TARGETING THE TUMOR BLOOD VESSELS:

VEGFR2 as a Biomarker and Therapeutic Target
in
Non Small Cell Lung Cancer

Inaugural Dissertation

zur

Erlangung des Doktorgrades

Dr. nat. med.

Der Medizinischen Fakultät
und
der Mathematisch-Naturwissenschaftlichen Fakultät
der Universität zu Köln

Vorgelegt von

Sampurna Chatterjee

aus Kalkutta

Berichterstatter: Prof. Dr. Mirka Uhlirova

                                Prof. Dr. Bent Brachvogel

Tag der letzten mündlichen Prüfung: 19.09.2014

To

Roland and my Parents

Table of Contents

1. Abstract

Blood vessels transport oxygen and nutrients within the body. However, blood vessels also nourish cancer. Numerous evidences indicate uniformly towards the fact that tumors cannot grow without access to and recruitment of blood vessels, a process widely known as tumor angiogenesis. It has been well described that endothelial cell migration and proliferation is primarily regulated by VEGF-A binding to its receptor VEGFR2. However molecular mechanisms that control the shift in angiogenic switch in Non Small Cell Lung Cancer remain poorly understood till date. In this PhD thesis we have identified a novel autocrine feed-forward loop active in the tumor where tumor-cell autonomous VEGF:VEGFR2 feed forward loop triggers signal amplification substantially amplifying the pro-angiogenic signal required for establishing fully angiogenic tumors in lung cancer. In 20% of lung cancer patients this feed forward loop was active as the level of VEGF: VEGFR2 binding in tumor cells and directly correlated with tumor angiogenesis. Disruption of this feed forward loop using inhibitors against VEGFR2 or knockdown was sufficient to prevent tumor growth in vivo. Furthermore, inhibition of tumor cell VEGFR2 induced feedback activation of the IRS/MAPK signalling pathway switching the tumor cells from an angiogenic to a proliferative phenotype. Combined pharmacological inhibition of VEGFR2 with ZD6474 and MEK with PD0325901

resulted in dramatic tumor shrinkage. We thereby propose that high expression of tumor VEGF:VEGFR2 can serve as a predictive biomarker for therapeutic efficacy of dual VEGFR2/MEK inhibition in the patients with NSCLC.

Our next project was to investigate the role of VEGFR2 in the tumor microenvironment using cancer cells, which do not have a high expression of VEGFR2. In most cancers, tumor vasculature is leaky, disorganized with a chaotic morphology resulting in a hostile tumor microenvironment characterized by increased hypoxia and high interstitial fluid pressure. These abnormal vessels interfere with effective delivery of drugs and supports tumor progression and resistance to treatment. The traditional concept of using anti-angiogenic therapy to eradicate tumors by starving them from oxygen and nutrient supply by destroying existing vessels has not seen much success. One reason for this failure can be attributed to the vessel-leakiness hindering homogeneous drug delivery within the tumor. Alternative strong evidences are emerging that transient application of anti-angiogenic agents can normalize the aberrant tumor vasculature and that cytotoxic therapy given during this normalization window might have the best outcome. Yet there remains a lack of clarity about how to optimize scheduling such drug combinations. In this PhD thesis, we observed that short-term treatment with the VEGFR / PDGFR inhibitor PTK787 or VEGFR2 inhibitor ZD6474 initiated a transient window of improved blood flow using $[^{15}O]$ H_2O Positron Emission Tomography (PET) in a preclinical mouse model of Non Small Cell Lung Cancer. This improvement was associated with reduced vessel leakiness and enhanced pericyte coverage. Initiation of cytotoxic treatment with erlotinib during this normalization

window resulted in improved treatment efficacy. Additionally intermittent PTK787 treatment also facilitated long-term tumor regression. Concisely, our findings offer strong evidence that short-term anti-angiogenic therapy can promote transient vessel normalization that can improve the delivery and efficacy of a targeted cytotoxic drug.

In summary, VEGFR2 expressed on tumor cells plays a pivotal role in driving tumor angiogenesis and the same receptor expressed in the tumor microenvironment is relevant for normalization of tumor vasculature. Hence VEGFR2 can serve as an effective therapeutic target, which may lead to eradication of tumors or survival advantage in advanced NSCLC patients in the clinic.

2. Zusammenfassung

Blutgefäße transportieren Sauerstoff und Nährstoffe im Körper. Damit unterstützen Blutgefäße aber auch das Wachstum von Tumoren. Zahlreiche Studien deuten darauf hin, dass Tumore nicht ohne Zugang zu Blutgefäßen bzw. der Neubildung von Blutgefäßen, einem Prozess, der unter Angiogenese bekannt ist, wachsen können. Es konnte gezeigt werden, dass die Migration und Ausbreitung der Endothelzellen hauptsächlich durch die Bindung von VEGF-A an seinen Rezeptor VEGFR2 reguliert wird. Allerdings sind die molekularen Mechanismen, die den Übergang des angiogenen – das Wachstum der Tumorgefäße stimulierenden - Schalters im nicht-kleinzelligen Bronchialkarzinomen steuern, zum jetzigen Zeitpunkt kaum verstanden. In dieser Doktorarbeit haben wir eine neue autokrine Rückkopplungsschleife identifiziert, die in den Tumorzellen aktiv ist. Diese autonome VEGF:VEGFR2 „Feed-Forward" Schleife löst eine Signalverstärkung aus, die das pro-angiogene Signal, das zur Erschaffung von angiogenen Tumoren in Lungenkrebs notwendig ist, wesentlich verstärkt. Wir konnten zeigen, dass bei 20% der Patienten mit Lungenkrebs diese Rückkopplungsschleife aktiv ist. Das Unterbrechen dieser „Feed-Forward" Schleife durch VEGFR2-Inhibitoren oder Gen-Knock-down war in vivo ausreichend das Wachstum des Tumors zu verhindern. Weiterhin hat die Inhibition des tumoreigenen VEGFR2 die

Aktivierung eines zweiten Signalweges, des IRS/MAPK Signalweges induziert, woraufhin die Tumorzellen von einem angiogenen zu einem proliferativen Phänotyp wechselten. Eine kombinierte pharmakologische Inhibition von VEGFR2 mit ZD6474 und MEK mit PD0325901 führte zu einer deutlichen Schrumpfung des Tumors. Wir konnten damit zeigen, dass eine hohe Expression des tumoreigenen VEGF:VEGFR2 als Biomarker für die therapeutische Wirksamkeit der kombinierten VEGFR2/ MEK Inhibition in Patienten mit nicht-kleinzelligen Bronchialkarzinom dient.   In unserem nächsten Projekt untersuchten wir die Rolle von VEGFR2 in der Tumorumgebung. In den meisten Krebsarten sind die Blutgefäße durchlässig, nicht organisiert und besitzen eine chaotische Gestalt, die zu einer Tumormikroumgebung führen, die durch Hypoxie und hohen Druck der Interstitialflüssigkeit charakterisiert ist. Diese abnormalen Blutgefäße behindern die effektive Medikamentenzufuhr und unterstützen die Entwicklung von Resistenzmechanismen des Tumors gegen eine Behandlung. Die bisherige Methode – der Einsatz einer anti-angiogene Therapie um den Tumor abzutöten, indem man vorhandene Blutzellen zerstört um so seine Sauerstoff- und Nährstoffzufuhr zu unterbrechen – hat keine großen Erfolge gezeigt. Ein Grund für dieses Versagen ist den undichten Blutgefäßen zuschreiben, die eine effiziente Zufuhr der Medikamente innerhalb des Tumors verhindern. Andererseits gibt es Hinweise dafür, dass eine kurzzeitige Anwendung von anti-angiogenen Medikamenten die abweichende Morphologie der Blutgefäße des Tumors kurzzeitig normalisieren kann, und somit eine zytotoxische Therapie in diesem Zeitfenster der Normalisierung möglicherweise den bestmöglichen Erfolg erzielen kann. Es war allerdings

bislang ungewiss, wie man eine derartige Medikamentenkombination optimal planen soll. In dieser Doktorarbeit haben wir unter Verwendung von [15O] H2O Positron Emission Tomographie (PET) in vorklinischen Mausmodellen nicht-kleinzelliger Bronchialkarzinome beobachtet, dass eine kurzzeitige Behandlung mit dem VEGFR / PDGFR Inhibitor PTK787 zu einer transienten Verbesserung der Durchblutung führt. Diese Verbesserung war mit einer verminderten Durchlässigkeit der Blutgefäße und einer verbesserten Perizytenabdeckung verbunden. Der Start der zytotoxischen Behandlung mit Erlotinib innerhalb dieses Zeitfensters resultierte in einer gesteigerten Behandlungswirksamkeit. Zusätzliche zwischenzeitliche Behandlung mit PTK787 verbesserte den langfristigen Rückgang des Tumors. Zusammenfassend zeigen unsere Untersuchungsergebnisse, dass eine kurzzeitige anti-angiogene Therapie zu einer kurzzeitigen Blutgefäßnormalisierung führen kann, die die Zufuhr und Wirksamkeit eines abgestimmten zytotoxischen Medikaments verbessern kann. Die Expression von VEGFR2 in Tumorzellen spielt eine ausschlaggebende Rolle bei der Tumorangiogenese. Derselbe Rezeptor ist in der Tumorumgebung ausschlaggebend für die Blutgefäßnormalisierung des Tumors. VEGFR2 kann somit als ein effektive, therapeutische Zielstruktur dienen, dessen gezielte Inhibierung zur Schrumpfung des Tumors und möglicherweise zur Erhöhung der Überlebenschancen bei Patienten mit fortgeschrittenen nicht-kleinzelligen Bronchialkarzinomen führt.

3. List of publications

I.

Sampurna Chatterjee, Lukas C. Heukamp, Maike Siobal, Jakob Schöttle, Caroline Wieczorek, Martin Peifer, Davide Frasca, Mirjam Koker, Katharina König, Lydia Meder, Daniel Rauh, Reinhard Buettner, Jürgen Wolf, Rolf A. Brekken, Bernd Neumaier, Gerhard Christofori, Roman K. Thomas and Roland T. Ullrich.

Tumor VEGF:VEGFR2 autocrine feed-forward loop triggers angiogenesis in lung cancer.

Journal of Clinical Investigation. 2013, 1732-1740.

II.

Sampurna Chatterjee, Caroline Wieczorek, Jakob Schöttle, Maike Siobal, Yvonne Hinze, Thomas Franz, Alexandra Florin, Joanna Adamczak, Lukas C. Heukamp, Bernd Neumaier and Roland T. Ullrich.

Transient antiangiogenic treatment improves delivery of cytotoxic compounds and therapeutic outcome in lung cancer.

Cancer Research. 2014, 2816-2824.

3.1. Individual contributions:

I.

All experiments have been planned, executed and analyzed by me unless and otherwise stated. In this project I designed the concept along with Gerhard Christofori, Roman Thomas and Roland Ullrich. I did the *in vitro* work including ELISA, immunoprecipitaion, Western blotting, FACS analysis. Additionally all *in vivo* work was also done by me including preparation of cell suspension from multiple NSCLC cell lines, xenografts, treatment of mice by oral gavage, tumor volume measurement, PET measurements, BLI measurements in the orthotopic murine lung cancer model, explantation of the xenografts and preparing tumor lysates. Lukas Heukamp, Reinhard Buettner and Jürgen Wolf gave me substantial support in immunohistochemistry and analyzing patient as well as xenografts samples. Davide Frasca assisted them. Rolf Brekken provided us an antibody that specifically recognizes VEGF binding to VEGFR2 on tumor cells. Bernd Neumaier synthesized the radiotracers FLT and MET. Daniel Rauh provided us the structural configuration of resistance gatekeeper mutation of VEGFR2. I received considerable support from Maike Siobal in establishing stable knockdown and the mutation in VEGFR2. Along with her I repeated some ELISA and Western Blots. Jakob Schöttle sometimes assisted me in PET measurements. Caroline Wieczorek performed proliferation assays in different cell lines. Martin Peifer provided the Affymetrix U133A array. Mirjam Koker provided technical support in establishing IP. Katharina König supplied us with a murine Ras-mutated lung cancer model in mice. Lydia Meder performed

VEGFR2 FACS measurement. I analyzed all data sometimes aided by Roland Ullrich and performed all statistical analysis. Roland Ullrich and Roman Thomas helped in editing and correcting the manuscript.

II.

All experiments have been planned, executed and analyzed by me unless and otherwise stated. I designed the project with Roland Ullrich. All in vivo work were carried out by me including preparation of cell suspension from multiple NSCLC cell lines, xenografts, treatment of mice by oral gavage, tumor volume measurement, measuring blood perfusion in tumors and proliferation using [^{15}O] H$_2$O and [^{18}F] FLT PET measurements respectively, injection of FITC Dextran via tail vein, perfusion of mice and explantation of the xenografts, preparation tumor lysates and Western Blotting. I also performed Immunofluorescence with tumor sections. Additionally I calculated pericyte coverage in the tumor blood vessels. Caroline Wieczorek supported me in repeating H$_2$O PET. Jakob Schöttle analyzed some H$_2$O PET data together with me. Maike Siobal provided technical support for Western Blotting. Thomas Franz and Yvonne Hinze measured erlotinib concentration within the tumors via mass spectrometric analysis. Lukas Heukamp and Alexandra Florin provided support in immunohistology of tumor samples. Together with Joanna Adamczak I performed perfusion of mice with 4% paraformaldehyde. Bernd Neumaier synthesized the radiotracers H$_2$O and FLT. I collected and analyzed all data, did the statistical analysis and wrote the manuscript. It was corrected and approved by Roland Ullrich and all co-authors.

4. Introduction:

4.1. Overview of lung cancer

Cancer is a disease attributed by uncontrolled growth of abnormal cells. Lung cancer is by far the second most common cancer and a leading cause of death due to cancer in men and women worldwide [1]. Lung cancer incidence rates are highest in North America and Europe accounting for 26% of all female cancer deaths and 28% of all male cancer deaths in 2013 in The United States. In Europe, lung cancer mortality rate was 16.8% in females and 26.1% in males in 2013. In Germany lung cancer remains the commonest cause of death due to cancer among men accounting for 25% of the deaths while it is the third most common in women (14%). Lung cancer is the most common or the second most common cancer in Asia except India, Japan, Mongolia and Taiwan with highest incidence rates in both males and females in Korea, Philippines, China and Singapore and the lowest in India and Sri Lanka. Lung cancer mortality rates are much higher for males than females in Asia exceeding 40 per 100,000 population in Philippines, Singapore and Korea and 37 per 100,000 in China and Taiwan. Females have the highest mortality rate in Singapore (18 per 100,000) followed by Taiwan and China (16/100,000).

4.2. Classification, causes and symptoms

The two major forms of lung cancer are Non Small Cell Lung Cancer (NSCLC) and Small Cell Lung Cancer (SCLC). NSCLC alone contributes to about 80 – 85% of all lung cancers [2]. NSCLC consists of three main histological subtypes:

adenocarcinoma (ADC), squamous cell carcinoma (SCC) and large cell carcinoma [3], [4]. Adenocarcinoma constitutes to about to 40% of all lung cancers arising from cells having glandular or secretory properties and often found in the peripheral lung tissue. Around 30% of all lung cancers are squamous cell carcinomas arising from multilayered squamous lining cells usually occurring at the centre of the lung near to the bronchi. Large cell carcinoma has a vaguely defined identity and can appear anywhere in the lungs.

Substances and exposures that might have different levels of cancer-causing potential and may cause cancer are called carcinogens. Smoking including passive smoking is associated with all major histological types of lung cancer but most strongly linked to small-cell and squamous-cell carcinomas than adenocarcinomas [5]. In contrast adenocarcinoma is the most common form of lung cancer in non smokers [6]. Cigarette smoke contains several thousand chemicals with over 60 identified carcinogens the most potent being polycyclic hydrocarbons (PAHs) like the tobacco specific nicotine-derived nitrosoaminoketone (NNK).

Chronic exposure to radon is nowadays known to be the second leading cause of lung cancer after smoking [7]. Exposure to certain chemicals including asbestos, arsenic, silica and air pollution (diesel exhaust, use of coal for

cooking) can cause lung cancer. Cancer survivors who received radiation or chemotherapy are at higher risk of lung cancer.

Factors that are unrelated to smoking include genetic (for e.g. p53 mutation), family history of lung cancer or viral (people with HIV or AIDS are at a higher risk of lung cancer because of their lower immunity) factors.
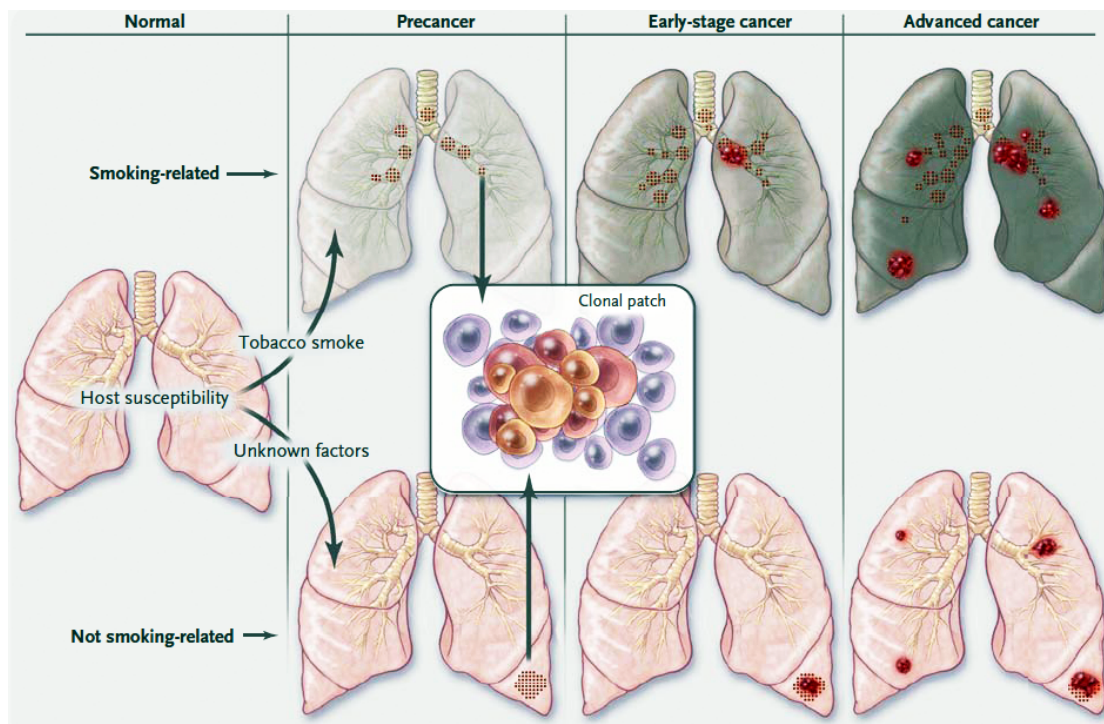

Figure 1: Evolution of lung cancer
Smoking related discolored patches mostly develop along the central airways of the lungs. These are usually squamous-cell or small-cell carcinoma. Most tumors unrelated to smoking are adenocarcinomas that arise in the peripheral airways. Genetic and epigenetic changes lead to aberrant pathway activation and cellular functions (uncontrolled proliferation and apoptosis) resulting in premalignant patches with clones and subclones of mutations (e.g. , *KRAS, p53, EGFR* etc) and loss of heterozygosity. (Image adapted from [2])

Signs or symptoms are not common in the early stages of lung cancer. However, symptoms develop as the disease progresses, which include

persisting cough associated with a change in colour of sputum (coughing up mucus and blood),

persistent breathlessness with chest pain while breathing,

feeling tired or lack of energy

loss of appetite and rapid weight loss

recurrent lung problems including infections such as bronchitis and pneumonia.

NSCLC is divided into five stages:

Stage 0 - the cancer is located within the inner lining of the lung

Stage 1 - the cancer is in the lung but has not spreaded to nearby lymph nodes

Stage 2 - the cancer has spreaded to some lymph nodes located near to the original tumor.

Stage 3 – the cancer has spreaded to the nearby tissue or lymph nodes far away (locally advanced disease)

Stage 4 – the cancer has spreaded to both lungs and / or to another organ for e.g. liver or brain (most advanced stage of lung cancer).

Depending on the stage of cancer diagnosis, NSCLC patients can be treated by surgery, chemotherapy, radiation or a combination of those. However success with traditional therapeutic regimens has reached a plateau and therefore new treatment approaches are needed to be developed [8].

4.3. Tumor angiogenesis

Sprouting of new capillaries from existing blood vessels is defined as angiogenesis [9]. Physiological angiogenesis is important for growth and development, reproduction and wound repair. Proliferation and migration of endothelial cells undergoing DNA synthesis are common hallmarks of angiogenesis [10].

About 30 years ago Judah Folkman pointed out that tumor growth cannot proceed without access to and recruitment of new blood vessels [11] a process defined as 'tumor angiogenesis' a term first coined by Shubi Phillipe [12]. Combination of genetic and epigenetic alterations activating oncogenes or inhibiting tumor suppressor genes lead to tumor development. Pathological angiogenesis is important for dormant tumors to grow beyond a microscopic size, maintain metabolic activity, survive and metastasize [13]. The tumor mass attains a critical size because of uncontrolled proliferation and tumor cells located far away from blood vessel lack supply of nutrients and oxygen thereby turning apoptotic, necrotic or hypoxic. However, to overcome this, tumor cells communicate with the microenvironment secreting substances first described as tumor angiogenesis factors [14] by Judah Folkman which induces sprouting of new capillaries from existing vessels[15]. This well defined, multistep transition from pre-vascular hyperplasia to densely vascularized and proliferating tumor is referred to as the ,angiogenic switch' [16].

In the past decades an assemblage of pro-angiogenic agents have been identified for example Vascular Endothelial Growth Factor (VEGF) [17], Fibroblast Growth Factor (FGF) [18], Platelet-derived Growth Factor (PDGF)

[19], angiopoietins [20], interleukins [21]. Simultaneously an arsenal of factors opposing angiogenesis (anti-angiogenic agents) have been characterized for example endostatins [22], thrombospondin [23], angiostatins [24].
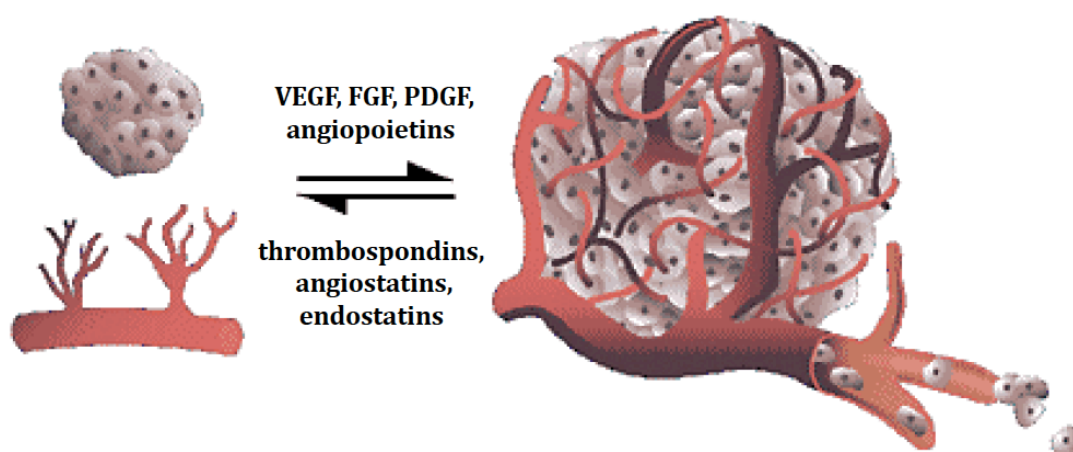

Figure 2: Angiogenic switch in cancer
Angiogenic switch refers to a discreet transition from dormant hyperplasia to vascularized, malignant tumor where the balance between pro-angiogenic factors (VEGF, FGF, PDGF etc) and anti-angiogenic factors (thrombospondins, angiostatins etc) is shifted in favour of a pro-angiogenic outcome. (Image modified from www.medscape.org)

The most widely studied pro-angiogenic polypeptide VEGF belongs to the mammalian glycoprotein family, which includes all the types VEGF-A, VEGF-B, VEGF-C, VEGF-D, and Placenta Growth Factor (PLGF) [25]. Best characterized subtype is VEGF-A which is expressed in different isoforms like 121, 165, 189 and 206 amino acid proteins with VEGF-A 165 being the predominant isoform [26]. VEGF is highly expressed in hypoxic condition and most commonly overexpressed in almost all kinds of human cancers[21, 27]. The classical VEGF receptors are the RTK VEGFRs – VEGFR1 (also known as FLT1), VEGFR2 (also known as KDR and FLK1) and VEGFR3 (also known as FLT4) [28]. VEGFR1 is a kinase impaired RTK and has a strong binding affinity for VEGF [29, 30]; in

contrast, the downstream intracellular signaling is much stronger and distinct when VEGF binds to VEGFR2 activating a broad range of downstream signaling cascades and inducing diverse biological responses [31]. VEGFR2 is the predominant RTK that drives VEGF mediated angiogenesis in endothelial cells [32]. Nowadays there are several reports confirming that a variety of tumor cells also express VEGFR2, which plays a pivotal role in mediating VEGF signaling [33]. VEGF-C and VEGF-D bind preferentially to VEGFR3 which is mostly expressed on lymphatic endothelial cells [26]. VEGFR3 plays an important role in lymphangiogenesis [34] and nowadays also known to induce lymphatic vessel sprouting thereby enhancing metastasis in some tumors for e.g. human large cell carcinoma of the lung [35]. Neuropillins (NRP-1 and NRP-2) primarily function as co-receptors to the VEGFRs [36]. They form complexes with VEGFR1 and VEGFR2 increasing their affinity for VEGF-A 165 [37]. Neuropillins have been also known to be expressed on both endothelial and tumor cells [38].
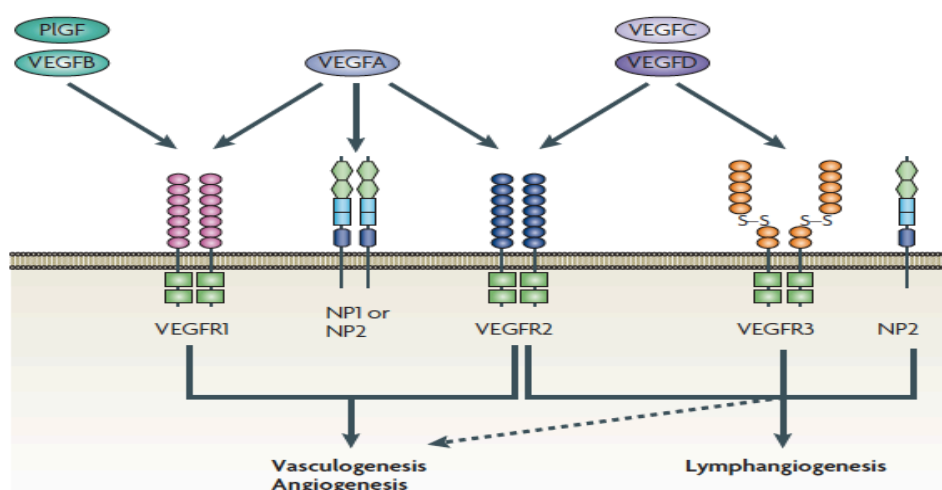

Figure 3: Overview of VEGF family members and their receptors
The mammalian family of VEGF ligands constitutes of VEGF-A, VEGF-B, VEGF-C, VEGF-D and PLGF. They bind to the VEGF receptor (VEGFR) tyrosine kinases activating downstream signaling. VEGF-A binds to both VEGFR1 and VEGFR2. VEGF-B and PLGF binds mainly to VEGFR1. VEGF-C and VEGF-D specifically binds to VEGFR3 and sometimes to VEGFR2. NRP-1 and NRP-2 act as co-receptors supporting binding of VEGF to VEGFRs. (Figure adapted from[26])
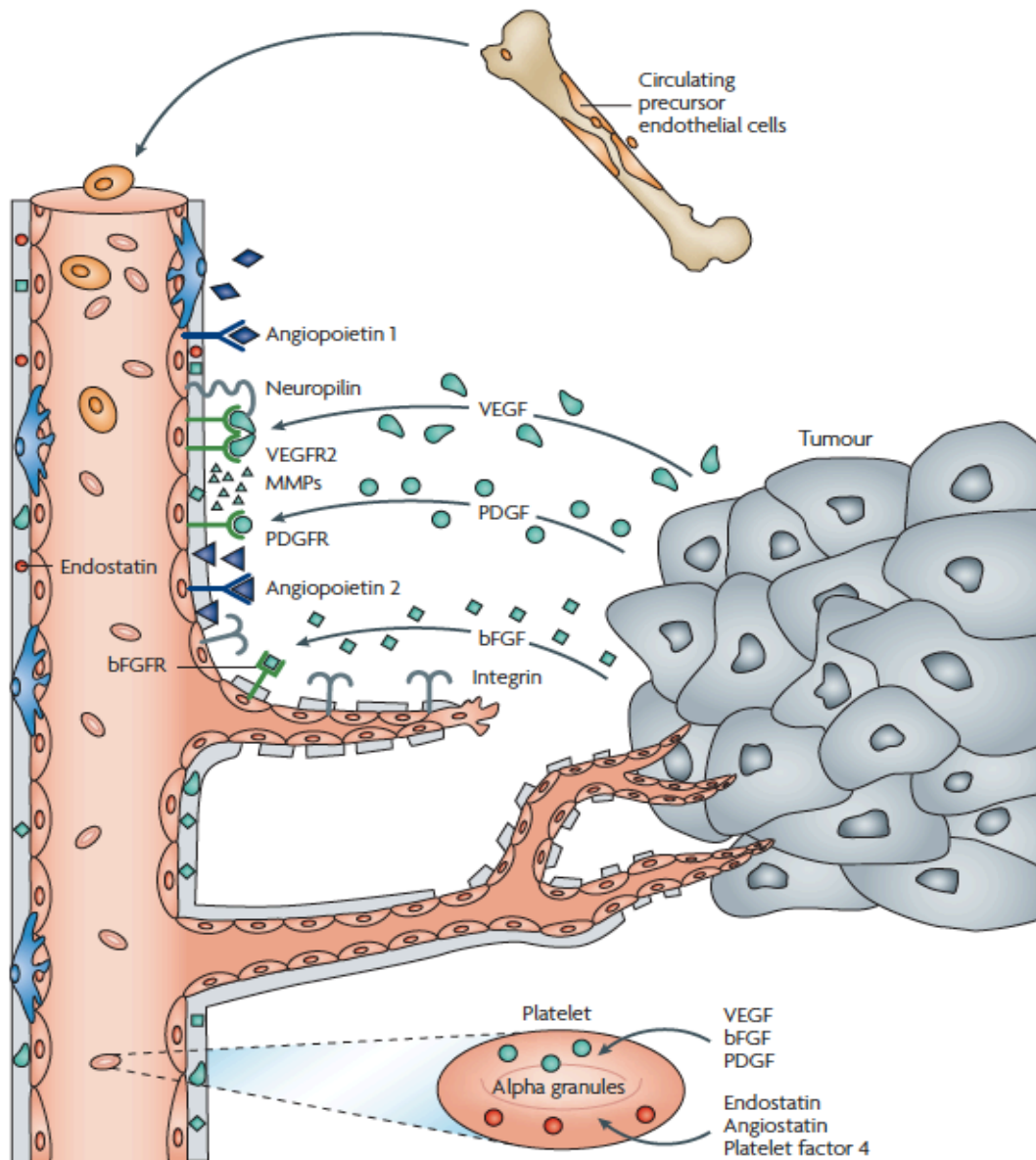
Figure 4: Schematic representation of tumor angiogenesis
Tumor cells secrete VEGF, which binds to VEGFR2 and NRP-1/NRP-2 on the endothelial cells. Matrix metalloproteinases (MMPs) are secreted simultaneously by endothelial and the VEGF-stimulated tumor cells. MMPs help in activating other pro-angiogenic factors from the stroma of tumor microenvironment. While angiopoietin1 (ANGPT1) tries to normalize the blood vessels, angiopoietin2 (ANGPT2) released by tumor cells degrades the vascular basement membrane inducing migration of endothelial cells promoting sprouting of new vessels. Other pro-angiogenic agents like FGF and PDGF can activate their receptors and facilitate tumor angiogenesis in similar manner. (Figure Adapted from [9])

The spontaneous progression from non-angiogenic hyperplasia to vascularized tumor is defined as the angiogenic switch. Angiogenic switch happens when the balance between pro- and anti-angiogenic agents is shifted in the favour of the pro-angiogenic factors.
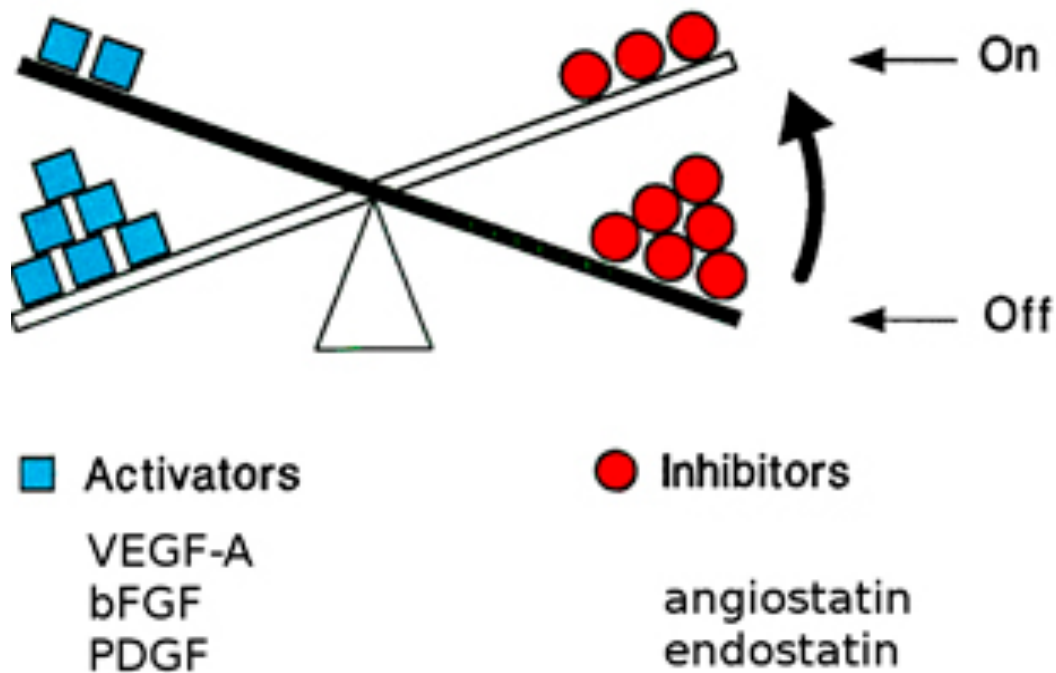

Figure 5: Angiogenic switch
In a healthy organism angiogenesis is tightly controlled and limited to physiological phenomena like wound healing, ovulation etc. However during tumor development the equilibrium between pro- and anti- angiogenic factors are shifted towards high levels of pro-angiogenic factors favouring the balance towards angiogenesis triggering the 'angiogenic switch'. This switch disrupts the delicate balance facilitating sprouting of new vessels and growth of tumor. (Figure adapted from [39])

The onset of angiogenic switch and extent of angiogenesis are critical determinants of tumor progression [40]. Molecular mechanisms underlying angiogenic switch is being studied extensively. Angiogenesis depends upon a complex interaction among tumor cells, endothelial cells and the tumor microenvironment including macrophages, stromal cells and pericytes in the

microvessels. Tumor angiogenesis on a molecular basis relies on a coordinated interplay among pro-angiogenic factors (VEGF, FGF, PDGF etc), coordination between migrating tip cells and proliferative stalk cells regulated by crosstalks between intracellular signaling molecules like VEGFR2 and NOTCH [41]. All these together activate the PI3K/AKT/mTOR pathway stimulating VEGF production and regulating cancer-cell induced angiogenesis [42-45]. Fast proliferating tumor cells create hypoxic regions within the tumor subsequently activating Hypoxia Inducible Factor 1 (HIF-1α) which has been identified as the transcriptional factor responsible for upregulation of VEGF under hypoxic conditions inducing the angiogenic switch [46, 47]. Macrophages cultured under hypoxic conditions release PDGF and FGF, which can stimulate endothelial cells modulating angiogenesis [48]. Recruitment of host blood vessels to the tumor sites is additionally triggered by genetic alterations (activation of oncogenes or loss of tumor suppressor genes) [49]. Potent oncogenes can interfere with expressions of both pro- and anti-angiogenic factors in tumors [50], (Table 1). For example, oncogenic *ras* mutants are known to upregulate VEGF production simultaneously downregulating thrombospondin-1(TSP-1) [51]. Tumor suppressor gene p53 inhibits angiogenesis by inducing expression of TSP-1 [52]. Another tumor suppression gene PTEN impede tumor angiogenesis by inhibiting PI3K [43]; simultaneously loss or inactivation of PTEN enhances tumor angiogenesis [53]. All these cumulatively results in a leaky tumor vasculature which is highly permeable, tortuous with increased interstitial pressure that might interfere with targeted delivery of cytotoxic agents [54].

Oncogene	Implicated pro-angiogenic activity
K-ras, H-ras	VEGF upregulation, TSP-1 downregulation
v-src	VEGF upregulation, TSP-1 downregulation
c-myb	TSP-2 downregulation
N-myc	angiogenic properties in neuroblastoma
c-myc	angiogenic properties in epidermis
HER-2	VEGF upregulation
EGFR	VEGF, bFGF, IL-8 upregulation
PyMT	TSP-1 downregulation
c-fos	VEGF expression
trkB	VEGF downregulation
HPV-16	secretion of VEGF and IFN-α
v-p3k	VEGF production and angiogenesis
ODC	novel angiogenic factor
PTTG1	VEGF and bFGF upregulation
E2a-Pbx1	induction of mouse angiogenin-3

Table 1: Role of several oncogenes as regulators of tumor angiogenesis (modified from [50])

Hence selective inhibition or destruction of tumor vasculature might lead to tumor regression. Since VEGF has been recognized as one of the key drivers of angiogenesis, studies over the past 20 years have provided significant development of therapeutic approaches that include antibodies against VEGF or VEGFRs and tyrosine kinase inhibitors (TKIs) against VEGFRs. Bevacizumab (BV), a humanized monoclonal antibody against VEGF was first reported in 1997 [55]. FDA has approved it for clinical trials involving patients with metastatic colorectal carcinoma (CRC), NSCLC and metastatic breast cancer in combination with chemotherapy [56-58]. Addition of BV to a standard double-agent chemotherapy regimen resulted in a significant improvement in overall survival (OV) and progression-free survival (PFS) in patients with NSCLC and metastatic CRC [56, 57]. VEGFR TKIs such as sorafenib and sunitinib have been approved

for clinical trials and they have shown efficacy as single agents in patients with renal cell carcinoma (RCC) [59-61]. Gefitinib and erlotinib, two small molecule TKIs of endothelial growth factor receptor (EGFR) which is overexpressed and mutated in solid tumors including NSCLC, are currently in clinical trials for patients with advanced NSCLC [62-66]. It is known that EGFR activation can regulate VEGF production and increase VEGFR expression in preclinical models and increased VEGF expression has been associated with resistance to EGFR inhibition in xenograft model of NSCLC [67-69]. Hence dual targeting of EGFR and VEGF by combining erlotinib with bevacizumab has been a particularly appealing therapeutic strategy in the clinic. A randomized Phase III trial comparing BV therapy with or without erlotinib significantly improved median PFS in the combination group [70]. However, modest impact on OS and increased toxicity associated with the combination treatment indicates towards the fact that this two-drug treatment regimen might not lead to new therapeutic developments in the clinic. Vandetinib (ZD6474, Zactima; AstraZeneca) competes with ATP binding in the catalytic domain of several tyrosine kinases. It is a potent inhibitor of VEGFR2 (50% inhibitory concentration IC_{50} 40 nM) [71]. Additionally it is also inhibits VEGFR3 (IC_{50} 110 nM) and EGFR (IC_{50} 500 nM) [71]. Based on promising results from Phase I studies with good tolerance of vandetinib upto 300mg daily [72-74], few Phase II and Phase III (ZEAL, ZEST, ZODIAC) trials using vandetinib as monotherapy and in combination with chemotherapy were conducted in advanced NSCLC patients [75, 76]. No statistically significant PFS or OS was observed in patients. However the ZODIAC study met its primary endpoint by showing statistically significant improvement

in the median PFS with 8.9 months for the arm vandetanib + chemotherapy compared to 4 months for the chemotherapy only arm. Adverse side effects were similar in all three trials most common being diarrhoea, rash, fatigue, nausea and hypertension. To date, the OS benefit in patients from only anti-angiogenic therapies remains modest. One major reason for disappointing results in the clinic is that there are no validated biomarker for anti-angiogenic drugs [77]. If we can identify specific biomarkers to select patients who can benefit from specific anti-angiogenic therapies then the survival advantage in those patients can be comparable to that from other targeted therapies [78]. In order to achieve this aim we need a better understanding of the molecular mechanisms that control the balance between anti- and pro-angiogenic factors and the resistance mechanisms of tumors against different antiangiogenic agents [77, 79, 80].

Bevacizumab only provided a survival advantage when used with chemotherapy or immune therapy in NSCLC, CRC, RCC, breast cancer [56-58, 81]. This might seem to be paradoxical since the original target of angiogenic therapy was to destroy tumor vasculature and chemotherapy or immune therapy needs functional blood vessels to deliver the drugs into the tumor. The hypothesis of 'normalization of tumor vasculature' suggested by Rakesh Jain might resolve this paradox [54]. Unlike normal vasculature, tumor blood vessels are leaky, tortuous, dilated and chaotic [82-86]. The vessel walls are leaky with inconsistent basement membrane and less pericyte coverage [87-89]. This leakiness leads to extravasation of plasma proteins increasing interstitial fluid pressure within the tumor. This abnormal phenotype of the tumor vasculature

supports tumor progression, aggravates tumor hypoxia, interferes with delivery of drugs and renders the cancer cells resistant to traditional treatment regimens [90]. The original concept of anti-angiogenic treatment was to inhibit tumor vessel growth thereby abrogating supply of nutrients and oxygen to the cells. However, anti-angiogenic treatment using DC101 (an antibody against VEGFR2) resulted in a reduction of tumor vessels but increased tumor invasiveness [91]. This is probably due to increased hypoxia within the tumor during anti-angiogenic therapy [92]. Higher doses of drugs to increase tumor concentration of drugs have not shown much success in the clinic. Since there are holes in the walls of the vessels it does not matter how much drug is administered. The drug and oxygen remain concentrated in some regions and do not reach the inaccessible areas of the tumor. However if the vessels can be repaired and made functional after anti-angiogenic therapy, then that would result in targeted and effective drug delivery. Here lies the rationale of normalizing tumor vasculature rather than destroying the blood vessels, which might explain the better treatment response in patients receiving chemotherapy with anti-angiogenic therapy. The concept of normalizing tumor vasculature using different anti-angiogenic agents has already been verified in xenograft models [93-96]. Clinical data from patients with rectal carcinoma showed that blocking VEGF using BV could indeed normalize tumor vessels [97, 98]. Most intriguing evidence in favour of vessel normalization came from change in blood perfusion data from clinic where anti-VEGF therapy improved tumor blood perfusion in some patients. Infact, patients with maximum vessel normalization and increased blood perfusion had the highest PFS and OS[99-101]. These

compelling pre-clinical and clinical evidences indicate clearly towards the fact that anti-angiogenic treatment which were originally developed to starve tumors can also be used to normalize tumor vessels improving blood perfusion and better delivery of cytotoxic drugs thereby prolonging patient survival. However, this raises a few sets of questions for example: When does vessel normalization begin? What is the optimal dose and schedule of anti-angiogenic drugs to induce vessel normalization? How long does the vasculature remains in this well fortified state? Does normalized vessels indeed deliver drugs into the tumor more efficiently? Is there any imaging technique other than magnetic resonance imaging (MRI) that can be used in the clinic to define and follow tumor perfusion after administration of anti-angiogenic therapy?
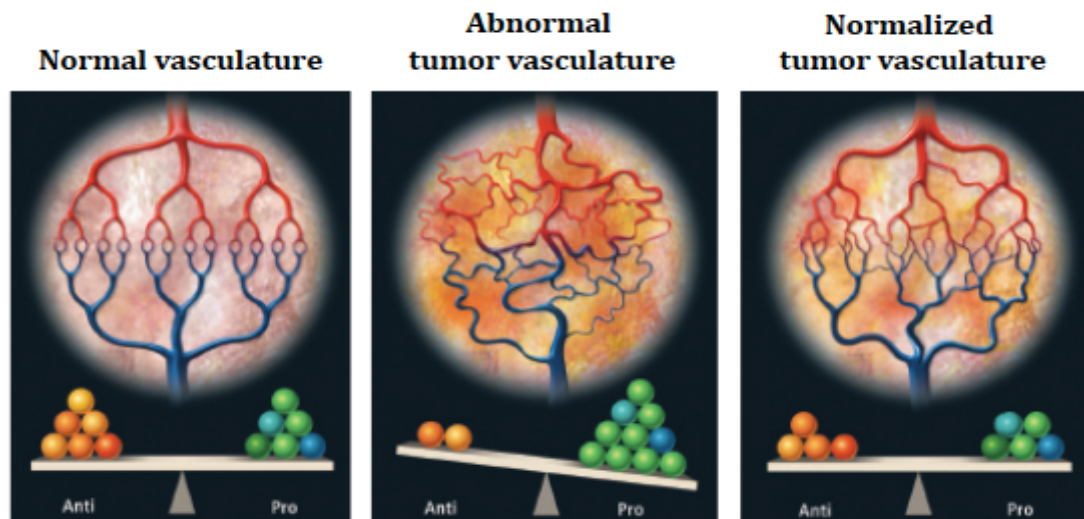

Figure 6: Hypothesis of vascular normalization
Vasculature can be: **normal (left):** equilibrium between angiogenic stimulators and inhibitors reinforces normal pathological angiogenesis with organized network of matured vessels branching into smaller ones, **abnormal (middle):** an imbalance created by a surplus of pro-angiogenic factors like VEGF, PDGF results in aberrant vessel sprouting creating a structurally and functionally abnormal vasculature, **normalized (right):** prudent anti-angiogenic therapy can initially prune chaotic sprouts improving the structure and function of existing vasculature leading to 'vascular normalization'. (Figure modified from [78])

5. Present Investigation

'VEGFR2 as a biomarker and effective therapeutic target in Non Small Cell Lung Cancer.'

5.1. Tumor VEGF:VEGFR2 autocrine feed-forward loop triggers angiogenesis in lung cancer.

Molecular mechanisms within the cancer cells controlling the angiogenic switch remains poorly understood till date. Identification of a potential biomarker on the tumor cells can be highly relevant for treating cancer in the clinic. In this study we aimed to investigate the impact of VEGFR2 expressed on tumor cells as a driver of angiogenic switch by inhibiting VEGFR2 in tumors combining pharmacological perturbation and multimodal imaging. Here I present my original work that has been published in [102] along with some additional results.

Materials and Methods

VEGFR2 expression in NSCLC cell lines

A. Affymetrix U133A array

VEGFR2 expression was analyzed in 53 NSCLC cell lines using Affymetrix U133A arrays. RNA extraction, hybridization and scanning of arrays were performed

using standard procedures. CEL files from U133A arrays were preprocessed as described previously [103].

B. Flow cytometry

Cell lines H1650, A549, H1975, H441 and HCC1359 were stained for VEGFR2 expression. 100,000 cells were fixed with 4% Formaldehyde for 20 min at 4°C, permeabilized with 0.5% saponin in PBS for 20 min at 4°C. Cells were stained with anti-VEGFR2 antibody (clone 55B11, 1:100, Cell Signaling) for 30 min at 4°C. Alexa-488 conjugated goat anti-rabbit antibody (A-11034, 1:1000, Life technologies) was used. Data of 10,000 cells per sample were acquired by a FACS Canto (BD Bioscience) and analyzed using FlowJo (Tree Star) software.

Cell lines and reagents

NSCLC cell lines H441, H1975, HCC1359, A549 and H1650 were purchased from the American Type Culture Collection (ATCC) and maintained in RPMI medium with 10% FCS and 1% (Penicillin+Streptomycin) antibiotic. VEGF was purchased from Tebu-bio GmbH, ZD6474 from Astra-Zeneca, PK90 from Axon Medchem, Torin1 from Tocris Bioscience, Rapamycin from LC labs. Compounds were stored at -20°C and dissolved in DMSO or vehicle on a rotating device at 4°C for invivo use.

Lentiviral RNAi, retroviral expression and stable transduction

The VEGFR2 V916M gatekeeper mutation was introduced into H1975 cells with a pBABE vector by site directed mutagenesis. Replication incompetent retroviruses were produced by co-transfection with the pCL ampho plasmid in

HEK 293T cells (Orbigen, USA) using TRANS-IT (Mirus, USA). Hairpins targeting the different genes were ordered from Sigma (www.sigmaaldrich.com). Replication incompetent lentiviruses were produced from pLKO.1 vector (www.broad.mit.edu/genome_bio/trc/) by co-transfection with Δ8.9 and pMGD2 in HEK 293T cells (www.broadinstitute.org/rnai/trc/lib) using TRANS-IT. Cells were transduced with polybrene and were selected with puromycin after transduction.

Western blotting

Western blotting was performed using the following antibodies: ß-actin clone C4 (MPBiomedicals LLC, USA), pAKT-S473 (1:500), AKT (1:1000), pS6K (1:1000), S6K (1:1000), IRS-1 (1:500), pERK (1:500), ERK (1:500), pVEGFR2 (1:500), VEGFR2 (1:500), VEGFR1 (1:500), pFoxO3a (1:500) (Cell Signaling Technology, USA), anti-rabbit-HRP- and anti-mouse-HRP-antibody (Millipore, Germany).

Immunoprecipitation

Protein A/G PLUS-Agarose beads (Santa Cruz Biotechnology, Inc) were washed twice in PBS and resuspended in 500μl of lysis buffer. Beads were incubated overnight with anti-PhosphoTyrosine antibody, clone 4G10 (1:50) (Millipore, Germany) in a rotating chamber at 4°C. Tubes were centrifuged at 3000 rpm for one minute and washed three times in ice-cold PBS. 500μg of cell lysate was added and volume was filled upto 1ml with lysis buffer. Tubes were incubated, centrifuged and washed as described previously. Supernatant was removed, beads were resuspended in 4x NuPage LDS buffer (Invitrogen) and heated at

80°C for ten minutes. Supernatant was carefully pipetted and loaded in a gel for western blotting. pVEGFR2 was used as the primary antibody.

ELISA

Cells were plated in 6-well plates and incubated for 24 hours in starving media. Cells were then stimulated with 40 ng VEGF-A 165 either alone or after pre-treatment with ZD6474 (1 µM) or with Rapamycin (100 nM) for 4 hours. Secretion of VEGF into cell culture supernatants was measured with the VEGF Human ELISA Kit from Tebu-Bio GmbH (cat. No. ELH-VEGF-001) according to the manufacturer's instructions.

Flow cytometry

Cells were plated in 6-well plates and incubated for 24 hours in starving media. Cells were then either treated with DMSO or stimulated with 40 ng VEGF-A 165 alone or after pretreatment with ZD6474 (0.5 and 1 µM) for 4 hours. The incorporated BrdU was stained with specific anti-BrdU fluorescent antibodies according to instructions for the BrdU Flow Kit from BD Pharmingen (cat. No. 559619). The levels of cell-associated BrdU were then measured with a Gallios Flow cytometer from Beckman Coulter. Results were calculated using Gallios FACS software.

Multimodal imaging

A. Positron Emission Tomography (PET)

Nude mice with macroscopic subcutaneous tumors were treated with an oral gavage of 75 mg/kg ZD6474 and imaged with a FOCUS microPET scanner

(Concord Microsystems, Inc., Knoxville, TN). [18F]FLT and [11C]MET were synthesized as described previously [104, 105]. 3'-deoxy-3'-fluorothymidine ([18F]FLT) is an analogue substrate of Thymidine. Clinical studies have already revealed significant correlation between [18F]FLT uptake and the in vitro proliferation marker Ki-67 in different tumors [106, 107]. Nucleoside transporters on the cell membrane regulate its uptake. Within the cell Thymidine Kinase 1 phosphorylates [18F]FLT to [18F]FLT monophosphate, di and triphosphate. In contrast to Thymidine, only a very small proportion of [18F]FLT is incorporated into the DNA [108].

Amino acid tracer such as [11C]methyl-L-Methionine ([11C]MET) has been used for diagnosis of tumors. Increase in [11C]MET uptake within the tumors is due to increased transport mediated by L-amino acid transporters mediated by growth factors that regulate mTOR signaling in tumors [109]. No-carrier-added [18F]FLT and [11C]MET were administered i.v. (tail vein) into the animals with a dose of 200 μCi/mouse and 400 μCi/mouse respectively. [18F]FLT PET and [11C]MET PET imaging were performed 60 min and 20 min after injection respectively. Data evaluation was based on a region of interest (ROI) analysis of the entire tumor using software VINCI. For data analysis the maximal voxel radioactivity within the tumors was taken. The mediastinum was chosen as a reference for determination of uptake ratio, since we observed constant uptake for [18F]FLT and [11C]MET in this region. All data were decay corrected.

B. Bioluminescence imaging (BLI)

This optical imaging method depends on the sensitive detection of light to visualize cellular and molecular processes. Bioluminescence is a kind of chemiluminescence where light energy is released as a result of an enzymatic reaction between luciferin, a substrate and it's enzyme luciferase. Bioluminescence has been observed in jellyfish (Aequorea), corals (Tenilla) and also several bacterial species (Vibrio fischeri). Most commonly used bioluminescence reporter in research is the D-luciferin from firefly (Photinus pyralis). Mammalian cells do not express the enzyme luciferase. Hence signal from bioluminescence imaging can be unambiguously attributed to the process under investigation generating images with high signal to background ratio.
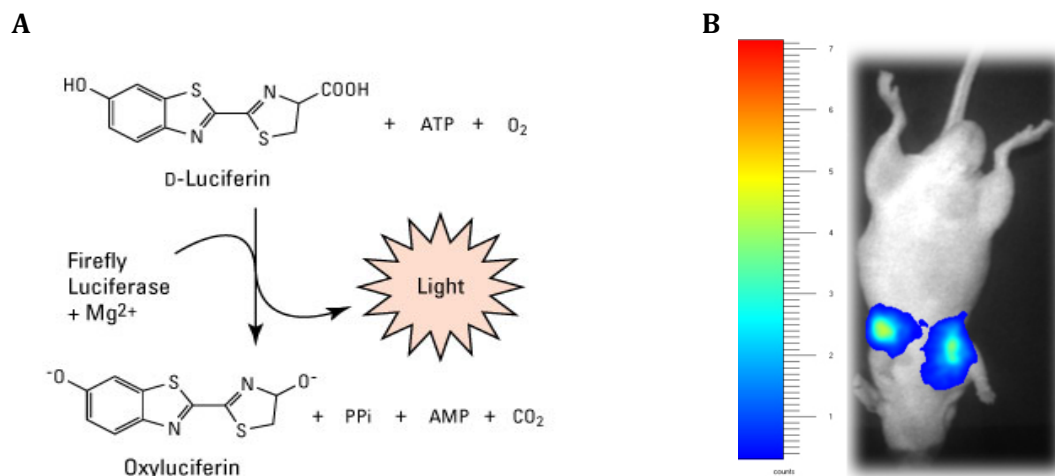

Figure 7: Principles of bioluminescence imaging
A. Enzyme luciferase oxidises luciferin emitting light (530-640nm) adapted from www.piercenet.com. **B.** $1x10^5$ H441 cells expressing luciferase were injected as single cell suspension intra venous (IV) via the tail vein in our lab. Three weeks later BLI signal from cancer cells in the lungs as recorded by Biospace imaging system.

Luc2 DNA was inserted in pBABE vector and HEK293T cells were transfected with Luc2 construct with retroviral particles. NSCLC cell lines were transduced

with virus containing Luc2, selected with antibiotics and implanted in mice. Analysis of luciferase gene expression was performed using an optical imaging system (Biospace, France). For bioluminescence detection, mice were injected intraperitoneally with D-luciferin (4 mg/animal in 200 µl PBS) and images were acquired 10 min after luciferin injection. Data evaluation was performed using ROI analysis of BLI images to determine maximum values in photons. Data were background subtracted.

Mouse models

All animal experiments and methodologies were approved in advance by the local animal protection committee and the local authorities. 5×10^6 cells (for each tumor) from individual cell lines suspended in plain RPMI were injected subcutaneously into male nude mice. Mice with established tumors (70 mm^3) or one day after tumor cell inoculation were treated daily by oral gavage of ZD6474 (75 mg/kg, dissolved in sterile, deionised water with 1% Tween 80), PD0325901 (12 mg/kg, dissolved in propylene glycol:water (1:1)), the combination of ZD6474 (75 mg/kg) and PD0325901 (12 mg/kg) or vehicle alone. Bevacizumab treatment was given i.p. (twice a week, 5mg/kg). Tumor size was monitored by measuring perpendicular diameters. Tumor volumes were calculated by determination of the largest diameter and its perpendicular according to the equation [tumor volume = $a \times (b^2/2)$]. The RasLO construct under the β-actin promoter is followed by a STOP codon flanked by LoxP sites. Human mutated Kras^{Val12} as well as a fusion molecule consisting of ovalbumin, S-tag and luciferase are expressed after excision of the STOP codon by Cre-

recombinase encoded in Adeno Virus. In order to induce tumor growth specifically in the lung, 10^7 PFU Adeno-Cre was applied intra-nasally in RasLO genotype positive mice between 6 to 8 weeks of age that had been previously anesthetized with Ketamin. Tumor progression or regression was non-invasively monitored by bioluminescence imaging (BLI) (Biospace) as described before.

Tumor samples and immunohistochemistry

All tumor samples were received from the CIO Biobank at the Institute of Pathology, University of Bonn, Germany. All tumors were clinically and pathologically identified as being the primary and only neoplastic lesion and classified according to World Health Organization (WHO) guidelines. 3μm thick sections of FFPE tumors were deparaffinized and antigen retrieval was performed by boiling the section in citrate buffer at pH6, or EDTA at pH9 for 20 min. Primary antibodies used were: VEGF (sc-152, 1:100, pH6, Santa Cruz Biotech); VEGF (Bevacizumab, 1:100, pH6, Roche; secondary anti human IgG-FITC, Dako), CD31 (SZ31, 1:50, pH6, Dianova), VEGFR2 (2479, 1:200, pH9, Cell signaling), ki-67 (mib-1, 1:100, pH6, Thermo scientific), pERK (4376, 1:50, pH6, Cell signaling), pMAPK (4631, 1:50, pH6, Cell signaling), IRS-1 (ab40777, 1:50, pH6, Abcam), VEGF:VEGFR (GV39M, 1:2, culture supernatant), HIF-1α (1:300). Corresponding secondary antibody detection kits on murine tissue were used (Histofine Simple Stain Mouse MAX PO, *Medac*, Hamburg, Germany) to minimize background and stained using automated LabVision Autostainer 480S from Thermo Scientific. The immunofluorescent double stainings of VEGF and

VEGFR2 was performed using the same primary antibodies and secondary antibodies. Three independent observers using a four-tier scoring system individually evaluated staining intensities. Statistical analysis was performed using a Fisher's exact test.

Results

Non small cell lung cancers express VEGFR2 differentially; VEGFR2 inhibition affects angiogenesis but not cellular proliferation; VEGF:VEGFR2 signaling induces a downstream feed forward loop via VEGFR2-PI3K-mTOR-VEGF cascade.

Human lung cancer cell lines H441, HCC1359 and H1975 with high expression of VEGFR2 and H1650, A549 with low VEGFR2 expression were chosen (**Figure 8A**). Mice implanted with H441 and H1975 were treated with the dual VEGFR2/EGFR inhibitor ZD6474, which has a 40-fold lower activity against Flt1 [71]. Both cell lines are resistant to EGFR inhibition, either due to a KRAS-mutation (H441) or to the presence of the T790M gatekeeper mutation of EGFR (H1975) [110]. Thus, any therapeutic impact of ZD6474 on these cell lines is primarily due to VEGFR2 inhibition and cannot be attributed to inhibition of EGFR. In macroscopic tumors ZD6474 treatment completely inhibited methionine uptake after one week of treatment, detected by [^{11}C]MET; (**Figure 8B**). However, uptake of [^{18}F]FLT, a marker of proliferation, was slightly increased (**Figure 8B**), suggesting that the cells continued to progress through

the cell cycle. Thus, VEGFR2 inhibition seems to inhibit a VEGFR2-dependent signaling pathway in tumor cells that affects amino acid transport without influencing cellular proliferation (**Figure 8B**).
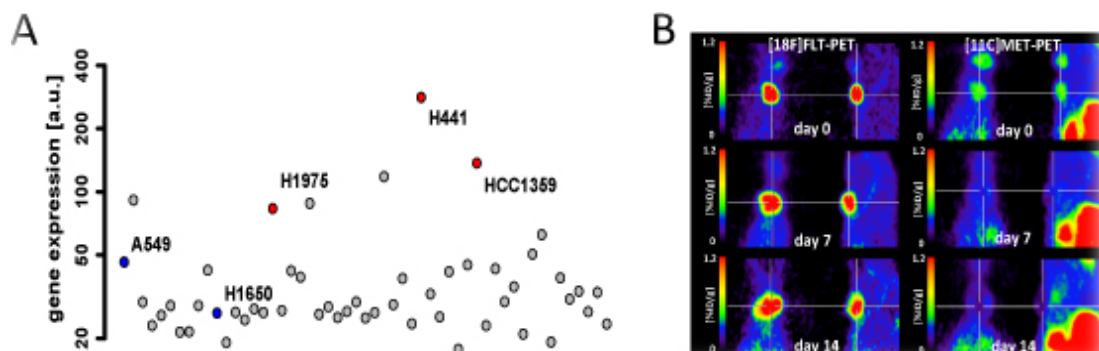

Figure 8: VEGFR2 expression profile and impact of VEGFR2 inhibition in NSCLC
A. VEGFR2 expression data from 53 NSCLC cell lines from Affymetrix U133A arrays. **B.** mice with established tumors (H1975) were treated with ZD6474 and PET imaging was performed on day 0 (before start of therapy) and at the indicated time points after treatment (left panels, [18F]FLT-PET; right panels, [11C]MET-PET).

To unravel if the reduction in MET uptake is specifically due to VEGFR2 inhibition, we introduced a resistant mutation against ZD6474-induced VEGFR2 inhibition. The substitution of Val916 with Met at the gatekeeper position of VEGFR2 creates a steric clash with ZD6474 that specifically prevents ZD6474 from binding to the VEGFR2 binding pocket **(Figure 9A)**. This gatekeeper mutation (H1975 VEGFR2^{V916M}) was sufficient to abrogate the inhibitory effect of ZD6474 on MET uptake (**Figure 9B)**. The cellular uptake of methionine is facilitated by the LAT1 transporter that is regulated by mTOR[111]. As VEGF secretion is partly regulated by mTOR, we sought to investigate if VEGF-VEGFR2 signaling induces a feed-forward loop via mTOR. Consistent the postulated existence of a feed-forward loop stimulating VEGF secretion in a VEGFR2-dependent manner, VEGF secretion was strongly induced by addition of exogenous VEGF in H1975, H441 and HCC1359 (**Figure 9C**) blunted by treatment with ZD6474 (**Figure 9C**). In

accordance with the hypothesis that VEGFR2-dependent secretion of VEGF is under the control of mTOR, which regulates methionine uptake via the LAT-1 transporter[112, 113], rapamycin treatment blunted VEGF-induced VEGF secretion of tumor cells **(Figure 9C)**. Another additional VEGFR2 inhibitor PTK787 also reduced secretion of VEGF validating our findings **(Figure 9C)**.
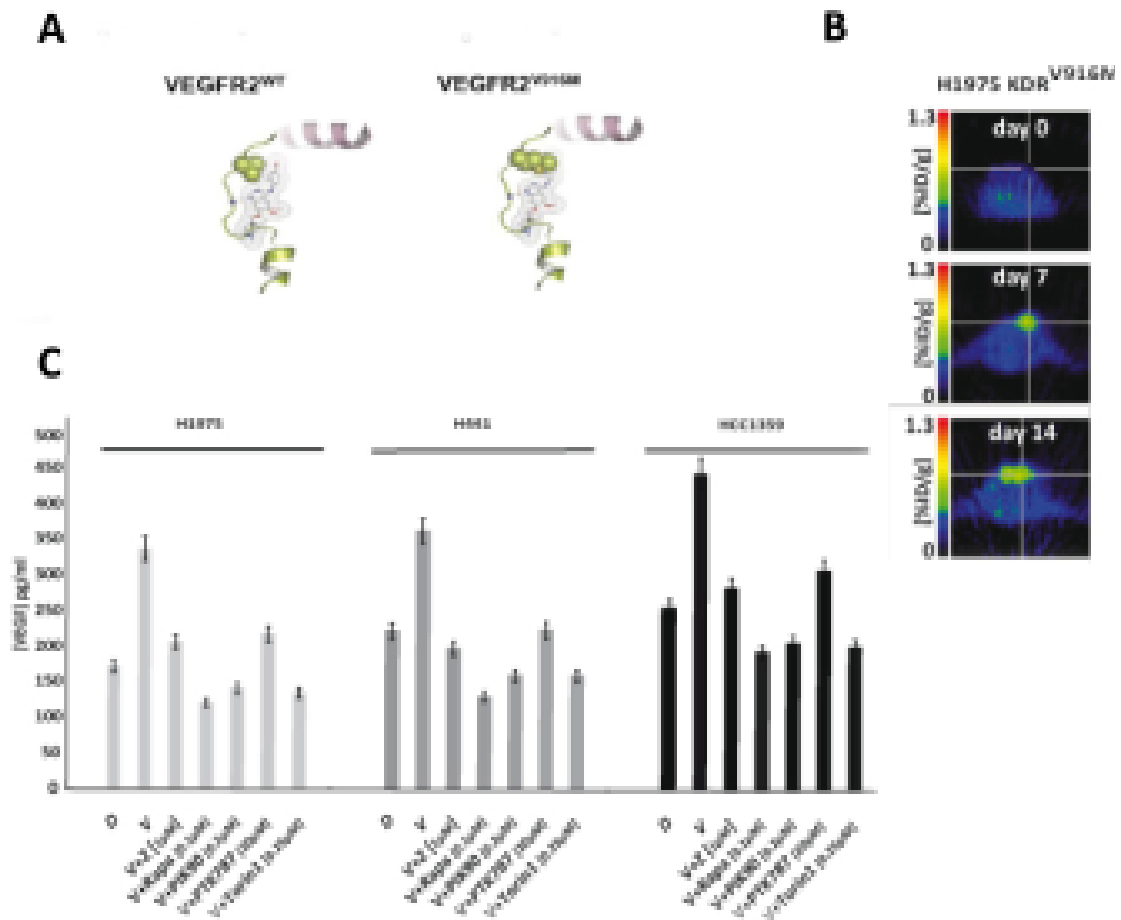

Figure 9: VEGF:VEGFR2 feed-forward loop in tumor cells boosts VEGF secretion
A. ZD6474 a classic Type I tyrosine kinase inhibitor binds to the hinge region of the kinase domain of VEGFR2^{WT}. Substitution of Val916 by Met at the gatekeeper position of VEGFR creates a steric clash with the inhibitor preventing ZD6474 from binding. **B.** mice with established tumors H1975 VEGFR2^{V916M} were treated with ZD6474 and [11C]MET-PET imaging was performed on day 0 (before start of therapy) and at the indicated time points after treatment. **C.** VEGF secretion by H1975, H441 and HCC1359 was measured in vitro by ELISA following stimulation with 40 ng VEGF (V). Cells pretreated with (Z=ZD6474 1 μM, Rapa=Rapamycin 0.2 μM, PIK90 0.2 μM, PTK787 20μM, Torin1 0.25 μM) were stimulated with 40 ng VEGF (V).

VEGF-mediated stimulation of VEGFR2 induced S6 phosphorylation (**Figure 10A**). Phosphorylation of S6 coincided with the activation of PDK1, which might provide an alternative route for mTOR activation (**Figure 10A)[114]**. In accordance with the induction of PI3K-mTOR-VEGF signaling, PI3K inhibition resulted in reduced VEGF secretion (**figure 9C**).

Additionally, we detected a consistent reduction in phosphorylation of ERK and of AKT (**Figure 10A**). Thus, under autocrine VEGF:VEGFR2 signaling, the slight reduction in tumor growth observed in response to VEGFR2 inhibition is likely to be independent of ERK-mediated proliferation. These results correlate with those of our PET experiments showing a continuous uptake of [18F]FLT **(Figure 8B)**. In H1975 VEGFR2^{V916M} mutant cells, VEGF levels were unaffected after addition of ZD6474 **(Figure 10B)**. Additionally ZD6474 failed to mediate VEGFR2-dephosphorylation and its downstream signaling target mTOR **(Figure 10C)**. Hence the observed ZD6474-mediated effects were specifically due to inhibition of VEGFR2 in tumor cells. In animal models, H1975 VEGFR2^{V916M} cells continued to grow overcoming tumor inhibiting effects of ZD6474 (**Figure 10D**). Thus, in accordance with the MET PET data, the ZD6474-mediated effects on tumor VEGF-VEGFR2-mTOR signaling were predominantly due to inhibition of VEGFR2 on the tumor cells and not due to inhibition of other kinases or VEGFR2 on endothelial cells.
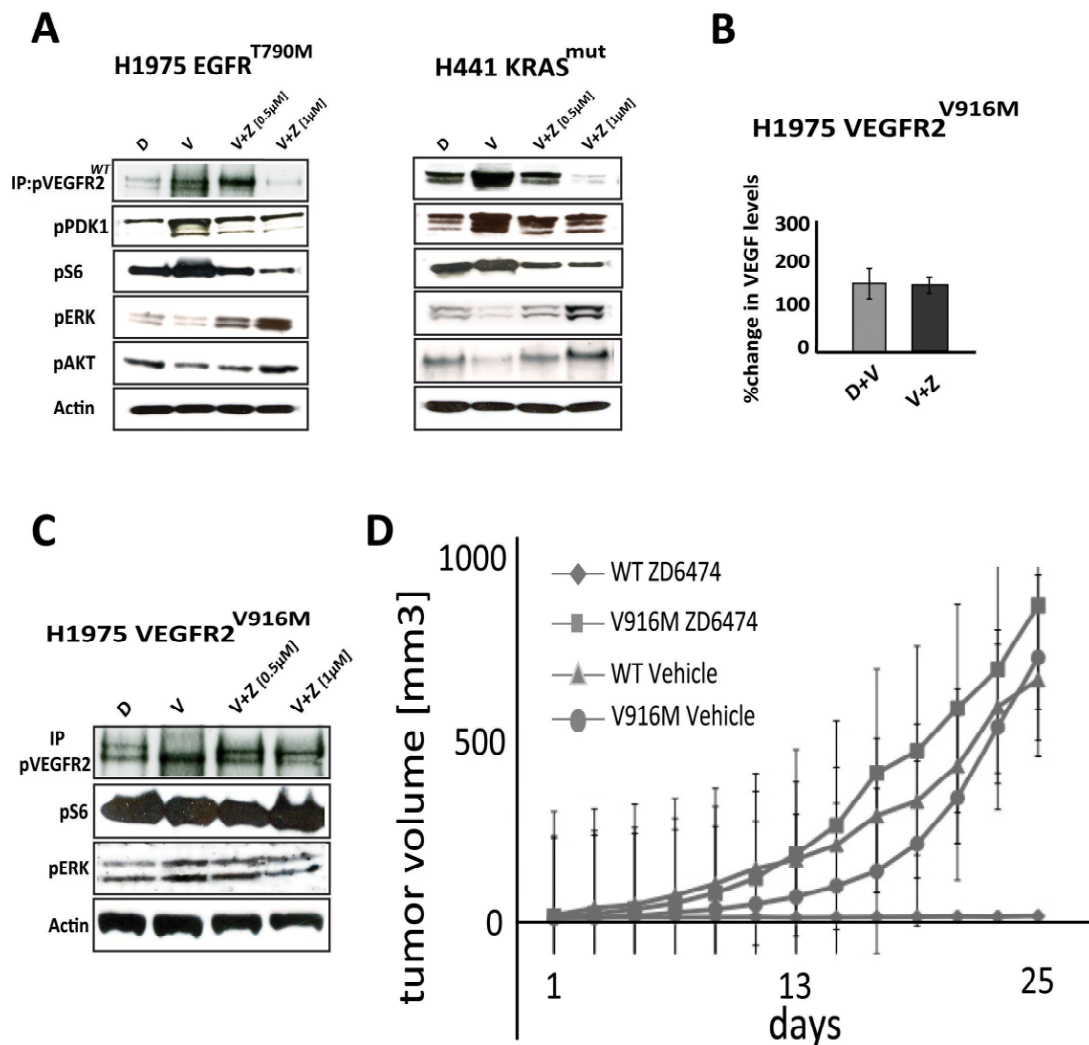
Figure 10: Tumor derived VEGFR2 is a key player in tumor angiogenesis
A. H1975 and H441 were treated with VEGF and indicated doses of ZD6474. Phosphorylation of VEGFR2 was determined by immunoprecipitation. The impact on activation of downstream signaling was determined by immunoblotting, employing the indicated phospho-specific antibodies. **B.** H1975 VEGFR2[V916M] mutants pretreated with the indicated dose of ZD6474 were stimulated with VEGF and VEGF levels were measured by ELISA. **C.** H1975 VEGFR2[V916M] was treated with VEGF and indicated doses of ZD6474. Phosphorylation of VEGFR2 was determined by immunoprecipitation. The impact on activation of downstream signaling was determined by immunoblotting, employing the indicated phospho-specific antibodies. **D.** H1975 xenografts expressing the VEGFR2[V916M] mutant or the VEGFR2[WT] control were injected into nude mice and treated with ZD6474 or vehicle on day 1 after tumor cell injections. Tumor volumes were recorded.

VEGF:VEGFR2 signaling is a key inducer of tumor development and angiogenic switch.

VEGFR2 was silenced with lentiviral shRNA in H1975 and H441 (**Figure 11A**). VEGFR2 knockdown did not reduce tumor cell proliferation in vitro but dramatically reduced secretion of VEGF by tumor cells in response to hypoxia (**Figure 11B**), thereby confirming that binding of VEGF to VEGFR2 amplifies VEGF secretion in a VEGFR2-dependent manner. VEGFR2 knockdown in tumor cells alone was sufficient to almost entirely abrogate initiation of tumor growth in vivo (**Figure 11C**), suggesting that autocrine VEGF:VEGFR2 signaling in tumor cells is essential for tumor development in vivo. While the large tumors transduced with empty control vector (H1975^{eV}) exhibited a highly angiogenic phenotype with many CD31-positive blood vessels, the small residual H1975^{VEGFR2KD} tumors lacked blood vessels almost completely (**Figure 11D**). H1975^{VEGFR2KD} tumors expressed almost no VEGF contrast to H1975^{eV} tumors (**Figure 11D**). Tumor derived (human) VEGF was stained using bevacizumab, which showed that silencing VEGFR2 on the tumor cells dramatically reduced the secretion of tumor-derived VEGF (**Figure 11D**). Furthermore, by staining with an antibody that specifically recognizes human VEGF bound to human VEGFR2[115], we could show that tumor cell-derived VEGF binds to VEGFR2 on tumor cells in H1975^{eV} but to a much lesser degree in H1975^{VEGFR2KD} xenograft tumors indicating the operation of autocrine stimulation in vivo (**Figure 11D**).
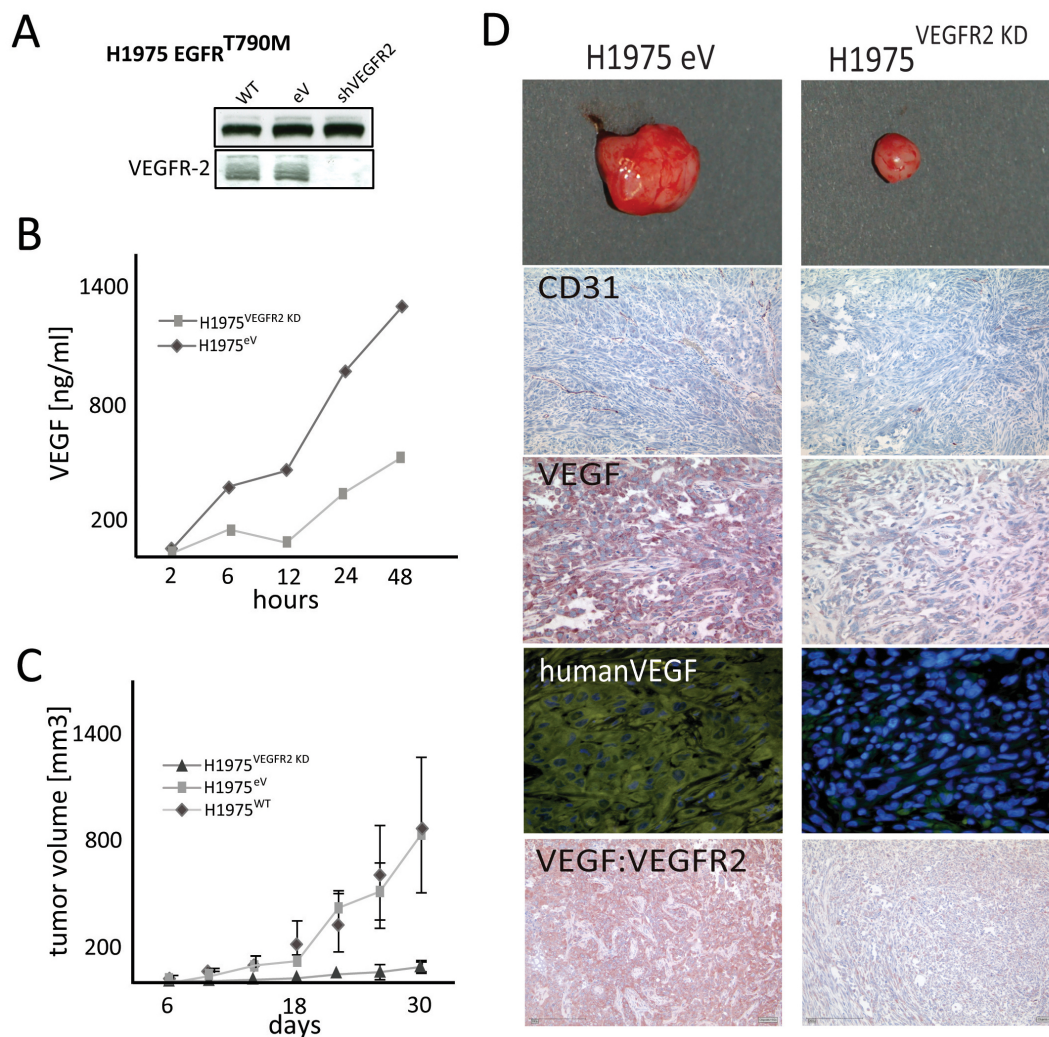
Figure 11: VEGF:VEGFR2 autocrine signaling is essential for induction of tumor angiogenesis

A. H1975^{WT} cells were stably transduced with lentiviral shRNA vectors targeting VEGFR2 (shVEGFR2) or with empty vector control (eV). Knockdown efficiency was determined by western blotting (upper panel, Flt-1; lower panel, VEGFR2). **B.** Stable cell lines were cultured and quantified under normoxic or hypoxic conditions (1% O_2). VEGF secretion was determined over time by ELISA. **C.** Stable cell lines were injected into nude mice and tumor growth was monitored over time. **D.** Tumors were harvested and stained for pan VEGF, CD31, human VEGF (employing GFP-labeled Avastin), human VEGF complexed with VEGFR2, and an antibody binding VEGF bound to VEGFR2.

As an alternative approach to determining whether VEGFR2 inhibition on tumor cells can prevent tumor formation, we treated mice with the VEGFR2 inhibitor ZD6474 simultaneous to tumor cell inoculation. Concomitant VEGFR2 inhibition in NSCLC-H1975 tumors expressing high levels of VEGFR2 completely

abrogated the establishment of tumors in vivo (**Figure 8I**), and was accompanied by a sharp reduction in tumor vessel density (**Figure 12A,B**). This blocking of tumor growth can be attributed to inhibition of VEGFR2, as the introduction of the resistance mutation VEGFR2^{V916M} in H1975 was sufficient to abrogate the ZD6474 mediated treatment effect **(Figure 8I)**. However in NSCLCs with low levels of VEGFR2 expression, such as H1650, pS6 levels remained unaffected under VEGFR2 inhibition (**Figure 12C**). Concomitant VEGFR2 inhibition also failed to abrogate tumor development in vivo (**Figure 12D**).
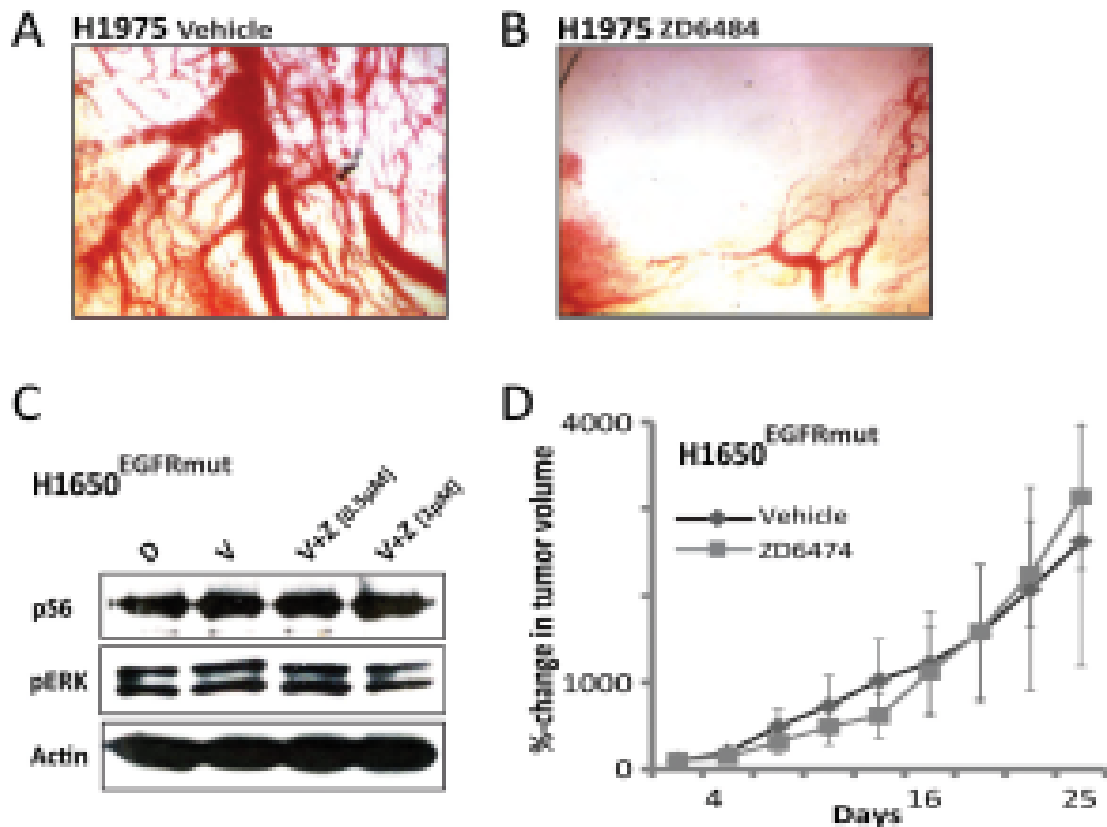

Figure12: Low VEGFR2 expressing tumor cell lines are unaffected by VEGFR2 inhibition

A,B. H1975^{WT} tumors were explanted from mice treated daily with an oral gavage of ZD6474 or vehicle for 2 weeks. Microvessels were imaged under a phase-contrast inverted-light microscope (Axiovert 135, Zeiss. LLC, US). **C.** H1650 cells with low VEGFR2 expression were pretreated with ZD6474 (Z) 0.5 and 1 µM for 4 hours and then stimulated with 40 ng VEGF (V) for 30 minutes. Cell lysates were immunoblotted with indicated phospho-specific antibodies. **D.** H1650 cells were injected into nude mice and treated with ZD6474 or vehicle on day 1 after tumor cell injections. Tumor volumes were recorded overtime.

In summary, the VEGF:VEGFR2 feed-forward loop is active only in tumor cells with high expression profile of VEGFR2 in vivo. It is essential for the establishment of fully angiogenic tumors and disruption of VEGF:VEGFR2 loop (either by VEGFR2 inhibition or blockade of VEGF) is sufficient to completely prevent tumor formation in vivo.

VEGF:VEGFR2 feed-forward loop is active in primary human lung adenocarcinoma; predictive biomarker for highly angiogenic phenotype.

Immunhistochemical analysis of VEGF and VEGFR2 in 117 surgically resected primary human lung adenocarcinomas was performed. VEGF expression correlated significantly with expression of VEGFR2 on the tumor cells ($p=2.612 \times 10^{-5}$) as well as with microvessel density ($p=2.2 \times 10^{-11}$); (**Table 2**), indicating that activated autocrine VEGF:VEGFR2 signaling loop is a feature of highly angiogenic lung adenocarcinomas.

VEGFR2 ($p=2.612 \times 10^{-5}$)

VEGF	0	1	2	3
0	0	1	0	1
1	0	11	8	1
2	0	10	42	16
3	0	0	13	10

CD31 ($p=2.2 \times 10^{-5}$)

VEGF	0	1	2	3
0	0	0	2	0
1	0	17	3	0
2	0	13	52	3
3	0	3	9	11

VEGFR2 ($p=0.01512$)

CD31	0	1	2	3
0	0	0	0	0
1	0	11	19	3
2	0	11	35	20
3	0	0	9	5

Table2: Tissue microarrays of 117 lung adenocarcinomas were stained with antibodies recognizing human VEGFR2, VEGF, CD31. Staining intensity of the different antibodies is given in chi-square tables scored on a 0-3 scale.

Immunofluorescence study also revealed that VEGF and VEGFR2 co-localized on tumors **(Figure 13B)**. Finally, staining of representative tumors with an antibody specifically recognizing human VEGF when bound to VEGFR2, confirmed that in the tumors co-expressing VEGF and VEGFR2, VEGF was indeed bound to VEGFR2 on tumor cells **(Figure 13B)**. Moreover, patients with adenocarcinomas that co-expressed high VEGF and VEGFR2, presented a highly angiogenic phenotype (**Figure 13B**).
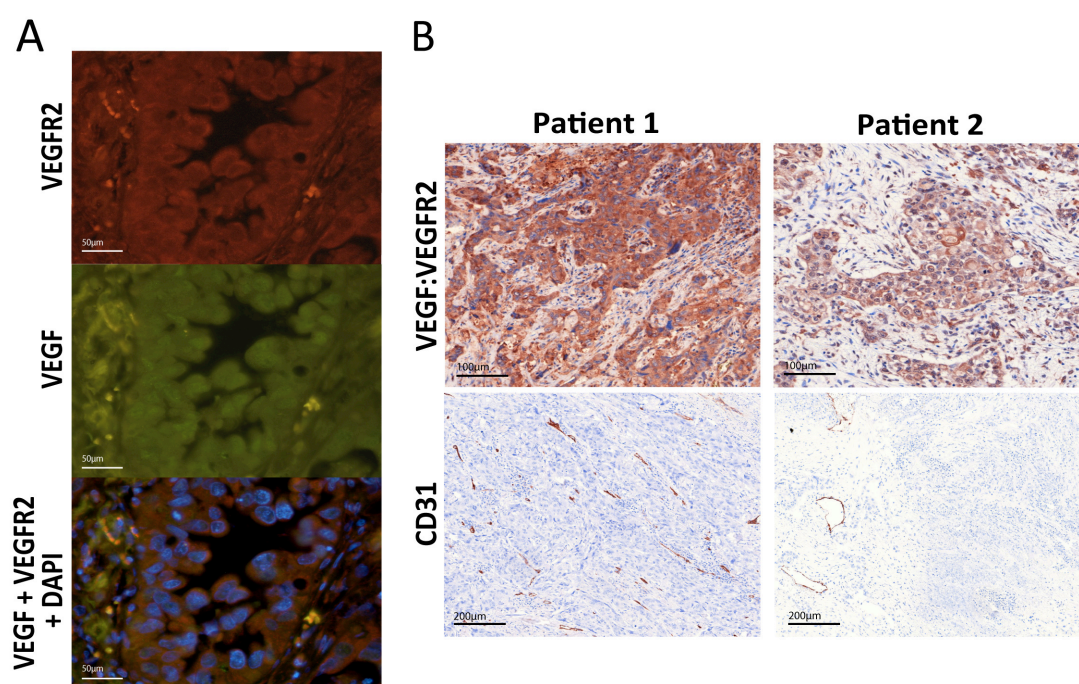

Figure 13. The VEGF:VEGFR2 feed-forward loop is active in primary human lung adenocarcinomas
A. Human adenocarcinomas were immunofluorescently stained to reveal co-expression of VEGF and VEGFR2 by the same tumor cell population. **B.** Patient 1 with a high angiogenic phenotype represented by strong VEGF:VEGFR2 staining and high CD31 positive cells. In contrast, patient 2 presents a low angiogenic phenotype with only moderate VEGF:VEGFR2 positive tumor cells, corresponding to a low density of CD31 positive cells.

These results support the hypothesis that the VEGF:VEGFR2 feed-forward loop also plays a critical role in the formation of primary lung tumors in patients.

Inhibition of VEGFR2 activates ERK signaling and sensitizes cancer cells to MAPK inhibition.

To our surprise we observed that H1975[VEGFR2KD] tumors exhibited increased levels of Ki67- and pERK-positive cells compared to H1975[eV] (**Figure 14A**). In the same manner, pERK signaling was reduced by VEGF stimulation in vitro and increased again on treatment with ZD6474 (**Figure 10A, 14B**). In concordance with the in-vitro data presented above, ZD6474 treatment induced inhibition of pS6 and an increase in pERK in vivo (**Figure 14C**). We thus hypothesized that inhibiting the VEGF:VEGFR2 feed-forward loop results in activation of the ERK signaling pathway and thereby appears to induce a ERK-dependant proliferative phenotype.
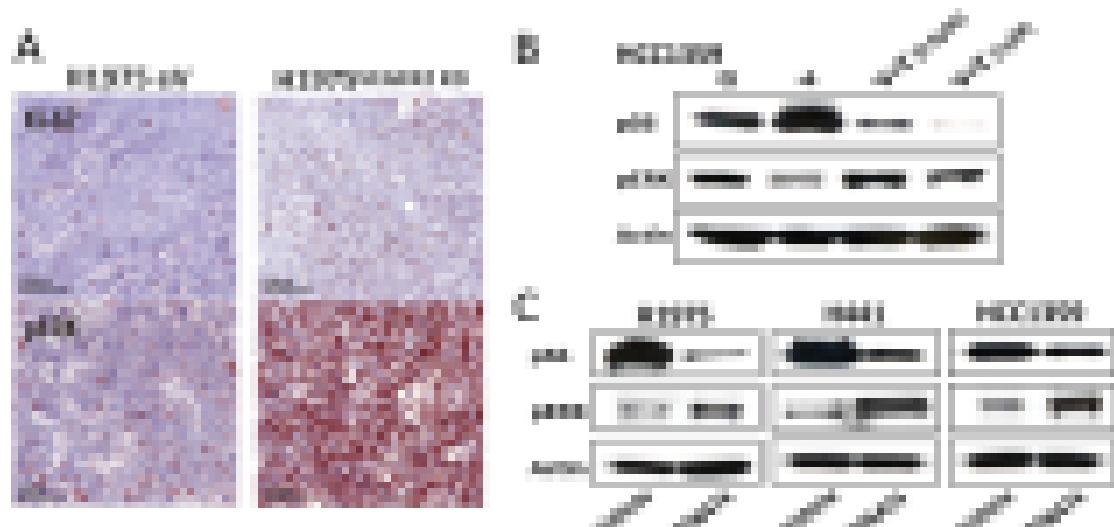

Figure 14: VEGFR2 inhibition decreases mTOR phosphorylation and induces pERK in high VEGFR2 expressing NSCLC
A. Tumors were harvested and stained for Ki67 and pERK . **B.** HCC1359 cells with very high VEGFR2 expression were pretreated with ZD6474 (Z) 0.5 and 1 μM for 4 hours and then stimulated with 40 ng VEGF (V) for 30 minutes followed by immunoblotting with specific antibodies. **C.** After treating mice over 14 days either with vehicle or ZD6474 (75mg/kg daily), tumors were explanted, lysed and immunoblotted for pS6 and pERK.

Recently, Rosen *et al.* described a negative feedback regulation of IGF signaling via mTOR and its transcriptional regulation of FOXO transcription factors [116]. In line with these findings, we found that inhibiting the VEGF-VEGFR2-mTOR autocrine feed-forward loop enhanced ERK signaling through activation of the insulin growth factor receptor (IGFR) signaling pathway via IRS-1, both in vivo and in vitro (**Figure 15A,B**). This activation of ERK was mediated by increased FOXO levels upon VEGFR2-mTOR inhibition in a time-dependent manner **(Figure 15B)**.
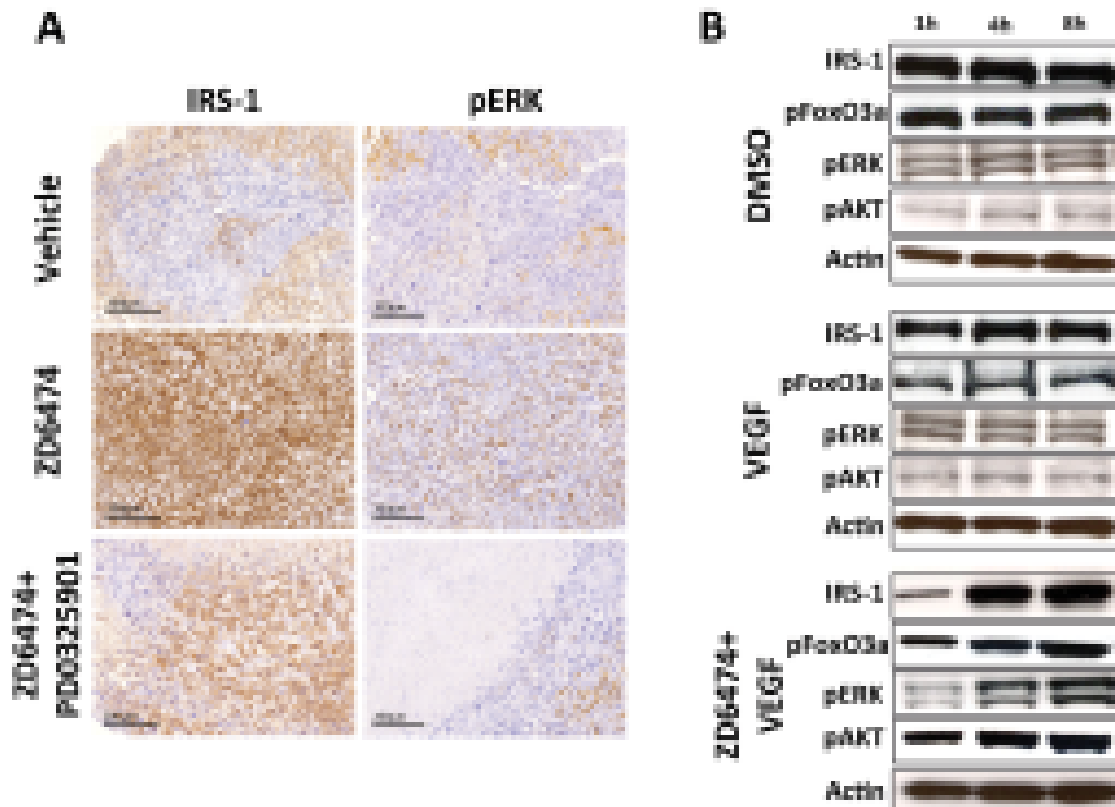

Figure 15: Inhibition of VEGFR2 enhances ERK signaling through insulin growth factor receptor (IGFR) signaling pathway via IRS-1
A,B. H1975 cells were engrafted subcutaneously in nude mice; mice with established tumors were treated with ZD6474 daily for 14 days. Tumors were explanted and impact of ZD6474 treatment on feed-forward activation of insulin receptor signaling was determined by IHC **(A)** and by western blots **(B)** employing the indicated antibodies.

Remarkably, combined inhibition of ERK by PD0325901 and VEGFR2 by ZD6474 resulted in a dramatic reduction of tumor cell proliferation, as indicated by [¹⁸F]FLT PET and complete tumor shrinkage **(Figure 16A, B).**
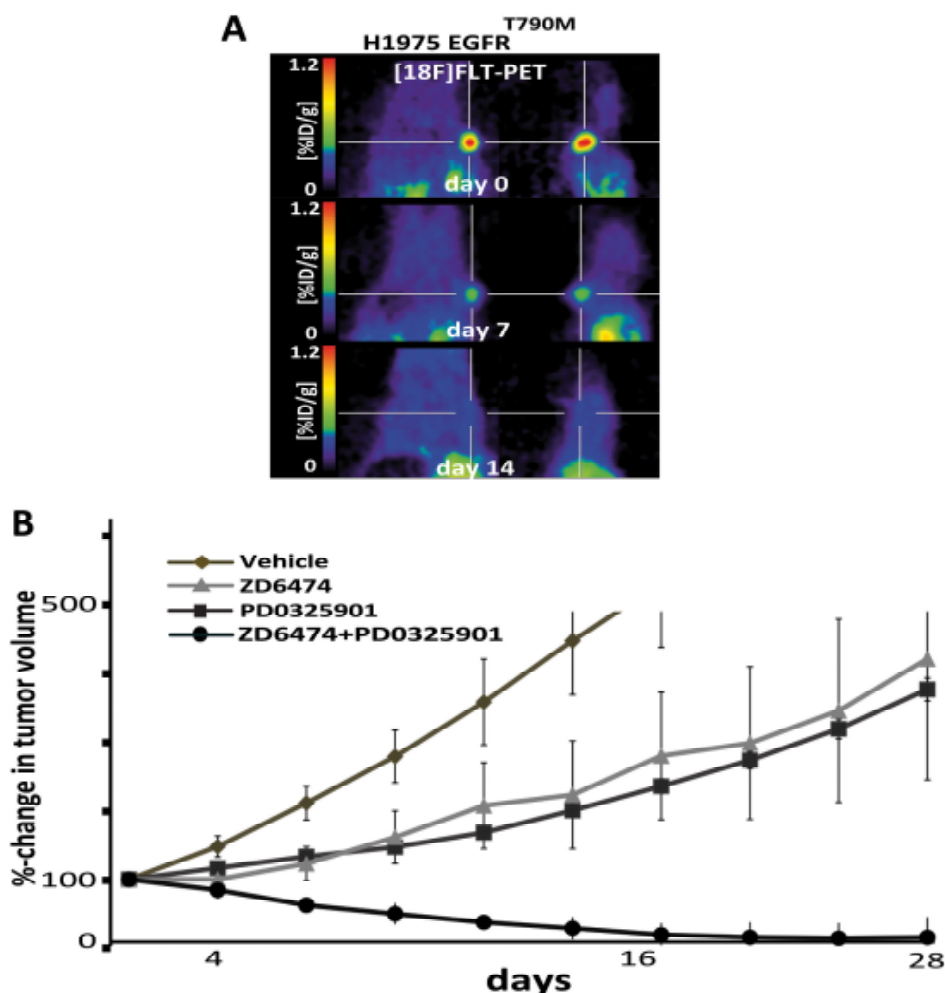

Figure 16. Combined inhibition of VEGFR2 and ERK signaling results in dramatic tumor shrinkage
A. H1975 cells were engrafted subcutaneously in nude mice; mice with established tumors were treated with combined ZD6474 plus PD0325901. [¹⁸F]FLT-PET imaging was performed on day 0 (before treatment) and at the indicated time points after treatment. Representative imaging results are shown. **B.** Tumor size of subcutaneously grown H1975 tumors was determined at the indicated time points under treatment with either vehicle, ZD6474 alone, PD0325901 (12 mg/kg) alone, or combined PD0325901 plus ZD6474.

In an orthotopic tumor model, where we applied a murine Ras-mutated lung cancer model expressing VEGFR2 on tumor cells **(Figure 17)**

combined PD0325901 and ZD6474 treatment resulted in substantial tumor regression as detected by bioluminescence imaging (BLI) **(Figure 17).**
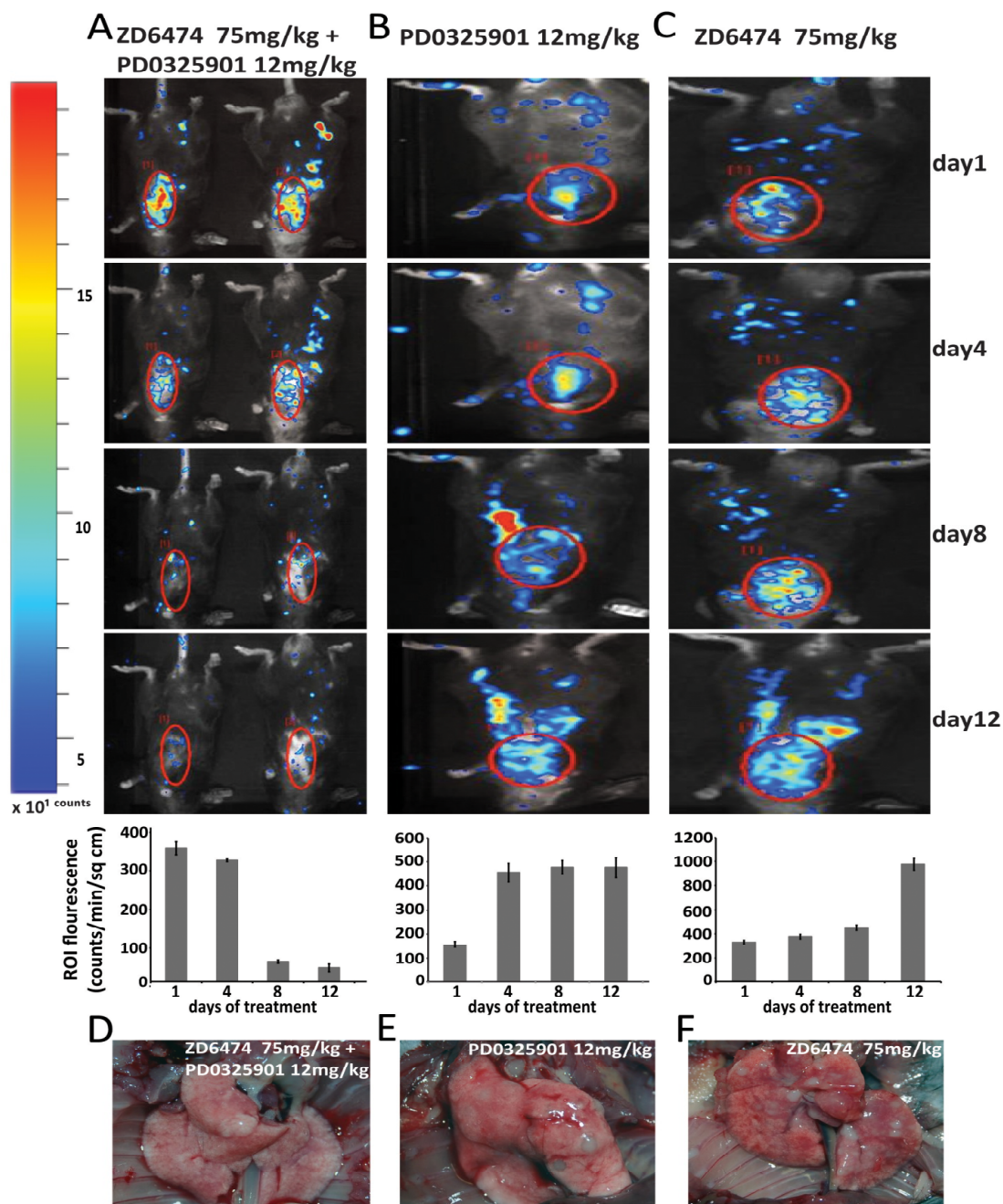

Figure 17. Combined inhibition of VEGFR2 and ERK signaling induces tumor shrinkage in an orthotopic Kras^{Val12} driven murine lung cancer model
A-C. Mice with Kras^{Val12} driven orthotopic murine Luc-positive tumors were treated and BLI imaging was performed on day 0 (before treatment) and at the indicated time points after treatment. Mice were treated with either ZD6474, PD0325901, or PD0325901 + ZD6474. **A-C.** Lower panels show quantification BLI signal based on region of interest analysis (ROI). **D-F.** Representative images of explanted lungs after treatment with ZD6474 + PD0325901 (**D),** PD0325901 only **(E)** or ZD6474 **(F)** only.

It is noteworthy that a response in the form of tumor shrinkage was associated with the expression levels of VEGFR2 on tumor cells. Consistent with our hypothesis, NSCLC-H1650 and A549 with only low VEGFR2 expressions failed to respond to combined VEGFR2 and ERK inhibition (**Figure 18C,D**) compared to excellent tumor shrinkage in high VEGFR2 expressing cells (**Figure 18A,B**)
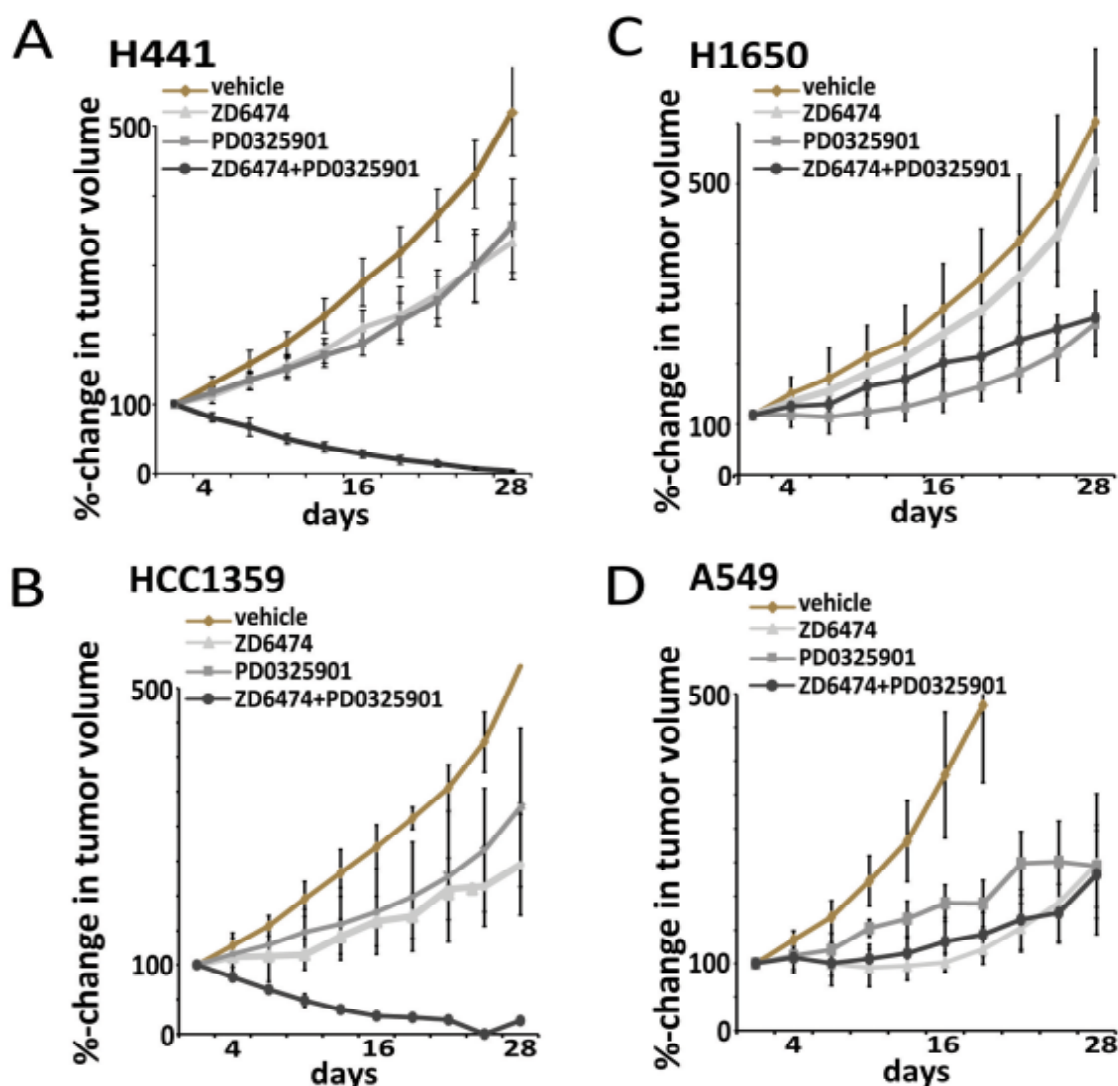

**Figure 18: Low VEGFR2 expressing NSCLCs are insensitive to combined VEGFR2 and ERK signaling**
Tumor volumes of subcutaneously engrafted H441, HCC1359 (high VEGFR2 expressing cell lines) **(A,B)** and H1650, A549 (low VEGFR2 expressing cell lines) **(C,D)** were recorded over time under treatment with either vehicle, ZD6474 alone, PD0325901 (12 mg/kg) alone, or PD0325901 combined with ZD6474.

Concluding remarks

Combining multimodal imaging and chemical genetics we have been able to unravel the molecular mechanism that initiate the angiogenic switch in NSCLC tumor. The preliminary pro-angiogenic signal is amplified via an autocrine feed-forward loop in lung cancer where tumor derived VEGF binds to tumor VEGFR2 activating mTOR inducing VEGF secretion.
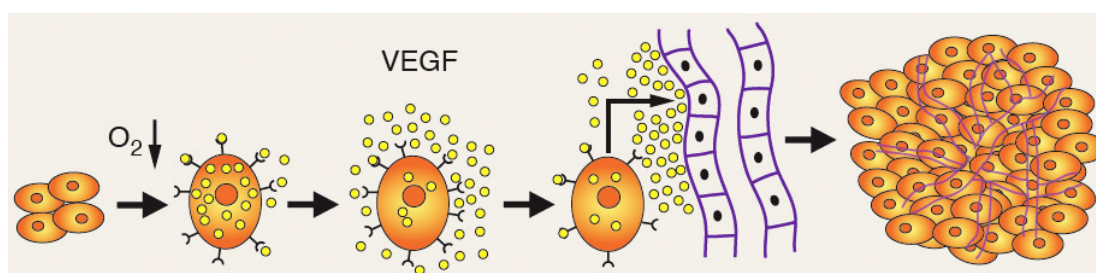
High coexpression of VEGF:VEGFR2 in NSCLC patients correlated to strong angiogenic tumors. Disruption of this feed-forward loop shifted the tumor cells from an angiogenic to proliferative phenotype sensitizing the tumor to MAPK inhibition.
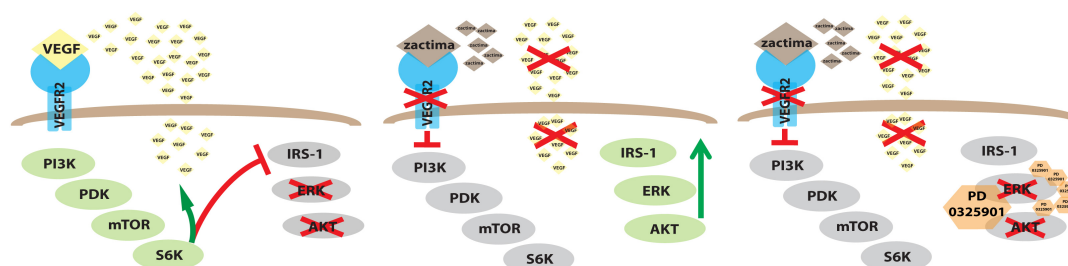
Hence we propose that high expression profile of VEGF:VEGFR2 can serve as a potential biomarker in the clinic to estimate which NSCLC patients might benefit from the therapeutic efficacy of combined VEGFR2 and MEK inhibition.

5.2. Transient anti-angiogenic treatment improves delivery of cytotoxic compounds and therapeutic outcome in lung cancer.

The popular concept of eradicating cancer by destroying tumor vasculature using anti-angiogenic agents has not seen much success in the last years. Prudent anti-angiogenic therapy might transiently normalize blood vessels improving tumor oxygenation and drug delivery. Clinical trials indicate towards the fact that anti-angiogenic therapy must be combined with cytotoxic treatment to obtain maximal efficacy. Yet there remains a lack of clarity about optimization of such drug combinations. Here we tend to investigate if inhibition of VEGFR2 in tumor microenvironment can promote normalization of tumor vasculature and improves the delivery and efficacy of a targeted cytotoxic drug in NSCLC. PTK787 (ZK 222584) and ZD6474 are potent inhibitors of VEGFR tyrosine kinases, PDGFR beta tyrosine kinase and c-Kit whereas ZD6474 additionally targets EGFR and RET. Imaging tumor vessel normalization induced by prudent anti-angiogenic agents PTK787 and ZD6474 were used to improve drug delivery of targeted compounds as erlotinib and GDC0941. Here I present my work that has been published in [117] along with some additional results.

Materials and Methods:

Cell lines and reagents

NSCLC cell lines H1975 and PC9 were purchased from the American Type Culture Collection (ATCC) and European Collection of Cell Cultures (ECACC)

respectively. Both cell lines were maintained in RPMI-1640 medium enriched with 10% FCS and 1% Penicillin+Streptomycin. ZD6474, PTK787, erlotinib were purchased from LC labs and GDC0941 from Axon Medchem. Compound stocks were stored at -20°C and dissolved in DMSO in vitro. For animal therapy ZD6474 and PTK787 were dissolved in sterilized, deionized water with 1% tween-80 at a concentration of 10mg/ml. Erlotinib was dissolved in 6% Captisol® (CyDex Inc., USA) at a concentration of 9mg/ml. GDC0941 was dissolved in MCT (0.5% methylcellulose with 0.2% Tween-80 in distilled water) at concentrations of 22.5mg/ml (monotherapy) and 15mg/ml (in combination with anti-angiogenic therapy). All solutions were stored on a rotating device at 4°C.

Western blotting

Western blotting was performed as described previously [118]. For Western blotting the following antibodies were used: ß-actin (clone C4) (MPBiomedicals LLC, USA), pEGFR, pAKT (S473), pERK (Cell Signaling Technology, USA), anti-rabbit-HRP- and anti-mouse-HRP-antibody (Millipore, Germany).

Immunofluorescence

Vascular leakage was assessed by i.v. injection of 0.1 ml 10 mg/ml FITC-dextran (200,000 kDa) from Sigma. After 30 min mice were anesthetized followed by perfusion with 4% paraformaldehyde injected into the aorta via an incision in the left ventricle and washed one time with PBS. Blood and fixative were allowed to pass out via the right atrium. Tumor sections were collected and immersed in 30% sucrose solution until samples dropped to the bottom of the

vials. A cold bath was prepared with dry ice and methanol. Tissue Tek wells were labeled and filled up with Jung tissue freezing medium (Leica Biosystems, Germany). Excess sucrose was removed from tissues and placed in the centre of wells and frozen by floating them on the methanol bath. Blocks were stored at -20°C and sliced at 10 to 20μm on cryostat. Slides were dried at room temperature for at least 2 hours and stained with anti-mouse CD31 (1:25, BD Pharmingen, Germany), anti-pVEGFR2 (1:300, Cell Signaling Technology, USA), fixed and processed for analysis in a Biorevo (Keyence) BZ-9000 microscope.

Tumor samples and immunohistochemistry

All tumors were stored in 4% paraformaldehyde overnight and transferred to PBS. Tissues were embedded in paraffin following standard protocol and stained with primary antibodies: mouse CD31 (1:25, BD Pharmingen), cleaved Caspase3 (1:750, Cell Signaling), pAKT (1:25, Cell Signaling) and alpha smooth muscle actin α-SMA (1:50) (Abcam) for marking pericytes. Corresponding secondary antibody detection kits for reduced background on murine tissue were used (Histofine Simple Stain Mouse MAX PO, medac) and stained on an automated stainer (LabVision Autostainer 480S, Thermo Scientific).

Xenograft experiments

All animal procedures were approved by the local animal protection committee and the local authorities (Bezirksregierung Cologne). 8 weeks old healthy *nu/nu* athymic male mice weighing 30g in an average were purchased from Janvier, Europe. Tumors were generated by s.c. injection of PC9 and H1975 cells (5×10^5

cells/tumor). Tumor-bearing mice were treated by oral gavage with the following set ups: PTK787 or ZD6474 75mg/kg daily as monotherapy, erlotinib 30mg/kg daily as monotherapy, GDC0941 75mg/kg daily as monotherapy, vehicle, erlotinib 30mg/kg or GDC0941 50mg/kg pretreated with PTK787 and continued as monotherapy during indicated timespan. The size of tumors ranged between 70 mm³ and 125 mm³. Monotherapy and vehicle of each drug was used as control. Tumor volume was recorded accordingly.

$[^{15}O]H_2O$ / $[^{18}F]FLT$ Positron Emission Tomography (PET) imaging:

Animals bearing macroscopic tumors were investigated on day 0 followed by start of treatment with PTK787 75mg/kg or ZD6474 75mg/kg daily, day 4, day 8 and day 18 using a FOCUS microPET scanner (Siemens Microsystems, Inc., Knoxville, TN, max. transaxial resolution 1.3mm). In total, 25 animals underwent $[^{15}O]H_2O$ and $[^{18}F]FLT$ imaging, each animal carried 3 tumors. The PTK787-treated group contained 15 animals, the vehicle treated group 10 mice. All animals underwent PET imaging at 4 different time points. We calculated percentage changes in tracer uptake with day 0 as baseline for each time point and tumor. $[^{15}O]H_2O$ PET imaging was performed before $[^{18}F]FLT$ PET. $[^{18}F]FLT$ PET was measured one hour after $[^{15}O]H_2O$ PET. $[^{15}O]H_2O$ was injected dynamically via tail vein and PET images were acquired for 2 min. after injection of 400 µCi/mouse. $[^{18}F]FLT$ was administered i.v. (200 µCi/mouse). PET imaging was performed 60 min. after injection [119]. Data evaluation was performed using in-house VINCI software. Data evaluation was based on a region of interest (ROI) analysis. For data analysis we used the maximal and the mean voxel

radioactivity of the defined ROI within the tumors. The mediastinum was chosen as a reference for determination of uptake ratio, since we observed constant uptake for $[^{18}F]FLT$ in this region. The heart was used as reference for calculation of the $[^{15}O]H_2O$ perfusion. All data were decay corrected.

Mass spectrometry

For absolute quantification of erlotinib and OSI-420 in positive ESI MRM (multi reaction monitoring) mode, an Acquitiy UPLC / Xevo™ TQ (Waters) with MassLynx and absolute quantification TargetLynx (Waters) were used. An Acquity UPLC BEH C18 1.7 µm, 2.1 x 50 mm column was used at 25°C. Solvent A was 0.1% formic acid (Biosolve) and B acetonitrile (Biosolve). A linear gradient from 95% A to 5% in 4.10 min at a flow rate of 0.4 ml/min was used. The following MRM transitions were used for erlotinib m/z 394.03 $(M+H^+)^+$ to 277.95 (quantifier), m/z 394.03 to 303.95 (qualifier), m/z 394.03 to 335.94 (qualifier), for OSI-420 m/z 380.03 to 277.85 (quantifier), m/z 380.03 to 249.89 (qualifier), m/z 380.03 to 321.93 (qualifier). All compounds were freshly prepared during 2 months and dissolved in 0.1% Formic acid (Biosolve) prepared with 0.22 µm MilliQ-Water. With erlotinib eluting at 2.94 min a standard calibration curve was calculated using following concentrations: 0.2, 0.5, 1, 5, 20, 50, 150, 300, 500, 750 ng/ml (prepared individually from stock solutions 100 µg/ml). With OSI-420 eluting at 2.51 min a standard calibration curve was calculated using following concentrations: 0.1, 0.5, 1, 2, 4, 6, 8, 10 ng/ml (prepared individually from stock solutions 100 µg/ml). Correlation coefficient: r < 0.990; response type: external standard, area; curve type linear;

weighting 1/x. The peak integrations were corrected manually, if necessary. Quality control standards of each standard were used during sample analysis and showed between 0.5% and 40% deviation respectively. Blanks after the standards, quality control and sample batch proved to be sufficient. No carry over was detected.

Statistics

Fisher's exact tests were performed using R version 2.7.1 (http://www.r-project.org). Data are presented as mean ±SD in all figure panels where error bars are shown. A level of significance of $p < 0.05$ was chosen (where mentioned).

Results:

Prudent anti-angiogenic treatment induces a time window of improved blood perfusion into the tumor.

In established human NSCLC cell line PC9 xenografts PTK787 treatment improved tumor blood flow after four days of treatment by 12% (n=45 where n represents total number of tumors), as determined by $[^{15}O]$-water PET ($[^{15}O]H_2O$; **Figure 19A, right panel, Figure 19B**). A steady increase in tumor blood flow by 33.58% (n=45) was measured until day 8 of treatment with PTK787 (p-value<0.001) probably mediated by a transient normalization of vessels followed by a sharp decrease of 17.23% (n=45) till day 18. In contrast, blood flow decreased consistently from day 4 to day 8 by 20.42% (n=30) and by 30.75% (n=30 where n represents total number of tumors) until day 18 in the vehicle-treated tumors (**Figure 19A, left panel, Figure 19B**). To explicate if improvement in blood flow can be also achieved by using other anti-angiogenic agents we used a dual VEGFR/EGFR inhibitor ZD6474 in H1975 xenografts which are resistant to EGFR inhibition due the presence of T790M gatekeeper mutation of EGFR. There was an increase in blood flow by 21.39% from day 0 to day 8 of ZD6474 treatment followed by a drop of 20.95% from day 0 to day 18 (**Figure 20A, right panel, Figure 20B**). Vehicle-treated tumors displayed a stable decrease in blood flow by 8.95% from day 0 to day 8 and by 14.78% on day 18 (**Figure 20A, left panel, Figure 20B**).
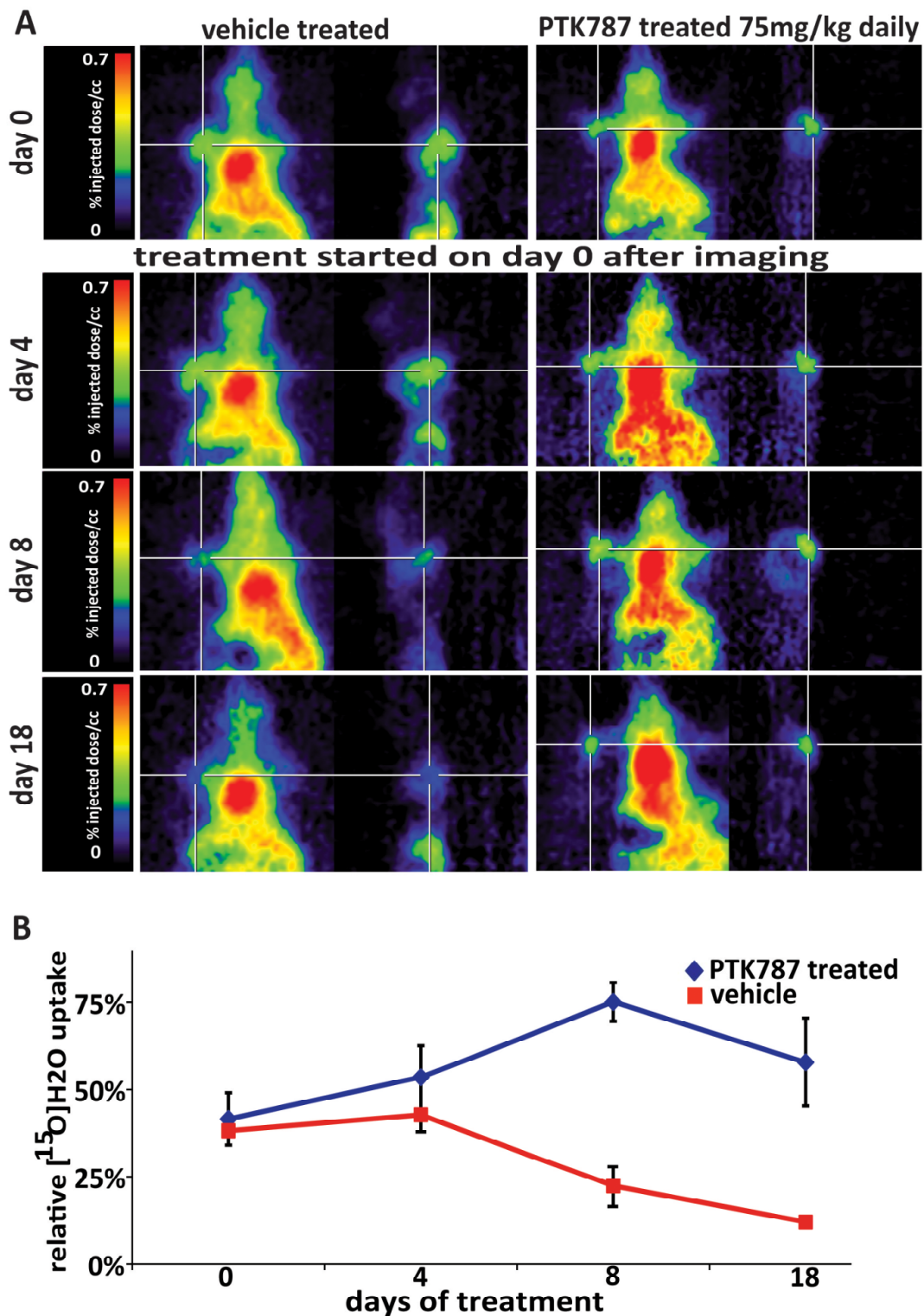
Figure 19: Multimodal imaging of tumor blood flow with [^{15}O]H$_2$O PET in PC9 xenografts using PTK787 as anti-angiogenic agent
 A. PET imaging was performed on nude mice with macroscopic subcutaneous tumors on day 0 (before start of therapy) and at the indicated time points after treatment with vehicle **(A, left panel)** and PTK787 **(A, right panel)**. **B.** Quantitative analysis of tumor blood perfusion before (day 0) and after 4, 8, 18 days of PTK787 treatment compared to vehicle sets.

Figure 20: Multimodal imaging of tumor blood flow with [¹⁵O]H₂O PET in H1975 xenografts using ZD6474 as anti-angiogenic agent.
A. PET imaging was performed on nude mice with macroscopic subcutaneous tumors on day 0 (before start of therapy) and at the indicated time points after treatment with vehicle (A, left panel) and ZD6474 (A, right panel). **B.** Quantitative analysis of tumor blood perfusion before (day 0) and after 4, 8, 18 days of ZD6474 treatment compared to vehicle sets.
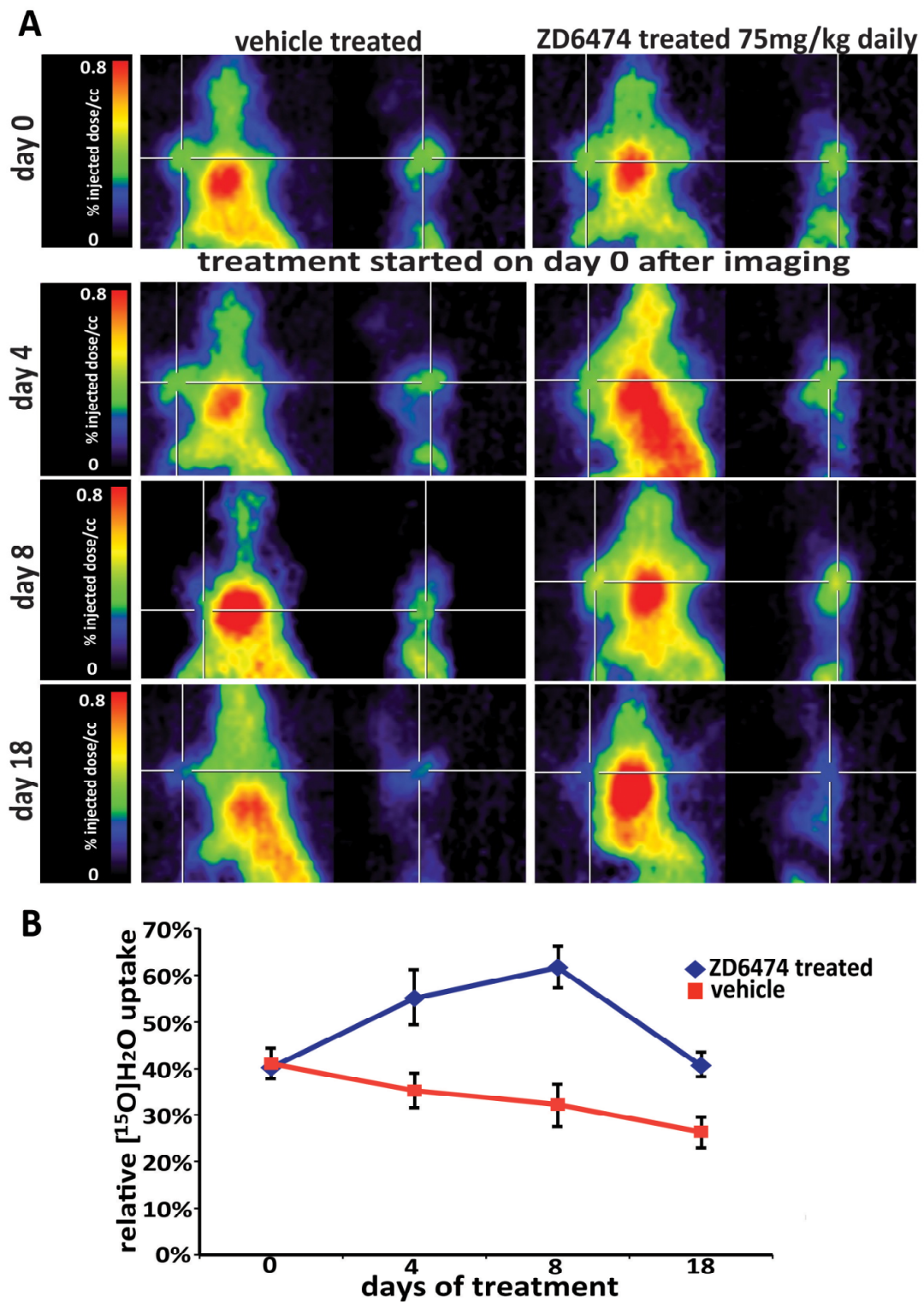
Simultaneously, during PTK787 therapy, uptake of [^{18}F]FLT, a marker of proliferation increased by 51.08% (day 0 to day 4) (n=30) and by 76% (day 0 to day 8 (n=30) (**Figure 21A,B,C**) suggesting that the cells continued to progress through the cell cycle. Proliferation remained unaffected also under ZD6474 therapy as measured by an increase in [^{18}F]FLT uptake by 67.1% (day 0 to day 4, n=30) and by 78.02% (day 0 to day 8, n=30) (**Figure 21D,E,F**).
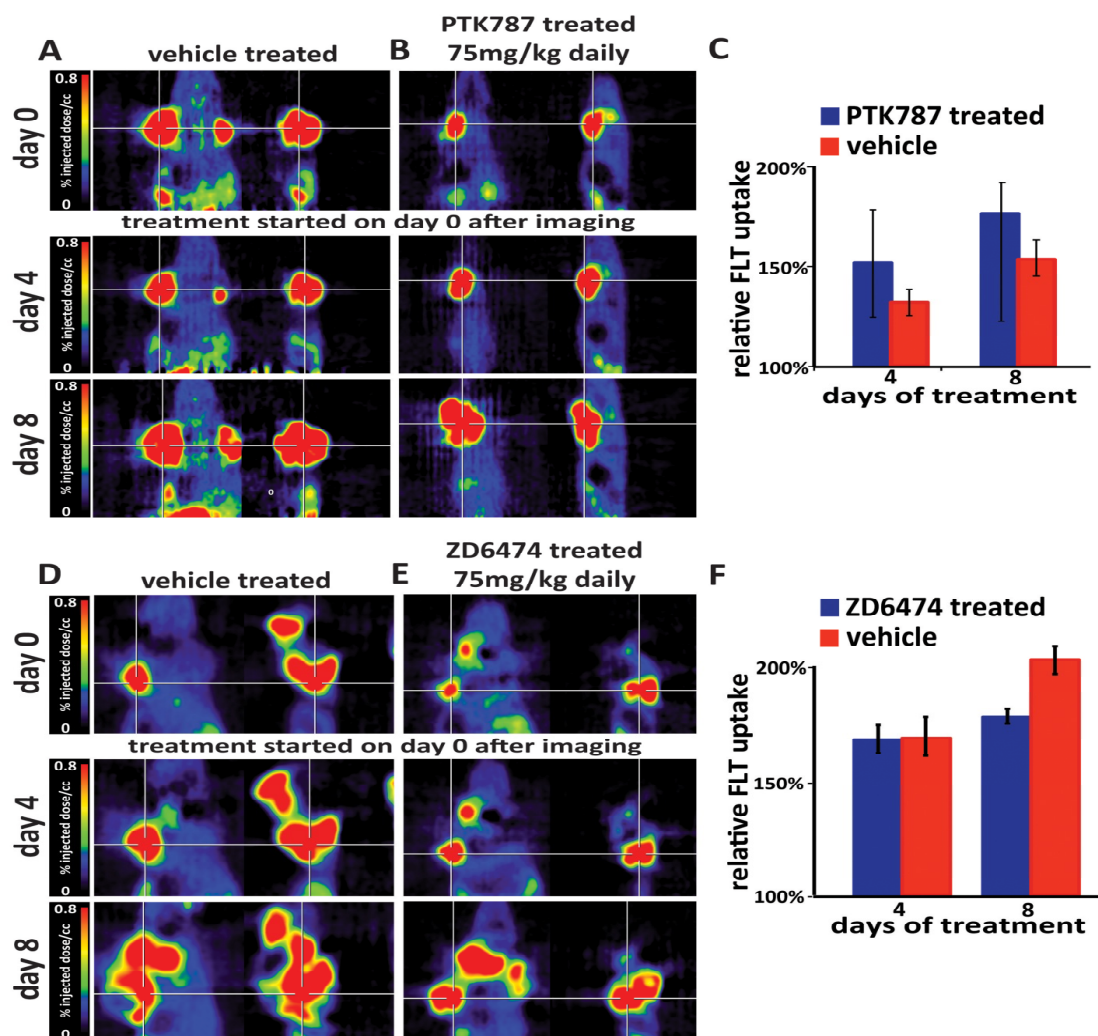

Figure21: Imaging of tumor cell proliferation using [^{18}F]FLT PET in PC9 and H1975 tumors.
Imaging of tumor cell proliferation using [^{18}F]FLT PET was performed on nude mice with macroscopic subcutaneous tumors PC9 **(A,B)** and H1975 **(D,E)** on day 0 (before start of therapy) and at the indicated time points after treatment with vehicle **(A,D)** and PTK787 **(B)** / ZD6474 **(E)**. Quantitative analysis of tumor cell proliferation before (day 0) and after 4 and 8 days of PTK787 treatment **(C)** / ZD6474 treatment **(F)** compared to vehicle sets.

These data indicate that prudent anti-angiogenic treatment induces a short-lived time window of about one week when tumor vessels are transiently normalized which can be monitored by an increase in blood into the tumor.

Short-time anti-angiogenic therapy reduces leakiness by improving pericyte coverage in tumor blood vessels in xenografts.

To elucidate if the improved blood flow into the tumors was indeed due to vessel normalization, permeability of the blood vessels were examined by fluorescence microscopy after tumor-bearing animals were perfused with FITC-dextran. Blood vessels of vehicle-treated tumors were dilated with haphazard morphological pattern and displayed extensive leakiness associated with massive extravasation of FITC-dextran in tumors from different mice (**Figure 22A,B, left panel,**) and correlated with high expression of CD31 and pVEGFR2 (**Figure 22A, left panel**). However, in tumors that were treated with PTK787 for four days blood vessels showed strikingly reduced leakiness with minimum extravasation of FITC-dextran (**Figure 22A, 22B, right panel**) supported by eight fold reduction in signal intensity (**Figure 22C**) accompanied by diminished CD31 and pVEGFR2 expression. (**Figure 22A, right panel**). Tumor vasculature was characterized by abnormal and discontinuous pericyte lining of vessels as indicated by arrows on day 0 (**Figure 22D**). 4 days of anti-angiogenic therapy transiently improved pericyte coverage in contrast to vehicle-treated tumors which still exhibited incoherent pericyte lining (**Figure 22D,E**). However, the number of blood vessels decreased remarkably in both control and treated tumors over 18 days of PTK787 treatment (**Figure 22D**).
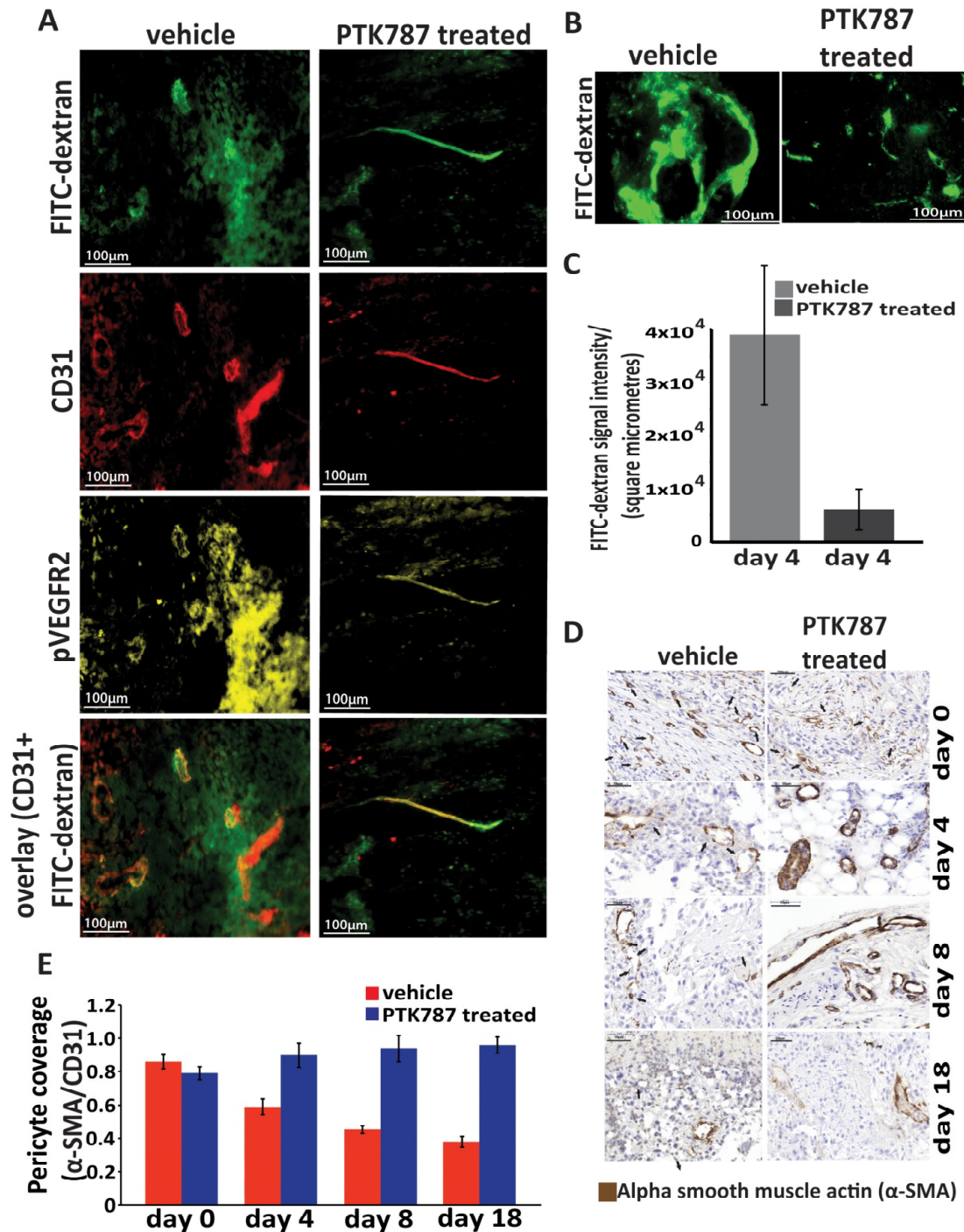
Figure 22: Blood vessel morphology and permeability
A,B. Vascular leakage was assessed by i.v. injection of 0.1 ml 10 mg/ml FITC-dextran (200,000 kDa). 10 to 20μm thick slices of perfused tumors were stained with anti-mouseCD31 and anti-pVEGFR2 antibody: control set **(A,B left panel)** and PTK787-treated tumors **(A,B right panel)**. **C.** Signal intensity of the total area of green staining (FITC-dextran) was quantified (four fields per tumor in both control and PTK787 treated groups). **D.** Histology of tumors stained for α-SMA (brown, pericytes) comparing untreated vasculature **(D, left panel)** with PTK787 sets **(D, right panel)**. **E.** Pericyte coverage was quantified (fraction of area covered) using four random fields from each tumor on day 0, day 4, day 8 and day 18 of PTK787 treatment or vehicle.

Anti-angiogenic treatment improves cytotoxic therapeutic outcome in NSCLC with enhanced delivery of erlotinib into the tumor.

To investigate if augmented blood flow induced by short-term anti-angiogenic treatment had any improved therapeutic efficacy in NSCLC, mice bearing macroscopic PC9 tumors were treated by an oral gavage of PTK787 (75mg/kg daily) for 1 week. Since water PET data indicated that tumor blood flow improves within a span of 7 days of anti-angiogenic therapy, erlotinib treatment was started within this 'Normalization window' from day 4 onwards and continued as monotherapy for 13 days. Mice receiving erlotinib therapy pretreated with PTK787 had a sharp initial increase in tumor volume from 100% on day 1 to 221.28% on day 4 followed by a massive reduction to 45.63% on day 7 and to almost complete shrinkage of tumor after 16 days of treatment (9.14% of original mass left) **(Figure 23A)**. Erlotinib as monotherapy restricted tumor proliferation resulting in a slow reduction (up to 50% of tumor mass) but not as strong as with intermittent PTK787 treatment (p-value<0.001) **(Figure 23A)**. There was no further shrinkage in tumor volume, which resulted in a stable disease. PTK787 monotherapy and vehicle treatment resulted in similar outcome with an increase in tumor volume to 245% and 220% respectively on day 4 **(Figure 23A)**.

To check if the normalized blood vessels were effectively delivering drugs into the tumors, erlotinib concentration within the tumor was measured via mass-spectrometric analysis. In tumor lysates from monotherapy sets with erlotinib, there was a slight improvement of the drug uptake into the tumor from day 1 (start of treatment) to day 4 by 20% **(Figure 23B)**. In contrast, tumors

pre-treated with PTK787 for 4 days displayed an improved erlotinib uptake by 140% on the first day of erlotinib treatment (day 4), which increased up to 160% on day 8 **(Figure 23B)**. Monotherapy sets showed reduction in erlotinib uptake by 42% on day 8 **(Figure 23B)** indicating towards a hindered delivery of the drug within the tumor.

Western blot analysis of lysates from tumors treated with different set-ups of PTK787 and erlotinib showed an time-dependent reduction in pEGFR signal from day 1 to day 4 corresponding to pAKT and pERK levels in the sets which received erlotinib pretreated with PTK787 **(Figure 23C)**. There was no change in signal intensity of pEGFR, pAKT or pERK in the vehicle or monotherapy sets (PTK787 alone or erlotinib alone) on day 1 **(Figure 23C)**. Western blot results correlated with histology where Ki67 positive cells were strongly reduced in PTK pretreated tumors receiving erlotinib on day 1 compared to tumors receiving erlotinib as monotherapy on day 1 (**Figure 23D**). Control tumors had a strong positive staining for Ki67 positive cells (**Figure 23D**). In PTK pretreated tumors receiving erlotinib, Ki67 positive cells continued reducing further in number from day 1 to day 4 until only a few Ki67 positive cells were left on day 8 (**Figure 23D**).
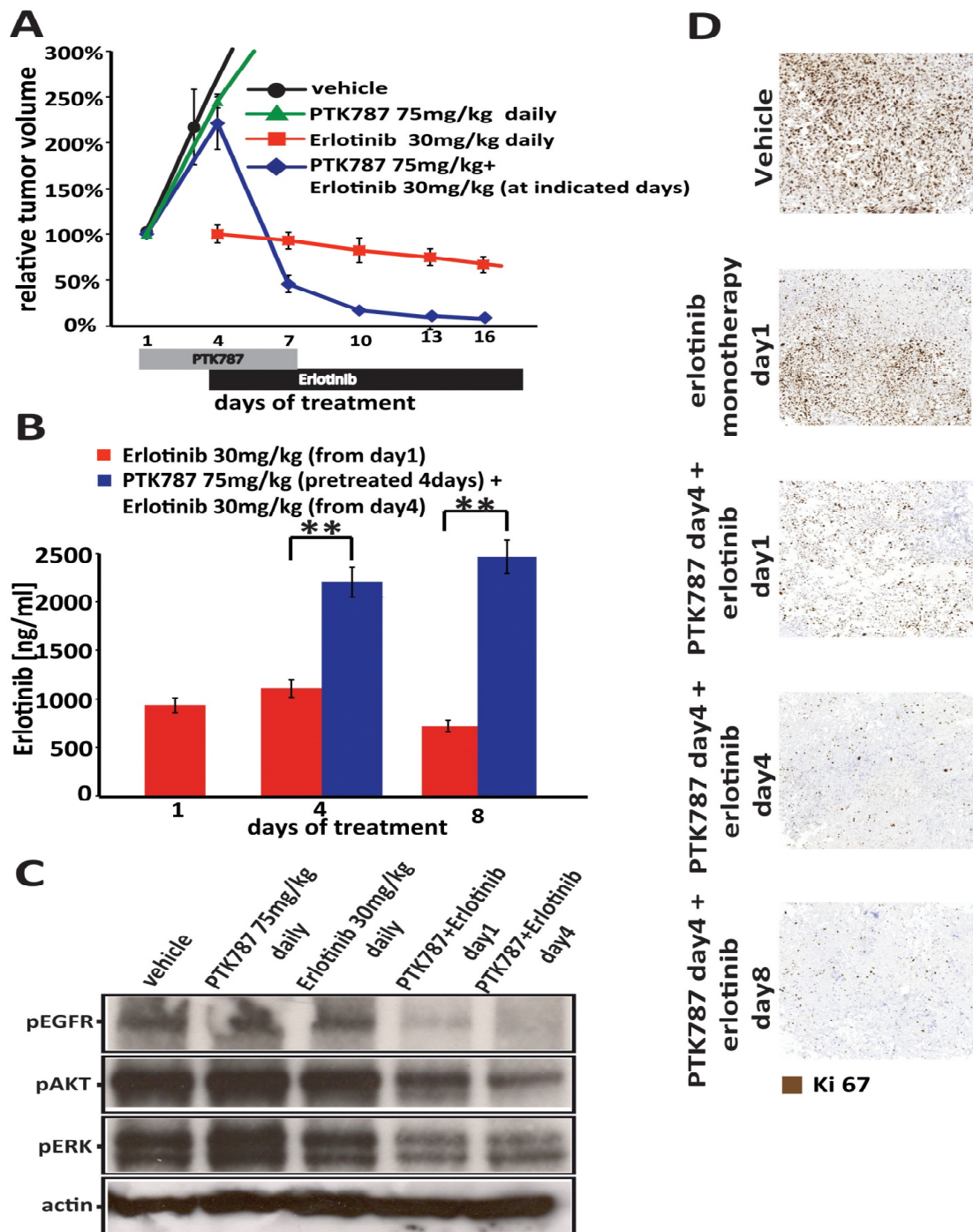
Figure 23: Prudent anti-angiogenic treatment improves delivery of erlotinib into the tumor and promotes therapeutic outcome

A. Tumor volumes in nude mice were recorded over time under treatment with PTK787 (75mg/kg), erlotinib (30mg/kg) and PTK787 (75mg/kg) + erlotinib (30mg/kg) and vehicle control at indicated days. **B.** Quantification of erlotinib uptake as measured by Mass-Spectrometry in PTK787 pre-treated tumors (blue column) between day 4 and 8 compared to uptake in the tumors receiving erlotinib just as monotherapy (4 independent tumors from different mice per set up). **C.** Tumor lysates from different therapy modules (as indicated) were immunoblotted with phospho-specific antibodies. Representative western blots are shown. **D.** Tumors under different treatment conditions were explanted on days mentioned and stained for Ki67 positive cells.

Histology results also showed complete inhibition of pAKT from day 0 to day 4 in PTK787 pretreated tumors receiving erlotinib **(Figure 24A)**. pAKT levels remained inhibited on day 8 with induction of necrosis **(Figure 24A)**. Even though tumor cells were healthy in both sets on day 0 **(Figure 24A),** heavy induction of apoptosis (cleaved caspase 3) was detected in tumors receiving erlotinib pretreated with PTK787 on day 4 **(Figure 24B)** which remained consistent till day 8 **(Figure 24B).** However, in erlotinib monotherapy sets displayed only moderate induction of apoptosis overtime **(Figure 24B)**.

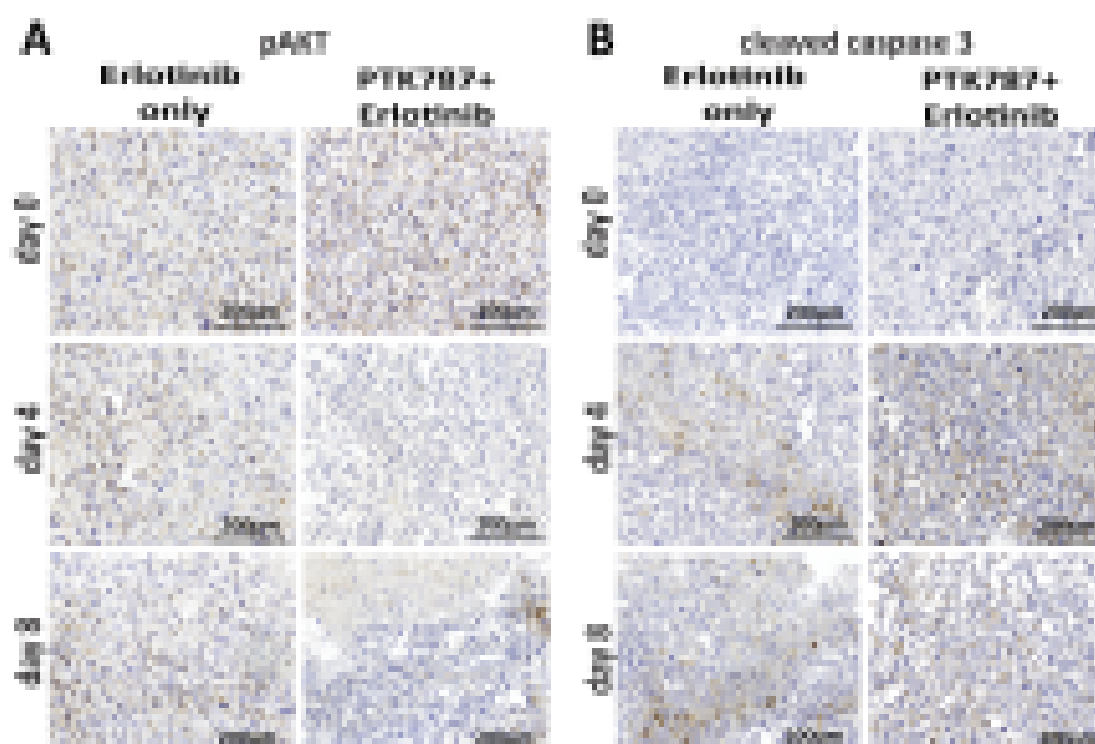**Figure 24: Erlotinib therapy pretreated with PTK induces strong pAKT inhibition and apoptosis in vivo**
A,B Histology of tumor samples from **23C** comparing pAKT expression **(A)** and induction of apoptosis (cleaved caspase 3) **(B)** in the same tumor samples between erlotinib monotherapy and erlotinib pre-treated with PTK787 tumors on day 0 (before start of treatment) and on indicated days after therapy

To confirm that this effect of tumor shrinkage was only due to better drug delivery facilitated by prudent anti-angiogenic treatment, macroscopic H1975 tumor-bearing mice pretreated with PTK787 were treated with PI3K kinase inhibitor GDC0941. Tumors receiving GDC0941 therapy pre-treated with PTK787 receded by 50% over 28 days compared to a mild growth-inhibition in GDC0941 monotherapy sets which tumor volumes surpassed by 250% on day 22 **(Figure 25)**. PTK787 monotherapy and vehicle treatment resulted in similar outcome with an increase in tumor volume over 250% on day 4 **(Figure 25)**.
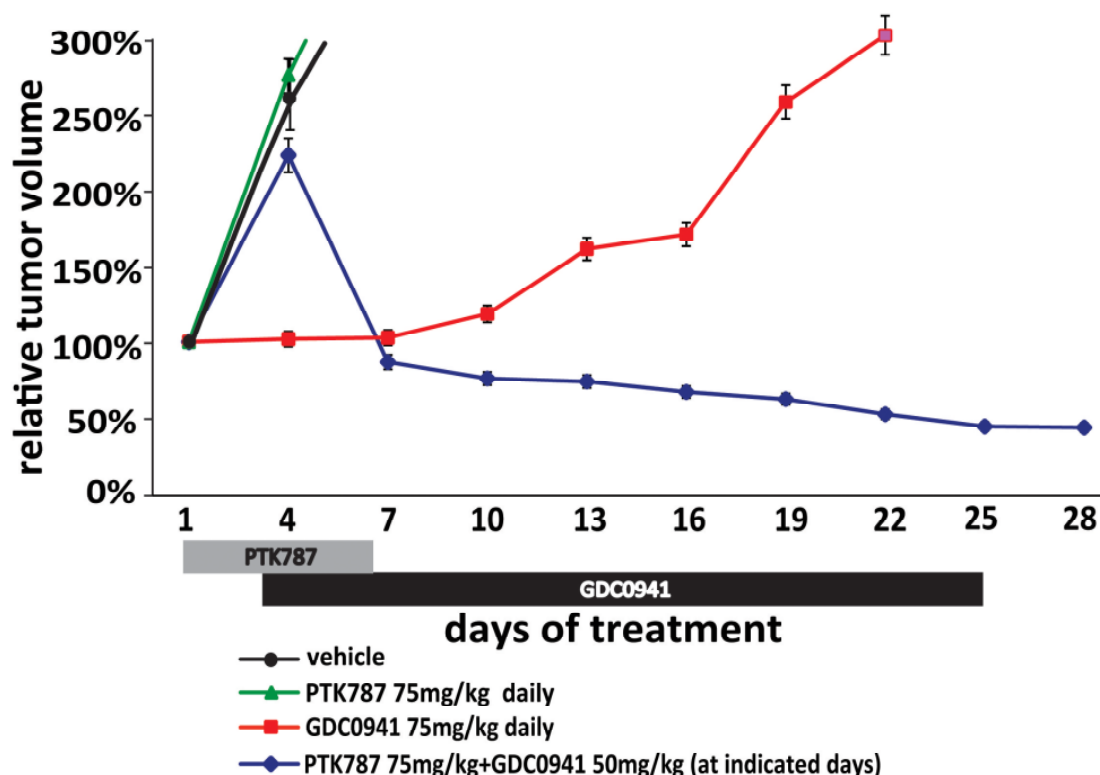

Figure 25: Short anti-angiogenic treatment improves therapeutic outcome of GDC0941 in vivo
PC9 cells were engrafted s.c. in nude mice and tumor volumes were recorded over time for 28 days under treatment with vehicle, PTK787 (75mg/kg), GDC0941 (75mg/kg) and PTK787 (75mg/kg) + GDC0941 (50mg/kg) at indicated days.

Intermittent anti-angiogenic treatment facilitates long-term tumor regression

A long-term xenograft study with subcutaneous PC9 tumors was performed where mice were treated with a continuous dose of erlotinib combined with a short PTK787 treatment every ten days. Tumors remained regressed in this combination model over the entire time span of 65 days **(Figure 26)**. However, in mice treated with erlotinib alone, there was an initial tumor regression up to 40% of original tumor volume until day 22 followed by a stable disease **(Figure 26)**.
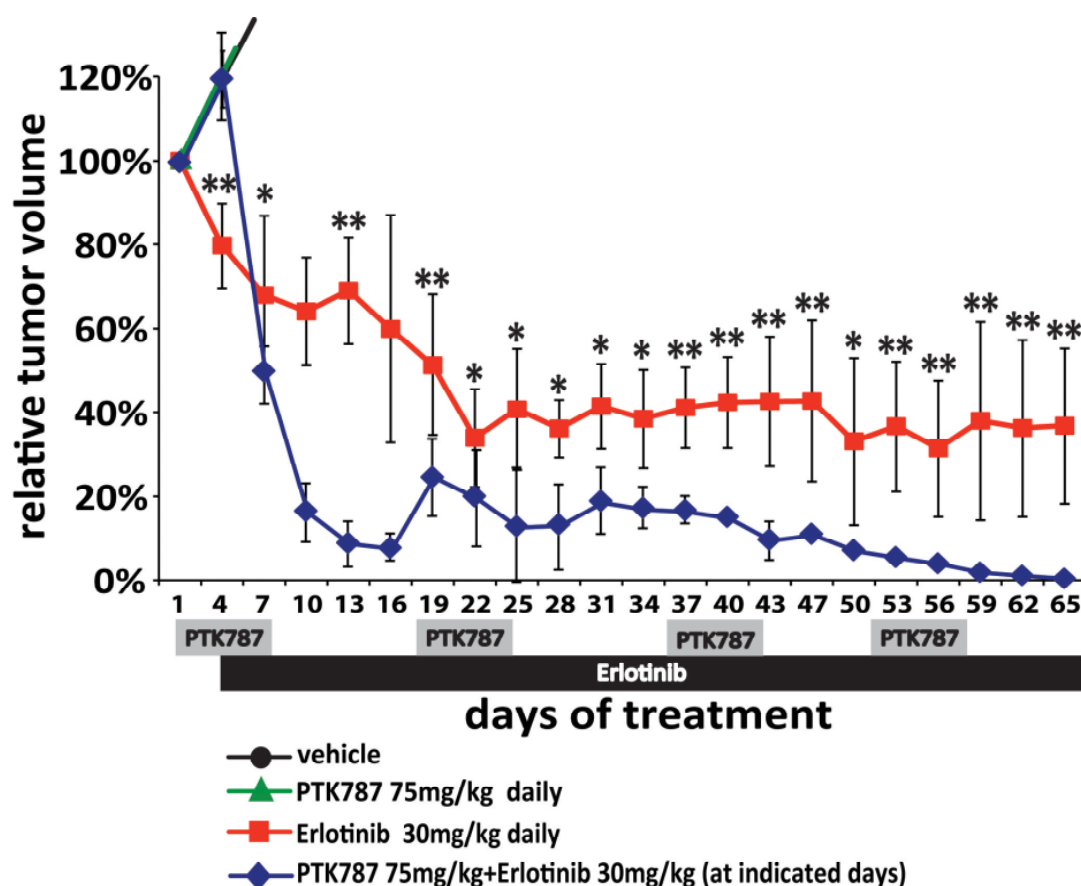

Figure 26: Intermittent anti-angiogenic therapy also promotes long-term tumor regression
PC9 cells were engrafted s.c. in nude mice and tumor volumes were recorded over time for 65 days under treatment with vehicle, PTK787 (75mg/kg), erlotinib (30mg/kg) and erlotinib (30mg/kg) with intermittent PTK787 treatment from day 1 to day 7, day 17 to day 25, day 35 to day 43 and day 51 to day 58.

Concluding remarks

Using $[^{15}O]H_2O$ Positron Emission Tomography (PET) imaging in a preclinical model of non small cell lung cancer we showed that short-term treatment with anti-angiogenic agents (PTK787/ZD6474) licensed a transient window of improved tumor blood perfusion. Initiation of cytotoxic treatment in this window of vessel normalization resulted in increased efficacy, as illustrated by improved outcome of erlotinib and GDC0941 therapy after initial anti-angiogenic treatment.
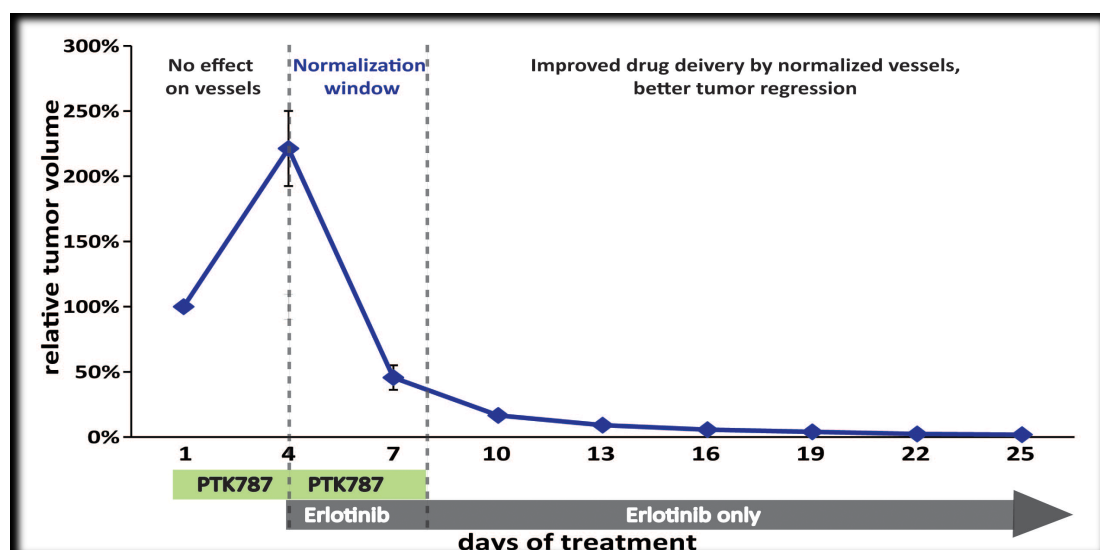
In summary, our findings are consistent with the vascular normalization hypothesis and offer strong evidence that prudent anti-angiogenic therapy leads to evanescent vessel normalization resulting in better cytotoxic therapeutic outcome. From this study it is tempting to speculate that optimized cytotoxic treatment starting with the 'normalization time frame' may provide maximum survival advantage in advance NSCLC patients.

6. Discussion

Considerable advances have been made to untangle the complex molecular mechanism that underlies tumor development from neoplasic lesions. Majority of solid tumors exhibit an aberrant vasculature afflicted with structurally and functionally abnormal vessels in response to excessive production of pro-angiogenic factors by the tumor [87]. The hypothesis of inhibiting tumors by destroying tumor vasculature has been speculated to yield satisfactory results in treating cancer. This has driven tremendous advances in the field of targeted therapies including anti-angiogenic agents such as bevacizumab (BV) as well as anti-VEGF receptor tyrosine kinase receptors (TKIs). However, clinical tools to predispose patients towards particular targeted therapeutic regimens have been lacking till date and results from clinical trials have been moderate or unsatisfactory or contradictory. This has triggered some important questions such as: why just some subsets of patients respond to anti-angiogenic therapy, some not at all and just a partial response is seen in other cases? Is the mechanism of action of the drug same in patients as deciphered in pre-clinical models? Why do tumors occasionally develop resistance to anti-angiogenic therapy? What additional pathways should be co-targeted with anti-angiogenic therapy to achieve maximum tumor regression and prolong survival? How to optimize drug scheduling and dosage to reach paramount drug efficacy without increasing toxic side effects? Could the overall survival in patients be improved beyond a few months? One of the biggest challenges to answer these questions is the lack of validated biomarker/s for

preselecting cancer patients who might benefit from anti-angiogenic therapy. Biomarkers can be classified into:

prognostic: biomarker that provide information about the likely outcome of cancer in patients irrespective of therapy [120, 121]

predictive: biomarker that provides information in advance of therapy about likely benefit of patients (in terms of tumor shrinkage or survival) from specific treatment [120, 122],

pharmacodynamic: a biomarker that is a measure of altered expression of a molecular target in response to a certain therapy [123, 124] and

surrogate: a biomarker used as a substitute for a clinically meaningful endpoint, which is a direct measure of how the patient feels, functions or survives [125].

Successful development and application of tyrosine kinase inhibitors largely depend on the predictive biomarkers for patient selection. The most extensively studied biomarker in cancer research is VEGF. Contradictory studies have raised questions regarding association between initial VEGF levels in patients and the outcome of anti-angiogenic treatment. In advanced NSCLC, baseline plasma VEGF levels correlated directly to progression-free survival but only in patients with low baseline levels of circulating VEGF [126]. On the other hand high levels of circulating VEGF in patients with metastatic NSCLC did not predict progression-free survival inspite of correlating with improved overall response rate in a phase II/III trial [127]. These discrepancies in the results raise doubts about the potential of circulating VEGF as a predictive biomarker.

In my PhD thesis, we have identified a novel tumor cell autonomous VEGF:VEGFR2 feed-forward loop in NSCLCs expressing high levels of VEGFR2

leading to amplification of VEGF secretion. VEGF secretion is boosted by activation of HIF-1α, which is specific to mTORC1 and remain unaffected by the status of mTORC2 [128]. We observed that mTORC1 inhibition using rapamycin can reduce VEGF expression induced by VEGFR2. Thus our data strongly indicates that VEGF:VEGFR2 signaling cascade functions via VEGFR2-PI3K-mTOR signaling, inducing an mTOR dependent upregulation of VEGF. Our observation that knockdown of VEGFR2 in tumor cells alone was sufficient to almost abolish formation of tumors in vivo supports a model where tumor cell-autonomous activation of VEGF:VEGFR2 feed-forward loop is absolutely indispensable for tumor initiation, switching the balance towards pro-angiogenesis promoting sprouting of new vessels. Proliferation in tumor with high expressions of VEGF:VEGFR2 remained at basal levels confirmed by our finding that VEGFR2/mTOR inhibition activated IRS/MAPK signaling overtime [116, 129]. Interfering the VEGF:VEGFR2 signaling cascade in xenografts switched the tumor towards a proliferative phenotype inciting therapeutic dependency on MAPK signaling. Combined targeting of angiogenesis (VEGFR2) with ZD6474 and proliferation (MAPK) with PD0325901 in tumors having high expression profile of VEGF:VEGFR2 proved to be very effective in regressing tumor mass substantially. In contrast, VEGF:VEGFR2 feed-forward loop was not active in tumors with low VEGFR2 expression and they remained unaffected by the combined ZD6474 and PD0325901 therapy. Consistent with our pre-clinical model, high VEGFR2 expression in 20% of lung cancer patients correlated with highly angiogenic tumors. To summarize the first part of our study, NSCLCs with high VEGFR2 expression exhibit highly angiogenic phenotype. Knockdown of

VEGFR2 or inhibition with anti-angiogenic therapy results in massive reduction of mTOR, VEGF and microvessels (CD31) simultaneously activating proliferative pathway via MAPK signaling as an escape mechanism. Co-targeting MAPK pathway results in massive tumor shrinkage. Cumulatively from our findings, we propose high co-expression of VEGF:VEGFR2 on tumor cells as a predictive biomarker for selecting advanced NSCLC patients who can benefit from therapeutic efficacy of dual VEGFR2/MEK inhibition.

Our findings have prompted to the development of a 'Phase I/II clinical trial with vandetinib and selumetinib in advanced EGFR^{WT} Non Small Cell Lung Cancer patients with high VEGF:VEGFR2 expression profile'. This trial is currently ongoing at the University Hospital of Cologne under the leadership of Prof. Jürgen Wolf from the Centre of Integrated Oncology (CIO Köln Bonn) and Lung Cancer Group Cologne (LCGC).

Tumor regression in response to anti-angiogenic therapies is often transitory owing to excessive pruning of vessels, increase in invasiveness due to elevated hypoxia within the tumor or due to intrinsic or acquired resistances to those particular agents. These adverse effects of anti-angiogenic therapy have lead to the concept of 'vascular normalization' rather than destruction using prudent anti-angiogenic treatment. Judicious administration of anti-angiogenic therapies has been shown to heal leakiness, reduce vascular permeability and interstitial fluid pressure improving pericyte coverage [96, 130, 131]. Several potential targets and drugs have been described to improve functionality of tumor vessels for example apricoxib, a Cox-2 inhibitor enhances maturity of tumor blood vessels [132]. Another study showed that dopamine could improve

activity of vessels by upregulating angiopoetin-1 and Krüppel-like factor-2 [131]. This might result in effective drug delivery within the tumor potentially sensitizing the cells to cytotoxic therapies and / or improving survival [96, 130, 133, 134]. Thus the inducers of vascular normalization can serve as potential biomarkers. Response monitoring in advanced NSCLC is complicated given that anti-angiogenic therapy does not lead to tumor shrinkage. Nowadays dynamic contrast-enhanced (DCE) MRI and PET are used in preclinical models and in clinic for non-invasive visualization and assessment of tumor response depending on the tracer types [135-137]. Tumor blood flow can be meticulously measured by $[^{15}O]$ H_2O flow which is a freely diffusible perfusion tracer. Even though $[^{15}O]$ H_2O PET has not been so frequently used in clinical study, subtle effects on tumor blood perfusion can be detected using $[^{15}O]$ H_2O PET making it as aspiring imaging technique [138].

Using $[^{15}O]$ H_2O PET imaging we have validated that prudent anti-angiogenic treatment with PTK787 improves blood flow in the tumor in vivo. Targeting VEGFR2 in the tumor microenvironment with PTK787 transiently normalized vasculature enhancing delivery and distribution of cytotoxic drugs like erlotinib into the tumors resulting in significant tumor regression. Improvement in tumor shrinkage is consistent with the notion that higher-dose EGFR-targeted drug exposure yields to more effective target inhibition [139]. Recent reports from Rakesh Jain indicate towards the fact that VGFE:VEGFR2 inhibition-induced vessel normalization effect is time and dose dependent [78, 140]. Applying $[^{15}O]$ H_2O PET imaging we could decipher the brief time frame during which tumor vasculature become normalized. PTK787 treatment created

a time window, which lasted atleast 8 days during which tumor blood flow improved, followed by a decline till day 18 of treatment. Similar results were obtained using ZD6474, which prompted normalization window to set in by increasing tumor blood perfusion from day 4 to day 8 followed by steady decrease in blood flow. ZD6474 is a tyrosine kinase inhibitor that primarily targets VEGFR2 and EGFR. However, since we used H1975 in this case, which are resistant to EGFR inhibition, the ZD6474 mediated effect on tumor vasculature can be attributed to inhibition of VEGFR2. Our findings strongly support the concept that tumor vascular normalization by anti-angiogenic therapy is time dependent. It has been shown that treatment with low doses of DC101 (an antibody against VEGFR2) can improve pericyte coverage in a preclinical model of breast cancer [141]. Our findings uniformly signify that the principal target to induce vascular normalization is probably VEGFR2, which might serve as a predictive biomarker of vascular normalization. However, vascular normalization effect seems to be transient as continued anti-angiogenic therapy with PTK787 or ZD6474 resulted in a deterioration of tumor blood flow beyond 8 days of treatment as visualized by our $[^{15}O]$ H_2O PET imaging. Considering that vessels remain well fortified only until day 8 of anti-angiogenic treatment, we decided to take this time frame as the 'normalization window' as a starting point of cytotoxic therapy. Implication of $[^{15}O]$ H_2O PET guided pretreatment with PTK787 and ZD6474 significantly improved the delivery and therapeutic efficacy of cytotoxic compounds erlotinib and GDC0941. Our data consolidate the benefit of using $[^{15}O]$ H_2O PET imaging in clinical studies to monitor tumor blood flow as a precise pharmacodynamic marker for vascular

normalization. Cytotoxic agents combined with anti-angiogenic therapy has shown mixed outcome in the clinic. Bevacizumab treatment in glioblastoma patients with high and stable perfusion receiving chemotherapy had significantly increased progression free and overall survival [100]. A Phase III study involving NSCLC patients receiving chemotherapy with bevacizumab displayed significant survival benefit over the chemotherapy group [142]. Still, there are some controversies and challenges that should be clarified before cancer therapy by vessel normalization can be clinically implicated. In a recent human study there was a rapid reduction of blood perfusion and docetaxel uptake in NSCLC after patients were administered with bevacizumab for four days [143]. In another Phase III trial, addition of bevacizumab to chemotherapy in newly diagnose GBM did not improve overall survival. This study is confirmed by our PET data that vascular normalization is only transient and continuous dosing of anti-angiogenic compounds can result in a reduction in tumor blood flow. In summary, our data strengthen the fact that prudent anti-angiogenic therapy leads to evanescent vessel normalization resulting in better drug delivery and therapeutic outcome. However, optimal designing of drug dosage and scheduling using [^{15}O] H$_2$O PET imaging are absolutely indispensable to achieve maximal clinical outcome.

7. References

1. Siegel R, Naishadham D, Jemal A: **Cancer statistics, 2013**. *CA Cancer J Clin*, **63**(1):11-30.
2. Herbst RS, Heymach JV, Lippman SM: **Lung cancer**. *N Engl J Med* 2008, **359**(13):1367-1380.
3. Sekido Y, Fong KM, Minna JD: **Progress in understanding the molecular pathogenesis of human lung cancer**. *Biochim Biophys Acta* 1998, **1378**(1):F21-59.
4. Uematsu K, He B, You L, Xu Z, McCormick F, Jablons DM: **Activation of the Wnt pathway in non small cell lung cancer: evidence of dishevelled overexpression**. *Oncogene* 2003, **22**(46):7218-7221.
5. Khuder SA: **Effect of cigarette smoking on major histological types of lung cancer: a meta-analysis**. *Lung Cancer* 2001, **31**(2-3):139-148.
6. Toh CK, Gao F, Lim WT, Leong SS, Fong KW, Yap SP, Hsu AA, Eng P, Koong HN, Thirugnanam A *et al*: **Never-smokers with lung cancer: epidemiologic evidence of a distinct disease entity**. *J Clin Oncol* 2006, **24**(15):2245-2251.
7. Robertson A, Allen J, Laney R, Curnow A: **The cellular and molecular carcinogenic effects of radon exposure: a review**. *Int J Mol Sci* 2013, **14**(7):14024-14063.
8. Schiller JH, Harrington D, Belani CP, Langer C, Sandler A, Krook J, Zhu J, Johnson DH: **Comparison of four chemotherapy regimens for advanced non-small-cell lung cancer**. *N Engl J Med* 2002, **346**(2):92-98.
9. Folkman J: **Angiogenesis: an organizing principle for drug discovery?** *Nat Rev Drug Discov* 2007, **6**(4):273-286.
10. Sholley MM, Ferguson GP, Seibel HR, Montour JL, Wilson JD: **Mechanisms of neovascularization. Vascular sprouting can occur without proliferation of endothelial cells**. *Lab Invest* 1984, **51**(6):624-634.
11. Folkman J: **Tumor angiogenesis: therapeutic implications**. *N Engl J Med* 1971, **285**(21):1182-1186.
12. Greenblatt M, Shubi P: **Tumor angiogenesis: transfilter diffusion studies in the hamster by the transparent chamber technique**. *J Natl Cancer Inst* 1968, **41**(1):111-124.
13. Rak J, Yu JL, Kerbel RS, Coomber BL: **What do oncogenic mutations have to do with angiogenesis/vascular dependence of tumors?** *Cancer Res* 2002, **62**(7):1931-1934.
14. Folkman J, Merler E, Abernathy C, Williams G: **Isolation of a tumor factor responsible for angiogenesis**. *J Exp Med* 1971, **133**(2):275-288.
15. Hanahan D, Weinberg RA: **Retrospective: Judah Folkman (1933-2008)**. *Science* 2008, **319**(5866):1055.
16. Baeriswyl V, Christofori G: **The angiogenic switch in carcinogenesis**. *Semin Cancer Biol* 2009, **19**(5):329-337.

17. Ferrara N, Henzel WJ: **Pituitary follicular cells secrete a novel heparin-binding growth factor specific for vascular endothelial cells**. *Biochem Biophys Res Commun* 1989, **161**(2):851-858.

18. Friesel RE, Maciag T: **Molecular mechanisms of angiogenesis: fibroblast growth factor signal transduction**. *FASEB J* 1995, **9**(10):919-925.

19. Battegay EJ, Rupp J, Iruela-Arispe L, Sage EH, Pech M: **PDGF-BB modulates endothelial proliferation and angiogenesis in vitro via PDGF beta-receptors**. *J Cell Biol* 1994, **125**(4):917-928.

20. Augustin HG, Koh GY, Thurston G, Alitalo K: **Control of vascular morphogenesis and homeostasis through the angiopoietin-Tie system**. *Nat Rev Mol Cell Biol* 2009, **10**(3):165-177.

21. Mizukami Y, Jo WS, Duerr EM, Gala M, Li J, Zhang X, Zimmer MA, Iliopoulos O, Zukerberg LR, Kohgo Y *et al*: **Induction of interleukin-8 preserves the angiogenic response in HIF-1alpha-deficient colon cancer cells**. *Nat Med* 2005, **11**(9):992-997.

22. O'Reilly MS, Boehm T, Shing Y, Fukai N, Vasios G, Lane WS, Flynn E, Birkhead JR, Olsen BR, Folkman J: **Endostatin: an endogenous inhibitor of angiogenesis and tumor growth**. *Cell* 1997, **88**(2):277-285.

23. Good DJ, Polverini PJ, Rastinejad F, Le Beau MM, Lemons RS, Frazier WA, Bouck NP: **A tumor suppressor-dependent inhibitor of angiogenesis is immunologically and functionally indistinguishable from a fragment of thrombospondin**. *Proc Natl Acad Sci U S A* 1990, **87**(17):6624-6628.

24. O'Reilly MS, Holmgren L, Shing Y, Chen C, Rosenthal RA, Moses M, Lane WS, Cao Y, Sage EH, Folkman J: **Angiostatin: a novel angiogenesis inhibitor that mediates the suppression of metastases by a Lewis lung carcinoma**. *Cell* 1994, **79**(2):315-328.

25. Ferrara N, Gerber HP, LeCouter J: **The biology of VEGF and its receptors**. *Nat Med* 2003, **9**(6):669-676.

26. Ellis LM, Hicklin DJ: **VEGF-targeted therapy: mechanisms of anti-tumour activity**. *Nat Rev Cancer* 2008, **8**(8):579-591.

27. Dvorak HF: **Vascular permeability factor/vascular endothelial growth factor: a critical cytokine in tumor angiogenesis and a potential target for diagnosis and therapy**. *J Clin Oncol* 2002, **20**(21):4368-4380.

28. Kowanetz M, Ferrara N: **Vascular endothelial growth factor signaling pathways: therapeutic perspective**. *Clin Cancer Res* 2006, **12**(17):5018-5022.

29. Rahimi N: **VEGFR-1 and VEGFR-2: two non-identical twins with a unique physiognomy**. *Front Biosci* 2006, **11**:818-829.

30. Tjwa M, Luttun A, Autiero M, Carmeliet P: **VEGF and PlGF: two pleiotropic growth factors with distinct roles in development and homeostasis**. *Cell Tissue Res* 2003, **314**(1):5-14.

31. Waltenberger J, Claesson-Welsh L, Siegbahn A, Shibuya M, Heldin CH: **Different signal transduction properties of KDR and Flt1, two receptors for vascular endothelial growth factor**. *J Biol Chem* 1994, **269**(43):26988-26995.

32. Goel HL, Mercurio AM: **VEGF targets the tumour cell**. *Nat Rev Cancer* 2013, **13**(12):871-882.

33. Spannuth WA, Nick AM, Jennings NB, Armaiz-Pena GN, Mangala LS, Danes CG, Lin YG, Merritt WM, Thaker PH, Kamat AA *et al*: **Functional significance of VEGFR-2 on ovarian cancer cells**. *Int J Cancer* 2009, **124**(5):1045-1053.

34. Alitalo K, Carmeliet P: **Molecular mechanisms of lymphangiogenesis in health and disease**. *Cancer Cell* 2002, **1**(3):219-227.

35. Laakkonen P, Waltari M, Holopainen T, Takahashi T, Pytowski B, Steiner P, Hicklin D, Persaud K, Tonra JR, Witte L *et al*: **Vascular endothelial growth factor receptor 3 is involved in tumor angiogenesis and growth**. *Cancer Res* 2007, **67**(2):593-599.

36. Neufeld G, Kessler O, Herzog Y: **The interaction of Neuropilin-1 and Neuropilin-2 with tyrosine-kinase receptors for VEGF**. *Adv Exp Med Biol* 2002, **515**:81-90.

37. Soker S, Miao HQ, Nomi M, Takashima S, Klagsbrun M: **VEGF165 mediates formation of complexes containing VEGFR-2 and neuropilin-1 that enhance VEGF165-receptor binding**. *J Cell Biochem* 2002, **85**(2):357-368.

38. Soker S, Takashima S, Miao HQ, Neufeld G, Klagsbrun M: **Neuropilin-1 is expressed by endothelial and tumor cells as an isoform-specific receptor for vascular endothelial growth factor**. *Cell* 1998, **92**(6):735-745.

39. Hanahan D, Folkman J: **Patterns and emerging mechanisms of the angiogenic switch during tumorigenesis**. *Cell* 1996, **86**(3):353-364.

40. Naumov GN, Bender E, Zurakowski D, Kang SY, Sampson D, Flynn E, Watnick RS, Straume O, Akslen LA, Folkman J *et al*: **A model of human tumor dormancy: an angiogenic switch from the nonangiogenic phenotype**. *J Natl Cancer Inst* 2006, **98**(5):316-325.

41. Geudens I, Gerhardt H: **Coordinating cell behaviour during blood vessel formation**. *Development* 2011, **138**(21):4569-4583.

42. Sabatini DM: **mTOR and cancer: insights into a complex relationship**. *Nat Rev Cancer* 2006, **6**(9):729-734.

43. Fang J, Ding M, Yang L, Liu LZ, Jiang BH: **PI3K/PTEN/AKT signaling regulates prostate tumor angiogenesis**. *Cell Signal* 2007, **19**(12):2487-2497.

44. Hu L, Hofmann J, Jaffe RB: **Phosphatidylinositol 3-kinase mediates angiogenesis and vascular permeability associated with ovarian carcinoma**. *Clin Cancer Res* 2005, **11**(22):8208-8212.

45. Seeliger H, Guba M, Kleespies A, Jauch KW, Bruns CJ: **Role of mTOR in solid tumor systems: a therapeutic target against primary tumor growth, metastases, and angiogenesis**. *Cancer Metastasis Rev* 2007, **26**(3-4):611-621.

46. Maxwell PH, Dachs GU, Gleadle JM, Nicholls LG, Harris AL, Stratford IJ, Hankinson O, Pugh CW, Ratcliffe PJ: **Hypoxia-inducible factor-1 modulates gene expression in solid tumors and influences both angiogenesis and tumor growth**. *Proc Natl Acad Sci U S A* 1997, **94**(15):8104-8109.

47. Rofstad EK, Danielsen T: **Hypoxia-induced angiogenesis and vascular endothelial growth factor secretion in human melanoma**. *Br J Cancer* 1998, **77**(6):897-902.

48. Kuwabara K, Ogawa S, Matsumoto M, Koga S, Clauss M, Pinsky DJ, Lyn P, Leavy J, Witte L, Joseph-Silverstein J *et al*: **Hypoxia-mediated induction of acidic/basic fibroblast growth factor and platelet-derived growth factor in mononuclear phagocytes stimulates growth of hypoxic endothelial cells**. *Proc Natl Acad Sci U S A* 1995, **92**(10):4606-4610.

49. Kerbel RS, Viloria-Petit A, Okada F, Rak J: **Establishing a link between oncogenes and tumor angiogenesis**. *Mol Med* 1998, **4**(5):286-295.

50. Rak J, Yu JL, Klement G, Kerbel RS: **Oncogenes and angiogenesis: signaling three-dimensional tumor growth**. *J Investig Dermatol Symp Proc* 2000, **5**(1):24-33.

51. Rak J, Mitsuhashi Y, Bayko L, Filmus J, Shirasawa S, Sasazuki T, Kerbel RS: **Mutant ras oncogenes upregulate VEGF/VPF expression: implications for induction and inhibition of tumor angiogenesis**. *Cancer Res* 1995, **55**(20):4575-4580.

52. Dameron KM, Volpert OV, Tainsky MA, Bouck N: **The p53 tumor suppressor gene inhibits angiogenesis by stimulating the production of thrombospondin**. *Cold Spring Harb Symp Quant Biol* 1994, **59**:483-489.

53. Giri D, Ittmann M: **Inactivation of the PTEN tumor suppressor gene is associated with increased angiogenesis in clinically localized prostate carcinoma**. *Hum Pathol* 1999, **30**(4):419-424.

54. Jain RK: **Normalization of tumor vasculature: an emerging concept in antiangiogenic therapy**. *Science* 2005, **307**(5706):58-62.

55. Presta LG, Chen H, O'Connor SJ, Chisholm V, Meng YG, Krummen L, Winkler M, Ferrara N: **Humanization of an anti-vascular endothelial growth factor monoclonal antibody for the therapy of solid tumors and other disorders**. *Cancer Res* 1997, **57**(20):4593-4599.

56. Hurwitz H, Fehrenbacher L, Novotny W, Cartwright T, Hainsworth J, Heim W, Berlin J, Baron A, Griffing S, Holmgren E *et al*: **Bevacizumab plus irinotecan, fluorouracil, and leucovorin for metastatic colorectal cancer**. *N Engl J Med* 2004, **350**(23):2335-2342.

57. Sandler A, Gray R, Perry MC, Brahmer J, Schiller JH, Dowlati A, Lilenbaum R, Johnson DH: **Paclitaxel-carboplatin alone or with bevacizumab for non-small-cell lung cancer**. *N Engl J Med* 2006, **355**(24):2542-2550.

58. Miller K, Wang M, Gralow J, Dickler M, Cobleigh M, Perez EA, Shenkier T, Cella D, Davidson NE: **Paclitaxel plus bevacizumab versus paclitaxel alone for metastatic breast cancer**. *N Engl J Med* 2007, **357**(26):2666-2676.

59. Goodman VL, Rock EP, Dagher R, Ramchandani RP, Abraham S, Gobburu JV, Booth BP, Verbois SL, Morse DE, Liang CY *et al*: **Approval summary: sunitinib for the treatment of imatinib refractory or intolerant gastrointestinal stromal tumors and advanced renal cell carcinoma**. *Clin Cancer Res* 2007, **13**(5):1367-1373.

60. Escudier B, Eisen T, Stadler WM, Szczylik C, Oudard S, Siebels M, Negrier S, Chevreau C, Solska E, Desai AA *et al*: **Sorafenib in advanced clear-cell renal-cell carcinoma**. *N Engl J Med* 2007, **356**(2):125-134.

61. Kane RC, Farrell AT, Saber H, Tang S, Williams G, Jee JM, Liang C, Booth B, Chidambaram N, Morse D *et al*: **Sorafenib for the treatment of advanced renal cell carcinoma**. *Clin Cancer Res* 2006, **12**(24):7271-7278.

62. Isobe T, Herbst RS, Onn A: **Current management of advanced non-small cell lung cancer: targeted therapy**. *Semin Oncol* 2005, **32**(3):315-328.

63. Fukuoka M, Yano S, Giaccone G, Tamura T, Nakagawa K, Douillard JY, Nishiwaki Y, Vansteenkiste J, Kudoh S, Rischin D *et al*: **Multi-institutional randomized phase II trial of gefitinib for previously treated patients with advanced non-small-cell lung cancer (The IDEAL 1 Trial) [corrected]**. *J Clin Oncol* 2003, **21**(12):2237-2246.

64. Kris MG, Natale RB, Herbst RS, Lynch TJ, Jr., Prager D, Belani CP, Schiller JH, Kelly K, Spiridonidis H, Sandler A *et al*: **Efficacy of gefitinib, an inhibitor of the epidermal growth factor receptor tyrosine kinase, in symptomatic patients with non-small cell lung cancer: a randomized trial**. *JAMA* 2003, **290**(16):2149-2158.

65. Thatcher N, Chang A, Parikh P, Rodrigues Pereira J, Ciuleanu T, von Pawel J, Thongprasert S, Tan EH, Pemberton K, Archer V *et al*: **Gefitinib plus best supportive care in previously treated patients with refractory advanced non-small-cell lung cancer: results from a randomised, placebo-controlled, multicentre study (Iressa Survival Evaluation in Lung Cancer)**. *Lancet* 2005, **366**(9496):1527-1537.

66. Pao W, Miller V, Zakowski M, Doherty J, Politi K, Sarkaria I, Singh B, Heelan R, Rusch V, Fulton L *et al*: **EGF receptor gene mutations are common in lung cancers from "never smokers" and are associated with sensitivity of tumors to gefitinib and erlotinib**. *Proc Natl Acad Sci U S A* 2004, **101**(36):13306-13311.

67. Ciardiello F, Caputo R, Damiano V, Troiani T, Vitagliano D, Carlomagno F, Veneziani BM, Fontanini G, Bianco AR, Tortora G: **Antitumor effects of ZD6474, a small molecule vascular endothelial growth factor receptor tyrosine kinase inhibitor, with additional activity against epidermal growth factor receptor tyrosine kinase**. *Clin Cancer Res* 2003, **9**(4):1546-1556.

68. Ciardiello F, Troiani T, Bianco R, Orditura M, Morgillo F, Martinelli E, Morelli MP, Cascone T, Tortora G: **Interaction between the epidermal growth factor receptor (EGFR) and the vascular endothelial growth factor (VEGF) pathways: a rational approach for multi-target anticancer therapy**. *Ann Oncol* 2006, **17 Suppl 7**:vii109-114.

69. De Luca A, Carotenuto A, Rachiglio A, Gallo M, Maiello MR, Aldinucci D, Pinto A, Normanno N: **The role of the EGFR signaling in tumor microenvironment**. *J Cell Physiol* 2008, **214**(3):559-567.

70. Johnson BE, Kabbinavar F, Fehrenbacher L, Hainsworth J, Kasubhai S, Kressel B, Lin CY, Marsland T, Patel T, Polikoff J *et al*: **ATLAS: randomized, double-blind, placebo-controlled, phase IIIB trial**

comparing bevacizumab therapy with or without erlotinib, after completion of chemotherapy, with bevacizumab for first-line treatment of advanced non-small-cell lung cancer. *J Clin Oncol* 2013, **31**(31):3926-3934.

71. Wedge SR, Ogilvie DJ, Dukes M, Kendrew J, Chester R, Jackson JA, Boffey SJ, Valentine PJ, Curwen JO, Musgrove HL *et al*: **ZD6474 inhibits vascular endothelial growth factor signaling, angiogenesis, and tumor growth following oral administration**. *Cancer Res* 2002, **62**(16):4645-4655.

72. Holden SN, Eckhardt SG, Basser R, de Boer R, Rischin D, Green M, Rosenthal MA, Wheeler C, Barge A, Hurwitz HI: **Clinical evaluation of ZD6474, an orally active inhibitor of VEGF and EGF receptor signaling, in patients with solid, malignant tumors**. *Ann Oncol* 2005, **16**(8):1391-1397.

73. Tamura T, Minami H, Yamada Y, Yamamoto N, Shimoyama T, Murakami H, Horiike A, Fujisaka Y, Shinkai T, Tahara M *et al*: **A phase I dose-escalation study of ZD6474 in Japanese patients with solid, malignant tumors**. *J Thorac Oncol* 2006, **1**(9):1002-1009.

74. de Boer R, Humblet Y, Wolf J, Nogova L, Ruffert K, Milenkova T, Smith R, Godwood A, Vansteenkiste J: **An open-label study of vandetanib with pemetrexed in patients with previously treated non-small-cell lung cancer**. *Ann Oncol* 2009, **20**(3):486-491.

75. Natale RB, Bodkin D, Govindan R, Sleckman BG, Rizvi NA, Capo A, Germonpre P, Eberhardt WE, Stockman PK, Kennedy SJ *et al*: **Vandetanib versus gefitinib in patients with advanced non-small-cell lung cancer: results from a two-part, double-blind, randomized phase ii study**. *J Clin Oncol* 2009, **27**(15):2523-2529.

76. Herbst RS, Sun Y, Eberhardt WE, Germonpre P, Saijo N, Zhou C, Wang J, Li L, Kabbinavar F, Ichinose Y *et al*: **Vandetanib plus docetaxel versus docetaxel as second-line treatment for patients with advanced non-small-cell lung cancer (ZODIAC): a double-blind, randomised, phase 3 trial**. *Lancet Oncol* 2010, **11**(7):619-626.

77. Jain RK, Duda DG, Willett CG, Sahani DV, Zhu AX, Loeffler JS, Batchelor TT, Sorensen AG: **Biomarkers of response and resistance to antiangiogenic therapy**. *Nat Rev Clin Oncol* 2009, **6**(6):327-338.

78. Jain RK: **Normalizing tumor microenvironment to treat cancer: bench to bedside to biomarkers**. *J Clin Oncol* 2013, **31**(17):2205-2218.

79. Bergers G, Hanahan D: **Modes of resistance to anti-angiogenic therapy**. *Nat Rev Cancer* 2008, **8**(8):592-603.

80. Carmeliet P, Jain RK: **Molecular mechanisms and clinical applications of angiogenesis**. *Nature* 2011, **473**(7347):298-307.

81. Rini BI, Halabi S, Rosenberg JE, Stadler WM, Vaena DA, Archer L, Atkins JN, Picus J, Czaykowski P, Dutcher J *et al*: **Phase III trial of bevacizumab plus interferon alfa versus interferon alfa monotherapy in patients with metastatic renal cell carcinoma: final results of CALGB 90206**. *J Clin Oncol* 2010, **28**(13):2137-2143.

82. Berdel WE, Danhauser S, Hong CI, Schick HD, Reichert A, Busch R, Rastetter J, Vogler WR: **Influence of 1-beta-D-**

arabinofuranosylcytosine conjugates of lipids on the growth and metastasis of Lewis lung carcinoma. *Cancer Res* 1988, **48**(4):826-829.

83. Brown EB, Campbell RB, Tsuzuki Y, Xu L, Carmeliet P, Fukumura D, Jain RK: **In vivo measurement of gene expression, angiogenesis and physiological function in tumors using multiphoton laser scanning microscopy**. *Nat Med* 2001, **7**(7):864-868.

84. Iurlaro M, Scatena M, Zhu WH, Fogel E, Wieting SL, Nicosia RF: **Rat aorta-derived mural precursor cells express the Tie2 receptor and respond directly to stimulation by angiopoietins**. *J Cell Sci* 2003, **116**(Pt 17):3635-3643.

85. Sarkar C, Chakroborty D, Chowdhury UR, Dasgupta PS, Basu S: **Dopamine increases the efficacy of anticancer drugs in breast and colon cancer preclinical models**. *Clin Cancer Res* 2008, **14**(8):2502-2510.

86. Vakoc BJ, Lanning RM, Tyrrell JA, Padera TP, Bartlett LA, Stylianopoulos T, Munn LL, Tearney GJ, Fukumura D, Jain RK *et al*: **Three-dimensional microscopy of the tumor microenvironment in vivo using optical frequency domain imaging**. *Nat Med* 2009, **15**(10):1219-1223.

87. Jain RK: **Molecular regulation of vessel maturation**. *Nat Med* 2003, **9**(6):685-693.

88. Baluk P, Hashizume H, McDonald DM: **Cellular abnormalities of blood vessels as targets in cancer**. *Curr Opin Genet Dev* 2005, **15**(1):102-111.

89. Nagy JA, Chang SH, Shih SC, Dvorak AM, Dvorak HF: **Heterogeneity of the tumor vasculature**. *Semin Thromb Hemost* 2010, **36**(3):321-331.

90. Fukumura D, Duda DG, Munn LL, Jain RK: **Tumor microvasculature and microenvironment: novel insights through intravital imaging in pre-clinical models**. *Microcirculation*, **17**(3):206-225.

91. Paez-Ribes M, Allen E, Hudock J, Takeda T, Okuyama H, Vinals F, Inoue M, Bergers G, Hanahan D, Casanovas O: **Antiangiogenic therapy elicits malignant progression of tumors to increased local invasion and distant metastasis**. *Cancer Cell* 2009, **15**(3):220-231.

92. Rapisarda A, Melillo G: **Role of the hypoxic tumor microenvironment in the resistance to anti-angiogenic therapies**. *Drug Resist Updat* 2009, **12**(3):74-80.

93. Yuan F, Chen Y, Dellian M, Safabakhsh N, Ferrara N, Jain RK: **Time-dependent vascular regression and permeability changes in established human tumor xenografts induced by an anti-vascular endothelial growth factor/vascular permeability factor antibody**. *Proc Natl Acad Sci U S A* 1996, **93**(25):14765-14770.

94. Hansen-Algenstaedt N, Stoll BR, Padera TP, Dolmans DE, Hicklin DJ, Fukumura D, Jain RK: **Tumor oxygenation in hormone-dependent tumors during vascular endothelial growth factor receptor-2 blockade, hormone ablation, and chemotherapy**. *Cancer Res* 2000, **60**(16):4556-4560.

95. Tong RT, Boucher Y, Kozin SV, Winkler F, Hicklin DJ, Jain RK: **Vascular normalization by vascular endothelial growth factor receptor 2 blockade induces a pressure gradient across the vasculature and improves drug penetration in tumors**. *Cancer Res* 2004, **64**(11):3731-3736.

96. Winkler F, Kozin SV, Tong RT, Chae SS, Booth MF, Garkavtsev I, Xu L, Hicklin DJ, Fukumura D, di Tomaso E *et al*: **Kinetics of vascular normalization by VEGFR2 blockade governs brain tumor response to radiation: role of oxygenation, angiopoietin-1, and matrix metalloproteinases**. *Cancer Cell* 2004, **6**(6):553-563.

97. Willett CG, Boucher Y, di Tomaso E, Duda DG, Munn LL, Tong RT, Chung DC, Sahani DV, Kalva SP, Kozin SV *et al*: **Direct evidence that the VEGF-specific antibody bevacizumab has antivascular effects in human rectal cancer**. *Nat Med* 2004, **10**(2):145-147.

98. Willett CG, Boucher Y, Duda DG, di Tomaso E, Munn LL, Tong RT, Kozin SV, Petit L, Jain RK, Chung DC *et al*: **Surrogate markers for antiangiogenic therapy and dose-limiting toxicities for bevacizumab with radiation and chemotherapy: continued experience of a phase I trial in rectal cancer patients**. *J Clin Oncol* 2005, **23**(31):8136-8139.

99. Sorensen AG, Batchelor TT, Zhang WT, Chen PJ, Yeo P, Wang M, Jennings D, Wen PY, Lahdenranta J, Ancukiewicz M *et al*: **A "vascular normalization index" as potential mechanistic biomarker to predict survival after a single dose of cediranib in recurrent glioblastoma patients**. *Cancer Res* 2009, **69**(13):5296-5300.

100. Sorensen AG, Emblem KE, Polaskova P, Jennings D, Kim H, Ancukiewicz M, Wang M, Wen PY, Ivy P, Batchelor TT *et al*: **Increased survival of glioblastoma patients who respond to antiangiogenic therapy with elevated blood perfusion**. *Cancer Res* 2012, **72**(2):402-407.

101. Emblem KE, Mouridsen K, Bjornerud A, Farrar CT, Jennings D, Borra RJ, Wen PY, Ivy P, Batchelor TT, Rosen BR *et al*: **Vessel architectural imaging identifies cancer patient responders to anti-angiogenic therapy**. *Nat Med* 2013, **19**(9):1178-1183.

102. Chatterjee S, Heukamp LC, Siobal M, Schottle J, Wieczorek C, Peifer M, Frasca D, Koker M, Konig K, Meder L *et al*: **Tumor VEGF:VEGFR2 autocrine feed-forward loop triggers angiogenesis in lung cancer**. *J Clin Invest* 2013, **123**(4):1732-1740.

103. Sos ML, Michel K, Zander T, Weiss J, Frommolt P, Peifer M, Li D, Ullrich R, Koker M, Fischer F *et al*: **Predicting drug susceptibility of non-small cell lung cancers based on genetic lesions**. *J Clin Invest* 2009, **119**(6):1727-1740.

104. Hamacher K, Coenen HH, Stocklin G: **Efficient stereospecific synthesis of no-carrier-added 2-[18F]-fluoro-2-deoxy-D-glucose using aminopolyether supported nucleophilic substitution**. *J Nucl Med* 1986, **27**(2):235-238.

105. Machulla H, Blocther A, Kuntzsch M, Piert M, Wei R, Grierson J: **Simplified labeling approach for synthesizing 3-deoxy-3-[F-18]fluorothymidine ([F-18]FLT)**. *J Radiochem Nucl Chem* 2000, **243**:843– 846.

106. Buck AK, Halter G, Schirrmeister H, Kotzerke J, Wurziger I, Glatting G, Mattfeldt T, Neumaier B, Reske SN, Hetzel M: **Imaging proliferation in lung tumors with PET: 18F-FLT versus 18F-FDG**. *J Nucl Med* 2003, **44**(9):1426-1431.

107. Wagner M, Seitz U, Buck A, Neumaier B, Schultheiss S, Bangerter M, Bommer M, Leithauser F, Wawra E, Munzert G *et al*: **3'-[18F]fluoro-3'-deoxythymidine ([18F]-FLT) as positron emission tomography tracer for imaging proliferation in a murine B-Cell lymphoma model and in the human disease**. *Cancer Res* 2003, **63**(10):2681-2687.

108. Krohn KA, Mankoff DA, Muzi M, Link JM, Spence AM: **True tracers: comparing FDG with glucose and FLT with thymidine**. *Nucl Med Biol* 2005, **32**(7):663-671.

109. Miyagawa T, Oku T, Uehara H, Desai R, Beattie B, Tjuvajev J, Blasberg R: **"Facilitated" amino acid transport is upregulated in brain tumors**. *J Cereb Blood Flow Metab* 1998, **18**(5):500-509.

110. Pao W, Miller VA, Politi KA, Riely GJ, Somwar R, Zakowski MF, Kris MG, Varmus H: **Acquired resistance of lung adenocarcinomas to gefitinib or erlotinib is associated with a second mutation in the EGFR kinase domain**. *PLoS Med* 2005, **2**(3):e73.

111. Fuchs BC, Bode BP: **Amino acid transporters ASCT2 and LAT1 in cancer: partners in crime?** *Semin Cancer Biol* 2005, **15**(4):254-266.

112. Brugarolas JB, Vazquez F, Reddy A, Sellers WR, Kaelin WG, Jr.: **TSC2 regulates VEGF through mTOR-dependent and -independent pathways**. *Cancer Cell* 2003, **4**(2):147-158.

113. Kanai Y, Segawa H, Miyamoto K, Uchino H, Takeda E, Endou H: **Expression cloning and characterization of a transporter for large neutral amino acids activated by the heavy chain of 4F2 antigen (CD98)**. *J Biol Chem* 1998, **273**(37):23629-23632.

114. Vasudevan KM, Barbie DA, Davies MA, Rabinovsky R, McNear CJ, Kim JJ, Hennessy BT, Tseng H, Pochanard P, Kim SY *et al*: **AKT-independent signaling downstream of oncogenic PIK3CA mutations in human cancer**. *Cancer Cell* 2009, **16**(1):21-32.

115. Brekken RA, Huang X, King SW, Thorpe PE: **Vascular endothelial growth factor as a marker of tumor endothelium**. *Cancer Res* 1998, **58**(9):1952-1959.

116. O'Reilly KE, Rojo F, She QB, Solit D, Mills GB, Smith D, Lane H, Hofmann F, Hicklin DJ, Ludwig DL *et al*: **mTOR inhibition induces upstream receptor tyrosine kinase signaling and activates Akt**. *Cancer Res* 2006, **66**(3):1500-1508.

117. Chatterjee S, Wieczorek C, Schottle J, Siobal M, Hinze Y, Franz T, Florin A, Adamczak J, Heukamp LC, Neumaier B *et al*: **Transient antiangiogenic treatment improves delivery of cytotoxic compounds and therapeutic outcome in lung cancer**. *Cancer Res* 2014, **74**(10):2816-2824.

118. Chatterjee S, Heukamp LC, Siobal M, Schottle J, Wieczorek C, Peifer M, Frasca D, Koker M, Konig K, Meder L *et al*: **Tumor VEGF:VEGFR2 autocrine feed-forward loop triggers angiogenesis in lung cancer**. *The Journal of clinical investigation* 2013, **123**(7):3183.

119. Ullrich RT, Zander T, Neumaier B, Koker M, Shimamura T, Waerzeggers Y, Borgman CL, Tawadros S, Li H, Sos ML *et al*: **Early detection of erlotinib treatment response in NSCLC by 3'-deoxy-3'-[F]-fluoro-L-thymidine**

([F]FLT) positron emission tomography (PET). *PLoS One* 2008, **3**(12):e3908.

120. Italiano A: **Prognostic or predictive? It's time to get back to definitions!** *J Clin Oncol* 2011, **29**(35):4718; author reply 4718-4719.

121. Oldenhuis CN, Oosting SF, Gietema JA, de Vries EG: **Prognostic versus predictive value of biomarkers in oncology**. *Eur J Cancer* 2008, **44**(7):946-953.

122. McShane LM, Altman DG, Sauerbrei W, Taube SE, Gion M, Clark GM: **REporting recommendations for tumor MARKer prognostic studies (REMARK)**. *Nat Clin Pract Urol* 2005, **2**(8):416-422.

123. Pan Y, Xu R, Peach M, Huang CP, Branstetter D, Novotny W, Herbst RS, Eckhardt SG, Holland PM: **Evaluation of pharmacodynamic biomarkers in a Phase 1a trial of dulanermin (rhApo2L/TRAIL) in patients with advanced tumours**. *Br J Cancer* 2011, **105**(12):1830-1838.

124. Sarker D, Workman P: **Pharmacodynamic biomarkers for molecular cancer therapeutics**. *Adv Cancer Res* 2007, **96**:213-268.

125. Katz R: **Biomarkers and surrogate markers: an FDA perspective**. *NeuroRx* 2004, **1**(2):189-195.

126. Hanrahan EO, Ryan AJ, Mann H, Kennedy SJ, Langmuir P, Natale RB, Herbst RS, Johnson BE, Heymach JV: **Baseline vascular endothelial growth factor concentration as a potential predictive marker of benefit from vandetanib in non-small cell lung cancer**. *Clin Cancer Res* 2009, **15**(10):3600-3609.

127. Dowlati A, Gray R, Sandler AB, Schiller JH, Johnson DH: **Cell adhesion molecules, vascular endothelial growth factor, and basic fibroblast growth factor in patients with non-small cell lung cancer treated with chemotherapy with or without bevacizumab--an Eastern Cooperative Oncology Group Study**. *Clin Cancer Res* 2008, **14**(5):1407-1412.

128. Duvel K, Yecies JL, Menon S, Raman P, Lipovsky AI, Souza AL, Triantafellow E, Ma Q, Gorski R, Cleaver S *et al*: **Activation of a metabolic gene regulatory network downstream of mTOR complex 1**. *Mol Cell* 2010, **39**(2):171-183.

129. Shi Y, Yan H, Frost P, Gera J, Lichtenstein A: **Mammalian target of rapamycin inhibitors activate the AKT kinase in multiple myeloma cells by up-regulating the insulin-like growth factor receptor/insulin receptor substrate-1/phosphatidylinositol 3-kinase cascade**. *Mol Cancer Ther* 2005, **4**(10):1533-1540.

130. Willett CG, Duda DG, di Tomaso E, Boucher Y, Ancukiewicz M, Sahani DV, Lahdenranta J, Chung DC, Fischman AJ, Lauwers GY *et al*: **Efficacy, safety, and biomarkers of neoadjuvant bevacizumab, radiation therapy, and fluorouracil in rectal cancer: a multidisciplinary phase II study**. *J Clin Oncol* 2009, **27**(18):3020-3026.

131. Chakroborty D, Sarkar C, Yu H, Wang J, Liu Z, Dasgupta PS, Basu S: **Dopamine stabilizes tumor blood vessels by up-regulating angiopoietin 1 expression in pericytes and Kruppel-like factor-2**

expression in tumor endothelial cells. *Proc Natl Acad Sci U S A* 2011, **108**(51):20730-20735.

132. Kirane A, Toombs JE, Larsen JE, Ostapoff KT, Meshaw KR, Zaknoen S, Brekken RA, Burrows FJ: **Epithelial-mesenchymal transition increases tumor sensitivity to COX-2 inhibition by apricoxib**. *Carcinogenesis* 2012, **33**(9):1639-1646.

133. Batchelor TT, Sorensen AG, di Tomaso E, Zhang WT, Duda DG, Cohen KS, Kozak KR, Cahill DP, Chen PJ, Zhu M *et al*: **AZD2171, a pan-VEGF receptor tyrosine kinase inhibitor, normalizes tumor vasculature and alleviates edema in glioblastoma patients**. *Cancer Cell* 2007, **11**(1):83-95.

134. Kamoun WS, Ley CD, Farrar CT, Duyverman AM, Lahdenranta J, Lacorre DA, Batchelor TT, di Tomaso E, Duda DG, Munn LL *et al*: **Edema control by cediranib, a vascular endothelial growth factor receptor-targeted kinase inhibitor, prolongs survival despite persistent brain tumor growth in mice**. *J Clin Oncol* 2009, **27**(15):2542-2552.

135. de Langen AJ, van den Boogaart VE, Marcus JT, Lubberink M: **Use of H2(15)O-PET and DCE-MRI to measure tumor blood flow**. *Oncologist* 2008, **13**(6):631-644.

136. Hahn OM, Yang C, Medved M, Karczmar G, Kistner E, Karrison T, Manchen E, Mitchell M, Ratain MJ, Stadler WM: **Dynamic contrast-enhanced magnetic resonance imaging pharmacodynamic biomarker study of sorafenib in metastatic renal carcinoma**. *J Clin Oncol* 2008, **26**(28):4572-4578.

137. Ullrich RT, Jikeli JF, Diedenhofen M, Bohm-Sturm P, Unruh M, Vollmar S, Hoehn M: **In-vivo visualization of tumor microvessel density and response to anti-angiogenic treatment by high resolution MRI in mice**. *PLoS One* 2011, **6**(5):e19592.

138. de Langen AJ, van den Boogaart V, Lubberink M, Backes WH, Marcus JT, van Tinteren H, Pruim J, Brans B, Leffers P, Dingemans AM *et al*: **Monitoring response to antiangiogenic therapy in non-small cell lung cancer using imaging markers derived from PET and dynamic contrast-enhanced MRI**. *J Nucl Med* 2011, **52**(1):48-55.

139. Shah NP, Kasap C, Weier C, Balbas M, Nicoll JM, Bleickardt E, Nicaise C, Sawyers CL: **Transient potent BCR-ABL inhibition is sufficient to commit chronic myeloid leukemia cells irreversibly to apoptosis**. *Cancer Cell* 2008, **14**(6):485-493.

140. Huang Y, Stylianopoulos T, Duda DG, Fukumura D, Jain RK: **Benefits of vascular normalization are dose and time dependent--letter**. *Cancer Res* 2013, **73**(23):7144-7146.

141. Huang Y, Yuan J, Righi E, Kamoun WS, Ancukiewicz M, Nezivar J, Santosuosso M, Martin JD, Martin MR, Vianello F *et al*: **Vascular normalizing doses of antiangiogenic treatment reprogram the immunosuppressive tumor microenvironment and enhance immunotherapy**. *Proc Natl Acad Sci U S A* 2012, **109**(43):17561-17566.

142. Lopez-Chavez A, Young T, Fages S, Leon L, Schiller JH, Dowlati A, Brahmer JR, Johnson DH, Sandler A: **Bevacizumab maintenance in patients with advanced non-small-cell lung cancer, clinical patterns, and**

outcomes in the Eastern Cooperative Oncology Group 4599 Study: results of an exploratory analysis. *J Thorac Oncol* 2012, **7**(11):1707-1712.

143. Van der Veldt AA, Lubberink M, Bahce I, Walraven M, de Boer MP, Greuter HN, Hendrikse NH, Eriksson J, Windhorst AD, Postmus PE *et al*: **Rapid decrease in delivery of chemotherapy to tumors after anti-VEGF therapy: implications for scheduling of anti-angiogenic drugs**. *Cancer Cell* 2012, **21**(1):82-91.

8. Appendix

8.1. List of Abbreviations

ADC: adenocarcinoma

ATP: adenosine triphosphate

AIDS: acquired immuno deficiency syndrome

ANGP: angiopoietin

BLI: bioluminescence imaging

BV: bevacizumab

BrdU: 5-bromo-2'-deoxyuridine

CRC: colorectal carcinoma

DNA: deoxyribonucleic acid

ELISA: enzyme linked immunosorbent assay

EGFR: endothelial growth factor receptor

[18F]FLT: [18F] 3'-deoxy-3'-[^{18}F]-fluoro-L-thymidine

FITC: fluorescein isothiocyanate

FGF: fibroblast growth factor

Flk1: fetal liver kinase 1

GBM: glioblastoma

HIV: human immunodeficiency virus

HIF: hypoxia inducible factor

IRS: insulin receptor substrate

IGFR: insulin growth factor receptor

KD: knockdown

KDR: kinase insert domain receptor

MAPK: mitogen-activated protein kinase

MEK: mitogen-activated protein kinase kinase

[11C]MET: methyl-L- [11C]-methionine

MMP: matrix metalloproteinase

MRI: magnetic resonance imaging

NNK: nitrosoaminoketone

NRP: neuropillin

NSCLC: non small cell lung cancer

OV: overall survival

PDGF: platelet derived growth factor

PDGFR: platelet derived growth factor receptor

PET: positron emission tomography

PAHS: polycyclic hydrocarbons

PFS: progression free survival

PLGF: placental growth factor

PBS: phosphate buffered saline

RTK: receptor tyrosine kinase

RCC: renal cell carcinoma

RNA: ribonucleic acid

ROI: region of interest

TSP: thrombospondin

TKI: tyrosine kinase inhibitor

SCLC: small cell lung cancer

SCC: squamous cell carcinoma

VEGF: vascular endothelial growth factor

VEGFR: vascular endothelial growth factor receptor

8.2. Publications

1.

Tumor VEGF:VEGFR2 autocrine feed-forward loop triggers angiogenesis in lung cancer. Journal of Clinical Investigation.

Sampurna Chatterjee, Lukas C. Heukamp, Maike Siobal, Jakob Schöttle, Caroline Wieczorek, Martin Peifer, Davide Frasca, Mirjam Koker, Katharina König, Lydia Meder, Daniel Rauh, Reinhard Buettner, Jürgen Wolf, Rolf A. Brekken, Bernd Neumaier, Gerhard Christofori, Roman K. Thomas and Roland T. Ullrich.

Journal of Clinical Investigation 2013, 1732-1740.

2.

Transient antiangiogenic treatment improves delivery of cytotoxic compounds and therapeutic outcome in lung cancer.

Sampurna Chatterjee, Caroline Wieczorek, Jakob Schöttle, Maike Siobal, Yvonne Hinze, Thomas Franz, Alexandra Florin, Joanna Adamczak, Lukas C. Heukamp, Bernd Neumaier and Roland T. Ullrich.

Cancer Research 2014, 2816-2824.

Research article

Tumor VEGF:VEGFR2 autocrine feed-forward loop triggers angiogenesis in lung cancer

Sampurna Chatterjee,[1] Lukas C. Heukamp,[2] Maike Siobal,[1] Jakob Schöttle,[1]
Caroline Wieczorek,[1] Martin Peifer,[1] Davide Frasca,[2] Mirjam Koker,[1] Katharina König,[2]
Lydia Meder,[2] Daniel Rauh,[3] Reinhard Buettner,[2] Jürgen Wolf,[4] Rolf A. Brekken,[5]
Bernd Neumaier,[1] Gerhard Christofori,[6] Roman K. Thomas,[1,2,3] and Roland T. Ullrich[1,4]

[1]Max Planck Institute for Neurological Research, with Klaus-Joachim-Zülch Laboratories of the Max Planck Society and the Medical Faculty of the
University of Cologne, Cologne, Germany. [2]Institute of Pathology, University Hospital Medical School, Cologne, Germany. [3]Fakultät Chemie,
Chemische Biologie, Technische Universität Dortmund, Dortmund, Germany. [4]Department I of Internal Medicine and Center for Integrated Oncology,
University Hospital of Cologne, Cologne, Germany. [5]Departments of Surgery and Pharmacology, Hamon Center for Therapeutic Oncology Research,
University of Texas Southwestern Medical Center, Dallas, Texas, USA. [6]Institute of Biochemistry and Genetics, Department of Biomedicine, Basel, Switzerland.

The molecular mechanisms that control the balance between antiangiogenic and proangiogenic factors and initiate the angiogenic switch in tumors remain poorly defined. By combining chemical genetics with multimodal imaging, we have identified an autocrine feed-forward loop in tumor cells in which tumor-derived VEGF stimulates VEGF production via VEGFR2-dependent activation of mTOR, substantially amplifying the initial proangiogenic signal. Disruption of this feed-forward loop by chemical perturbation or knockdown of VEGFR2 in tumor cells dramatically inhibited production of VEGF in vitro and in vivo. This disruption was sufficient to prevent tumor growth in vivo. In patients with lung cancer, we found that this VEGF:VEGFR2 feed-forward loop was active, as the level of VEGF/VEGFR2 binding in tumor cells was highly correlated to tumor angiogenesis. We further demonstrated that inhibition of tumor cell VEGFR2 induces feedback activation of the IRS/MAPK signaling cascade. Most strikingly, combined pharmacological inhibition of VEGFR2 (ZD6474) and MEK (PD0325901) in tumor cells resulted in dramatic tumor shrinkage, whereas monotherapy only modestly slowed tumor growth. Thus, a tumor cell-autonomous VEGF:VEGFR2 feed-forward loop provides signal amplification required for the establishment of fully angiogenic tumors in lung cancer. Interrupting this feed-forward loop switches tumor cells from an angiogenic to a proliferative phenotype that sensitizes tumor cells to MAPK inhibition.

Introduction

Several receptor tyrosine kinases, such as VEGFR2, Flt1/VEGFR1, VEGFR3, or PDGFR, have been implicated in tumor angiogenesis. When activated through binding of the respective ligand, they regulate related, yet distinct, processes involved in neoangiogenesis. Endothelial cell survival, migration, and proliferation of blood vessels is regulated primarily by VEGF-A binding to VEGFR2 (1). In the canonical model, tumor cells express VEGF, which binds to VEGFR2 on endothelial cells (2), thus stimulating tumor vessel formation. This change from prevascular hyperplasia to highly vascularized tumors has been referred to as the angiogenic switch (1). In recent years, several studies have reported expression of VEGFR1 as well as VEGFR2 on tumor cells (3–5). An intriguing finding related to tumor cell expression of Flt1 was the observation that VEGF secreted by tumor cells triggers tumor cell proliferation by binding Flt1 (6). Moreover, in patients with lung cancer, an increase in VEGFR2 gene copy number is associated with chemoresistance and shorter survival (7). Here, we have sought to analyze the impact of VEGFR2 inhi-

bition on tumor cells by combining genetically controlled pharmacological perturbations with multimodal PET imaging.

Results

VEGFR2 is differentially expressed on non-small-cell lung cancer – VEGFR2 inhibition alters amino acid transport in tumor cells but does not affect tumor cell proliferation. We used the human lung cancer cell lines H441 and H1975, which each expressed high levels of VEGFR2 (Figure 1A and Supplemental Figure 1A; supplemental material available online with this article; doi:10.1172/JCI65385DS1). We treated mice engrafted with these 2 cell lines with the dual VEGFR2/EGFR inhibitor ZD6474, which has a 40-fold lower activity against VEGFR1 (8). Both cell lines are resistant to EGFR inhibition, due either to a *KRAS* mutation (H441) or to the presence of the T790M gatekeeper mutation of EGFR (H1975) (ref. 9 and Supplemental Figure 1B). Thus, any therapeutic impact on subcutaneous tumor growth of these cell lines is primarily due to VEGFR2 inhibition and cannot be attributed to inhibition of EGFR. In established tumors, ZD6474 treatment completely abolished methionine uptake after 7 days of treatment, as determined by methyl-L-[11C]-methionine ([11C]MET) PET (Figure 1B and Supplemental Figure 1C). By contrast, uptake of 3′-deoxy-3′-[18F]-fluoro-L-thymidine ([18F]FLT), a marker of proliferation (10), was slightly increased (Figure 1B and Supplemental Figure 1C), suggesting that the cells continued to progress through the cell cycle. Thus, VEGFR2 inhibition seems to inhibit a VEGFR2-dependent signaling pathway in tumor cells that affects amino acid transport without affecting cellular proliferation

(Figure 1B). To investigate whether the reduction in [11C]MET uptake is specifically due to ZD6474-mediated VEGFR2 inhibition, we used a chemical genetic approach, which introduces a gatekeeper resistant mutation against ZD6474-induced VEGFR2 inhibition. The substitution of Val916 to Met at the gatekeeper position of VEGFR2 creates a steric clash with the inhibitor that specifically prevents ZD6474 from binding to VEGFR2 (Figure 1C and ref. 11). The introduction of this resistant gatekeeper mutation was sufficient to abrogate the inhibitory effect of ZD6474 on [11C]MET uptake (Supplemental Figure 1D). The cellular uptake of methionine is facilitated by the LAT1 transporter that is regulated by mTOR (12). Hence, we hypothesized that VEGF-bound VEGFR2 on tumor cells induces a VEGFR2 signaling pathway via mTOR. Moreover, as VEGF secretion is regulated by mTOR, we sought to investigate whether VEGF/VEGFR2 signaling induces a feed-forward loop via mTOR.

VEGF/VEGFR2 signaling induces a feed-forward loop that is mediated by a VEGFR2/PI3K/mTOR/VEGF signaling cascade. Consistent with a feed-forward loop stimulating VEGF secretion in a VEGFR2-dependent fashion, VEGF secretion was strongly induced by addition of exogenous VEGF in the VEGFR2-expressing tumor cell lines H1975, H441, and HCC1359 (Figure 1D and Supplemental Figure 2B), and this induction was blunted by treatment of cells with the VEGFR2 inhibitor ZD6474 (Figure 1D and Supplemental Figure 2B). To validate the specificity of VEGFR2 as the relevant target for inhibition of VEGFR2-dependent VEGF secretion, we used the gatekeeper resistant mutation against ZD6474-induced VEGFR2 inhibition (*V916M*) (Figure 1C). Introducing this mutation in H1975 cells was sufficient to abrogate the ZD6474-induced inhibition of VEGF secretion (Figure 1E). Under hypoxic conditions, induction of VEGF secretion was similarly inhibited by VEGFR2 inhibition (Supplemental Figure 3C), suggesting that this autocrine loop is also active in the physiological response to hypoxia. Rapamycin treatment similarly blunted VEGF-induced VEGF secretion of tumor cells, supporting the hypothesis that VEGFR2-dependent secretion of VEGF is under the control of mTOR (13), which also regulates methionine uptake via the LAT-1 transporter (ref. 14 and Figure 1D). Moreover, VEGF-mediated stimulation of VEGFR2 induced S6 phosphorylation in tumor cells expressing high levels of VEGFR2 (Figure 1F, Supplemental Figure 2A, and Supplemental Figure 3A). Phosphorylation of S6 coincided with the activation of PDK1, which might provide an alternative route for mTOR activation (Supplemental Figure 2A and ref. 15). In accordance with the induction of PI3K/mTOR/ VEGF signaling, PI3K inhibition resulted in reduced VEGF secretion (Supplemental Figure 2B). We next formulated a general mathematical model describing the postulated VEGF:VEGFR2 feed-forward mechanism. We then demonstrated that the behavior of the model was consistent with the experimental results obtained (Supplemental Figure 4 and Supplemental Note).

Additionally, we detected a consistent reduction in phosphorylation of ERK and of AKT in H1975, H441, and HCC1359 cells (Figure 1F and Supplemental Figure 3A). Thus, in the setting of autocrine VEGF/VEGFR2 signaling, the slight reduction in tumor growth observed in response to VEGFR2 inhibition is likely to be independent of ERK-mediated proliferation. These results agree with those of our PET experiments, showing a continuous uptake of [18F]FLT (Figure 1B). Finally, we confirmed that the observed ZD6474-mediated effects were due to inhibition of VEGFR2 in tumor cells by ectopically expressing the ZD6474-resistant mutant

of VEGFR2 (*V916M*) in H1975 cells (Figure 1, E and G, and ref. 11). This mutant abolished ZD6474-mediated VEGFR2 dephosphorylation and activation of mTOR (Figure 1G). Most strikingly, this VEGFR2 gatekeeper mutant against ZD6474 was sufficient to rescue the tumor growth–inhibiting effects of ZD6474 in vivo (Figure 1H). Thus, in concordance with the [11C]MET PET data, the ZD6474-mediated effects on tumor VEGF/VEGFR2/mTOR signaling are predominantly due to inhibition of VEGFR2 on the tumor cells and not due to inhibition of other kinases or VEGFR2 on endothelial cells.

We next sought to validate our findings on inhibition of VEGF/ VEGFR2/mTOR signaling with an additional VEGFR2 inhibitor, PTK787. As with ZD6474, treatment with PTK787 inhibited phosphorylation of S6 and reduced the level of secreted VEGF (Supplemental Figure 2, A and B). Further, we found that, in the absence of VEGF, ZD6474 had only a little effect on the activation on ERK and S6 kinase (Supplemental Figure 3E).

VEGF/VEGFR2 signaling is needed for the induction of tumor angiogenesis and tumor formation in vivo. To validate our finding with an alternative approach, we stably silenced VEGFR2 with lentiviral shRNA in H1975 and H441 non-small-cell lung cancer (NSCLC) cells (Figure 2A and Supplemental Figure 5B). Consistent with the [18F]FLT PET data, selective silencing of VEGFR2 by shRNA did not reduce tumor cell proliferation in vitro (Supplemental Figure 5A). By contrast, silencing of VEGFR2 dramatically reduced secretion of VEGF by tumor cells in response to hypoxia (Figure 2B), thereby confirming that binding of VEGF to VEGFR2 amplifies VEGF secretion in a VEGFR2-dependent manner. Most strikingly, knockdown of VEGFR2 in tumor cells alone was sufficient to almost entirely abolish initiation of tumor growth in vivo (Figure 2C and Supplemental Figure 5B), suggesting that autocrine VEGF/VEGFR2 signaling in tumor cells is required for the establishment of tumors in vivo. While the large tumors transduced with empty control vector (H1975[eV] tumors) exhibited a highly angiogenic phenotype with many CD31-positive blood vessels, the small residual tumors in which VEGFR2 had been stably silenced (H1975[VEGFR2KD] tumors) almost completely lacked blood vessels (Figure 2D). In concordance with the tissue culture results, these tumors lacked expression of VEGF, while H1975[eV] tumors expressed high amounts of VEGF (Figure 2D). Using bevacizumab (Avastin), we specifically stained for (human) tumor cell–derived VEGF. We herewith could demonstrate that silencing VEGFR2 on tumor cells dramatically reduced the secretion of tumor cell–derived VEGF (Figure 2D). We next analyzed whether the raised levels of VEGF in the VEGFR2 WT cells were due to elevated hypoxia. HIF-1α was equally expressed in wild-type (H1975[WT]), H1975[eV], and H1975[VEGFR2KD] tumors (Supplemental Figure 5C). By staining with an antibody that specifically recognizes human VEGF bound to human VEGFR2, we confirmed that tumor cell–derived VEGF binds to VEGFR2 on tumor cells in H1975[eV] tumors but to a much lesser degree in H1975[VEGFR2KD] xenograft tumors (16), supporting the presence of an autocrine loop in vivo (Figure 2D). Furthermore, H1975[VEGFR2KD] tumors had a markedly reduced uptake of [15O]H$_2$O, a measure of tumor blood flow as a functional readout of angiogenesis (17), when compared with that of H1975[eV] tumors (Supplemental Figure 5D). As an alternative approach to determine whether VEGFR2 inhibition on tumor cells can prevent tumor formation, we treated mice with the VEGFR2 inhibitor ZD6474 immediately after

research article
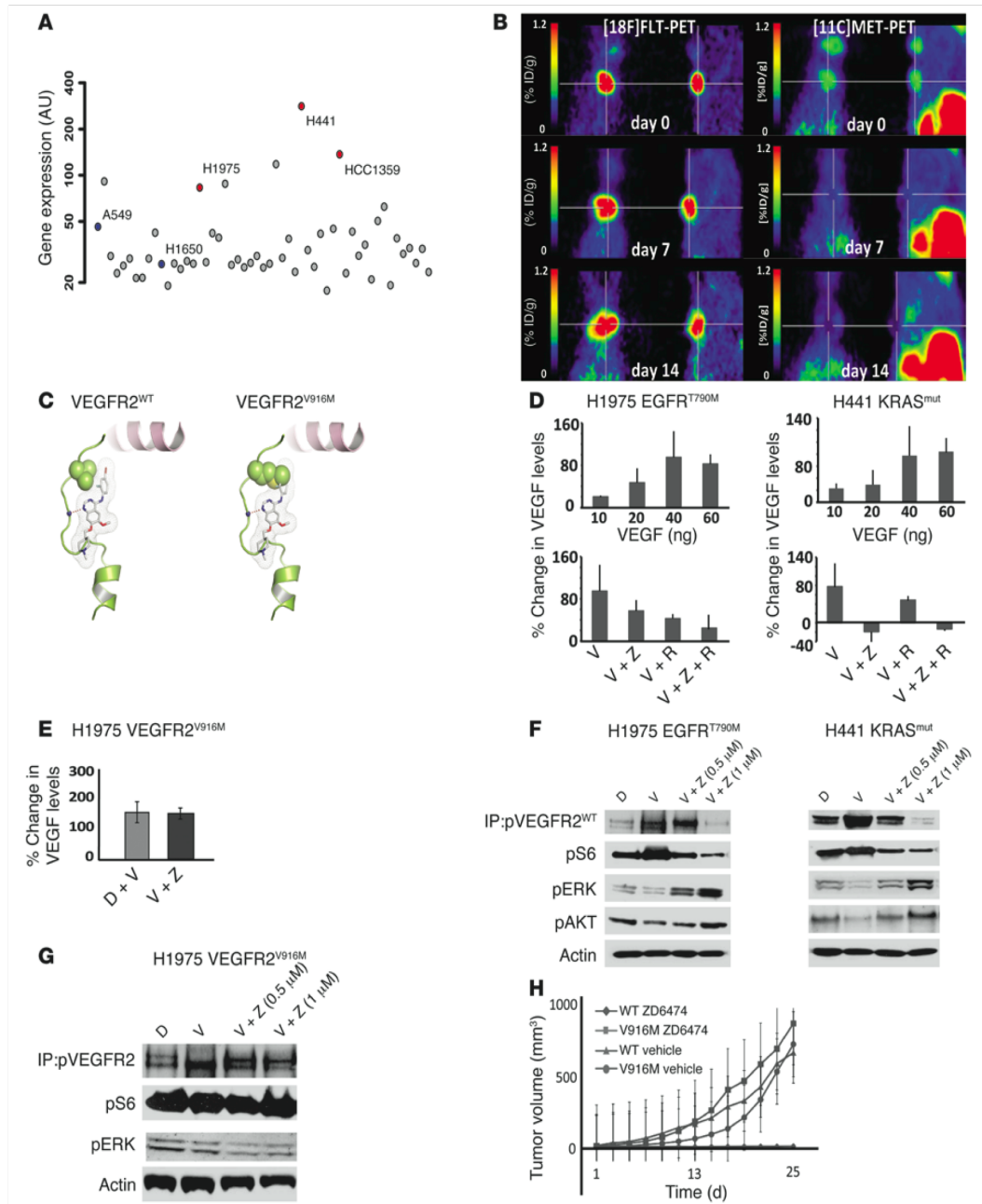
Figure 1
A VEGF:VEGFR2 feed-forward loop in tumor cells boosts VEGF secretion. (**A**) *VEGFR2* expression data from the 53 NSCLC cell lines were obtained using Affymetrix U133A arrays (21). (**B**) Mice with established tumors (H1975) were treated with ZD6474, and PET imaging was performed on day 0 (before start of therapy) and at the indicated time points after treatment (left panels, [18F]FLT-PET; right panels, [11C]MET-PET). (**C**) Substitution of Val916 by Met at the gatekeeper position of VEGFR2 creates a steric clash with the inhibitor and prevents ZD6474 from binding. (**D**) Secretion of VEGF by H1975, H441, and (**E**) H1975 mutant cells (VEGFR2^{V916M}) was determined in vitro by ELISA (**D**) following stimulation with increasing amounts of recombinant VEGF. H1975 and H441 cells were stimulated with the indicated concentrations of VEGF (V) and pretreated with the indicated compounds (ZD6474 [Z], 1 μM; rapamycin [R], 100 nM). (**F** and **G**) Cells were treated with VEGF and the indicated dose of ZD6474, and phosphorylation of VEGFR2 was determined by immunoprecipitation. (**F**) The impact on activation of downstream signaling was determined by immunoblotting. (**H**) H1975 mutant cells (VEGFR2^{V916M}) or the wild-type control cells were injected into nude mice and treated with ZD6474 or vehicle on day 1 after tumor cell injections.

105
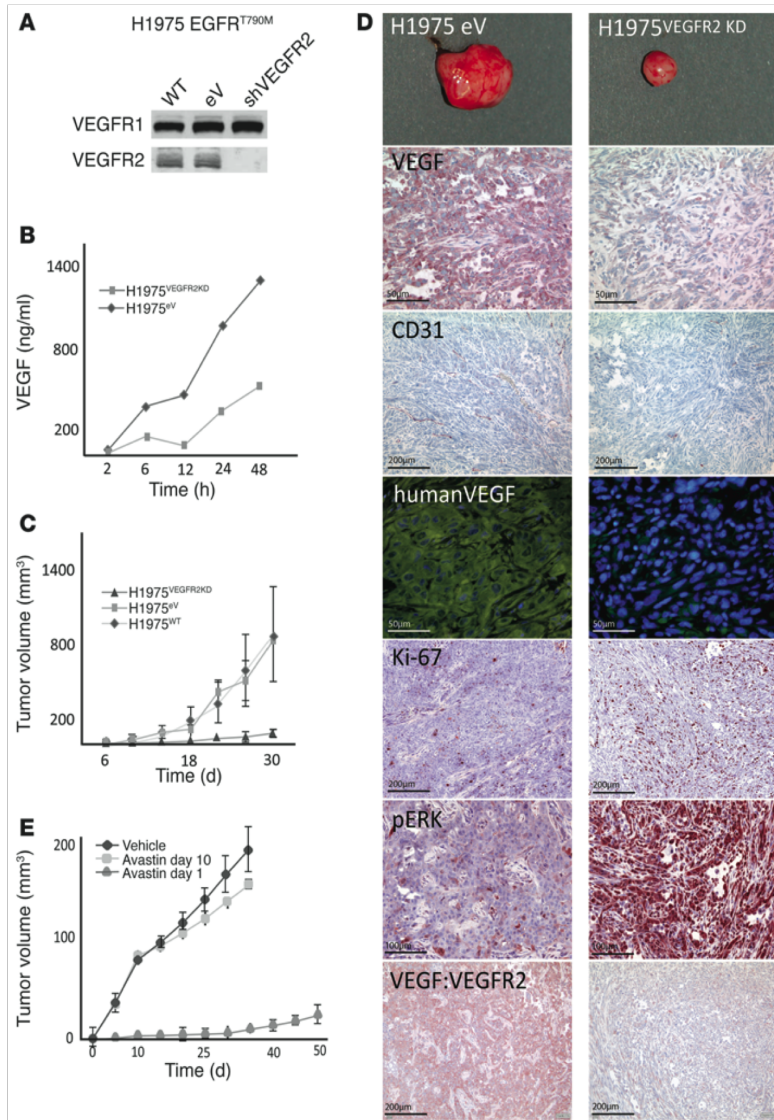
Figure 2
Requirement of autocrine VEGF/VEGFR2 signaling for induction of angiogenesis and tumor formation in vivo. (**A**) H1975 cells (WT cells) were stably transduced with lentiviral shRNA vectors targeting VEGFR2 (shVEGFR2) or with empty vector control (eV). Knockdown efficiency was determined by Western blotting (top panel, Flt1; bottom panel, VEGFR2). (**B**) Stable cell lines were cultured over time and quantified under normoxic conditions or exposed to hypoxia (1% O_2). VEGF secretion was determined over time by ELISA. (**C**) Stable cell lines were injected into nude mice, and tumor growth was monitored over time. (**D**) Tumors were harvested and stained for pan VEGF, CD31, human VEGF (using GFP-labeled Avastin), human VEGF complexed with VEGFR2, Ki67, pERK, and an antibody binding VEGF to VEGFR2. (**E**) H1975 cells were injected into nude mice and treated with Avastin or vehicle on day 1 and day 10 after tumor cell injections. Scale bar: 50 μm (VEGF, human VEGF); 100 μm (pERK); 200 μm (CD31, Ki67, VEGF:VEGFR2).

tumor cell inoculation. In concordance with the results obtained with VEGFR2-knockdown cells, concomitant VEGFR2 inhibition in NSCLC-H1975 tumors expressing high levels of VEGFR2 completely abrogated the establishment of tumors in vivo (Figure 1H), paralleled by a strong reduction in tumor vessel density (Supplemental Figure 5F). This blocking of tumor growth can be attributed to inhibition of VEGFR2, as the introduction of the resistance mutation VEGFR2^{V916M} in the H1975 cells was sufficient to abrogate the ZD6474-mediated treatment effect (Figure 1H). In contrast, tumor cells with low levels of VEGFR2 expression, such as H1650 and A549, were unaffected by concomitant VEGFR2 inhibition (Supplemental Figure 5E). In the same manner, treatment of mice with bevacizumab at the same time of tumor cell inoculation abrogated the establishment of tumors in vivo (Figure 2E). In summary, the VEGF:VEGFR2 feed-forward loop is active in tumor cells expressing high levels of VEGFR2 in vivo and is

required for the establishment of fully angiogenic tumors, and its disruption (either by VEGFR2 inhibition or blockade of VEGF) is sufficient to completely prevent tumor formation in vivo.

VEGF:VEGFR2 feed-forward loop is active in primary human lung adenocarcinomas. We next performed immunohistochemical analysis of VEGF and VEGFR2 in 117 surgically resected primary human lung adenocarcinomas (Figure 3A), revealing that VEGF expression correlated significantly with expression of VEGFR2 on the same tumor cells ($P = 2.612 \times 10^{-5}$) as well as with microvessel density ($P = 2.2 \times 10^{-11}$; Table 1 and Supplemental Figure 6). This indicates that activation of the autocrine VEGF/VEGFR2 signaling loop is a feature of highly angiogenic lung adenocarcinomas. Finally, staining of representative tumors with an antibody specifically recognizing VEGF bound to VEGFR2 confirmed that, in the tumors with coexpression of VEGF and VEGFR2, VEGF was indeed bound to VEGFR2 on tumor cells (Figure 3B). Moreover, adenocarcinomas
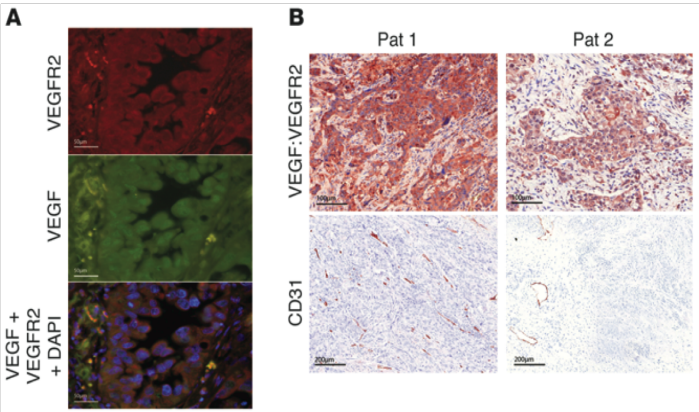
research article

Figure 3
The VEGF:VEGFR2 feed-forward loop in primary human lung adenocarcinomas. (**A**) Human adenocarcinomas were immunofluorescently stained to reveal coexpression of VEGF and VEGFR2 by the same tumor cell population. Scale bar: 50 μm. (**B**) A representative patient (Pat 1) with an high angiogenic phenotype represented by high VEGF:VEGFR2 staining and high levels of CD31-positive cells. In contrast, another patient (Pat 2) presents a low angiogenic phenotype, with only moderate levels of VEGF:VEGFR2–positive tumor cells, corresponding to a low density of CD31-positive cells. Scale bar: 100 μm (top panels); 200 μm (bottom panels).

that exhibited coexpression and autocrine binding of VEGF and VEGFR2 presented a highly angiogenic phenotype (Figure 3B). These results support a critical function for the VEGF:VEGFR2 feed-forward loop in primary lung tumors in patients.

Inhibition of VEGFR2 induces ERK signaling and sensitizes to MAPK inhibition. To our surprise, we found that H1975[VEGFR2KD] tumors exhibited increased levels of Ki67- and pERK-positive cells compared with H1975[eV] tumors (Figure 2D). In the same manner, VEGF stimulation in vitro reduced pERK signaling that was again increased upon ZD6474 treatment (Figure 1F and Supplemental Figure 3A). Consistent with the in vitro data presented above, ZD6474 treatment induced inhibition of pS6 and an increase in pERK in vivo (Supplemental Figure 7E). We thus hypothesized that inhibiting the VEGF:VEGFR2 feed-forward loop results in activation of the ERK signaling pathway and thereby appears to induce a ERK-dependant proliferative phenotype. Recently, Rosen and colleagues described a negative feedback regulation of IGF signaling via mTOR and its transcriptional regulation of FOXO transcription factors (18). In line with these findings, we observed that inhibiting the VEGF/VEGFR2/mTOR autocrine feed-forward loop enhanced ERK signaling, as a result of activation of the insulin growth factor receptor (IGFR) signaling pathway via IRS-1 (Figure 4, C and D). This activation of ERK was mediated by increased FOXO levels upon inhibition of VEGFR2/mTOR signaling (Figure 4D). Remarkably, combined inhibition of ERK signaling by PD0325901 and VEGFR2 resulted in a dramatic reduction of tumor cell proliferation, as indicated by [18F]FLT PET data, and, finally, in complete tumor shrinkage in vivo (Figure 4, A and B, and Supplemental Figure 7, A and B). In order to confirm our findings on tumor response after combined PD0325901 and ZD6474 treatment in an orthotopic tumor model, we applied a murine *Ras*-mutated lung cancer model expressing VEGFR2 on tumor cells (Figure 5 and Supplemental Figure 7H). In accordance with our xenograft data, combined PD0325901 and ZD6474 treatment resulted in substantial tumor regression, as detected by bioluminescence imaging (BLI) (Figure 5). These findings support the hypothesis of a recent study that combined MEK and VEGFR inhibition enhances inhibition of tumor growth (19). Of note, complete tumor shrinkage was associated with the expression levels of VEGFR2 on tumor cells. In line with our hypothesis, NSCLC-H1650 and A549, which express only low levels of VEGFR2, did not respond to combined ZD6474 and PD0325901 treatment (Supplemental Figure 7, C and D).

Discussion

We have identified a VEGF:VEGFR2 feed-forward loop in NSCLC cells expressing VEGFR2 that leads to a signal amplification and a boost in VEGF secretion, which is required for establishment of fully angiogenic tumors in vivo. This VEGF/VEGFR2 signaling cascade via VEGFR2/PI3K/mTOR induces a mTOR-dependent regulation of VEGF secretion (13). VEGF secretion is induced by the upregulation of HIF-1α, which has been shown to be specific to mTORC1 and unaffected by the status of mTORC2 (20). This is supported by our observation that mTORC1 inhibition with rapamycin can prevent elevated VEGF expression induced by the feed-forward loop. Treatment with Torin1, an inhibitor of TORC1 and TORC2, did not further reduce VEGF levels in comparison to rapamycin (Supplemental Figure 2B). Thus, our data strongly support that VEGFR2/mTOR-induced VEGF secretion is mediated via mTORC1.

Table 1
Tissue microarrays of 117 lung adenocarcinomas

Intensity	0	1	2	3
VEGFR2 intensity[A]				
VEGF intensity 0	0	1	0	1
VEGF intensity 1	0	11	8	1
VEGF intensity 2	0	10	42	16
VEGF intensity 3	0	0	13	10
CD31 intensity[B]				
VEGF intensity 0	0	0	2	0
VEGF intensity 1	0	17	3	0
VEGF intensity 2	0	13	52	3
VEGF intensity 3	0	3	9	11
VEGFR2 intensity[C]				
CD31 intensity 0	0	0	0	0
CD31 intensity 1	0	11	19	3
CD31 intensity 2	0	11	35	20
CD31 intensity 3	0	0	9	5

Tissue microarrays of 117 lung adenocarcinomas were stained with antibodies recognizing human VEGFR2, VEGF, and CD31. Association of staining intensity, scored on a 0–3 scale, of the different antibodies in the same cohort is given in χ^2 tables. Levels of significance were determined using Fisher's exact test. [A]$P = 2.612 \times 10^{-5}$; [B]$P = 2.2 \times 10^{-11}$; [C]$P = 0.01512$.

107
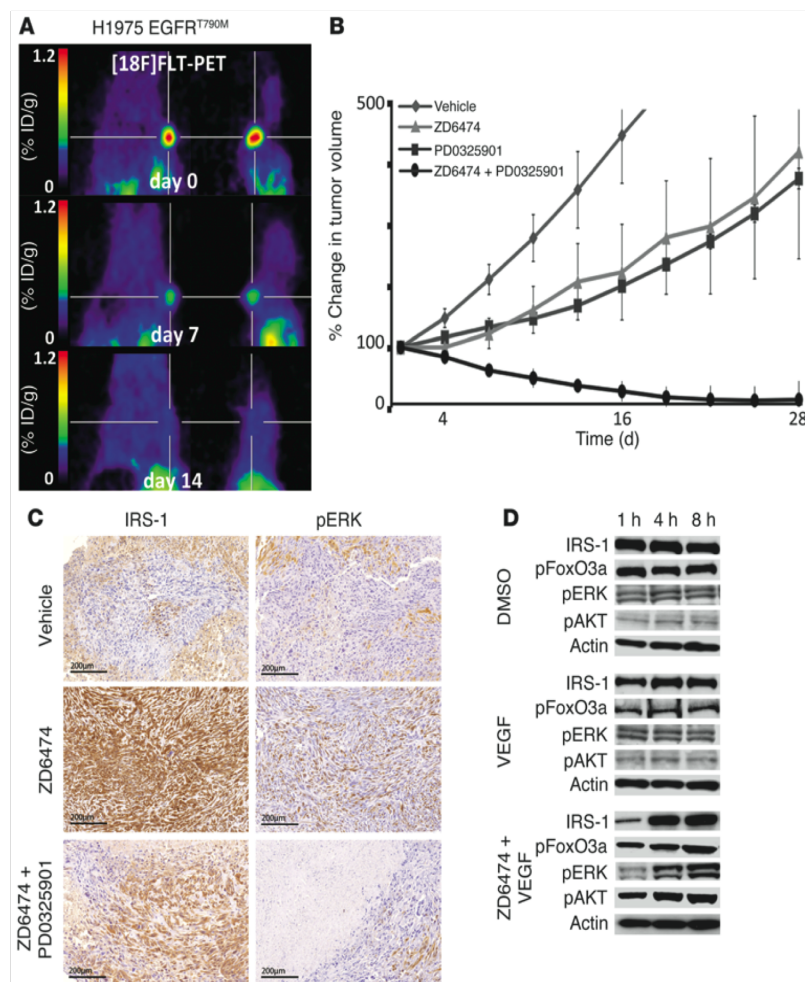
Figure 4
Combined inhibition of VEGFR2 and ERK signaling results in dramatic tumor shrinkage. (**A**) H1975 cells were engrafted subcutaneously in nude mice; mice with established tumors were treated with a combination of ZD6474 plus PD0325901, and [18F]FLT-PET imaging was performed on day 0 (before treatment) and at the indicated time points after treatment. Representative imaging results are shown. ID, injected dose. (**B**) Tumor size of subcutaneously grown H1975 tumors was determined at the indicated time points under treatment with vehicle, ZD6474 alone, PD0325901 (12 mg/kg) alone, or a combination of PD0325901 plus ZD6474. (**C** and **D**) Impact of ZD6474 treatment on feed-forward activation of insulin receptor signaling was determined (**C**) by IHC and (**D**) by Western blots using the indicated antibodies. Scale bar: 200 μm.

Our study supports a model wherein tumor cell-autonomous autocrine VEGF signaling loops form an integral part of the early phase of tumor development, promoting blood supply through angiogenesis. Consistent with this notion, we hypothesize that tumor cells reduce the proliferation in a VEGF/VEGFR2–dependent manner as long as the nutrient supply remains decreased. This hypothesis is confirmed by our finding that inhibition of VEGFR2/mTOR signaling results in a time-dependent feedback activation of IRS/MAPK signaling (18). Interrupting the VEGF:VEGFR2 feed-forward loop induces a therapeutically relevant dependency on MAPK signaling in vivo. As a consequence, combined inhibition of VEGFR2 and ERK signaling results in substantial tumor shrinkage in tumors in which this VEGF:VEGFR2 feed-forward loop is active. Our findings provide a potential mechanism for synergistic treatment effects of combined VEGFR2 and MAPK inhibition by PD0325901 and ZD6474. Finally, we have found that about 20% of patients with lung cancer show high tumor cell VEGFR2 expression, which correlates with a highly angiogenic phenotype. We therefore propose that high expression of VEGF:VEGFR2 on tumor cells could serve as a predictive marker for therapeutic efficacy of dual VEGFR2/MEK inhibition in patients with lung cancer. In summary, this study demonstrates the existence of a novel autocrine VEGF/VEGFR2 signaling loop, which amplifies VEGF secretion by tumor cells and is required to provide a switch for development of fully angiogenic tumors in vivo.

Methods

VEGFR2 expression in NSCLC cell lines. VEGFR2 expression data for the 53 NSCLC cell lines were obtained using Affymetrix U133A arrays (http://www.ncbi.nlm.nih.gov/geo/query/acc.cgi?acc=GSE14925). RNA extraction, hybridization, and scanning of arrays were performed using standard procedures. CEL files from U133A arrays were preprocessed as described previously (21).

Cell lines and reagents. NSCLC cell lines, H441, H1975, A549, and H1650, were maintained in RPMI medium with 10% FCS and 1% (penicillin plus streptomycin) antibiotic. VEGF was purchased from Tebu-bio GmbH, ZD6474 was purchased from AstraZeneca, rapamycin was purchased from LC Labs, Torin 1 was purchased from Tocris Bioscience, and PK90 was purchased from Axon Medchem. Compound stocks were stored at –20°C and dissolved in DMSO or vehicle solution in a rotating device at 4°C for animal therapy.

research article
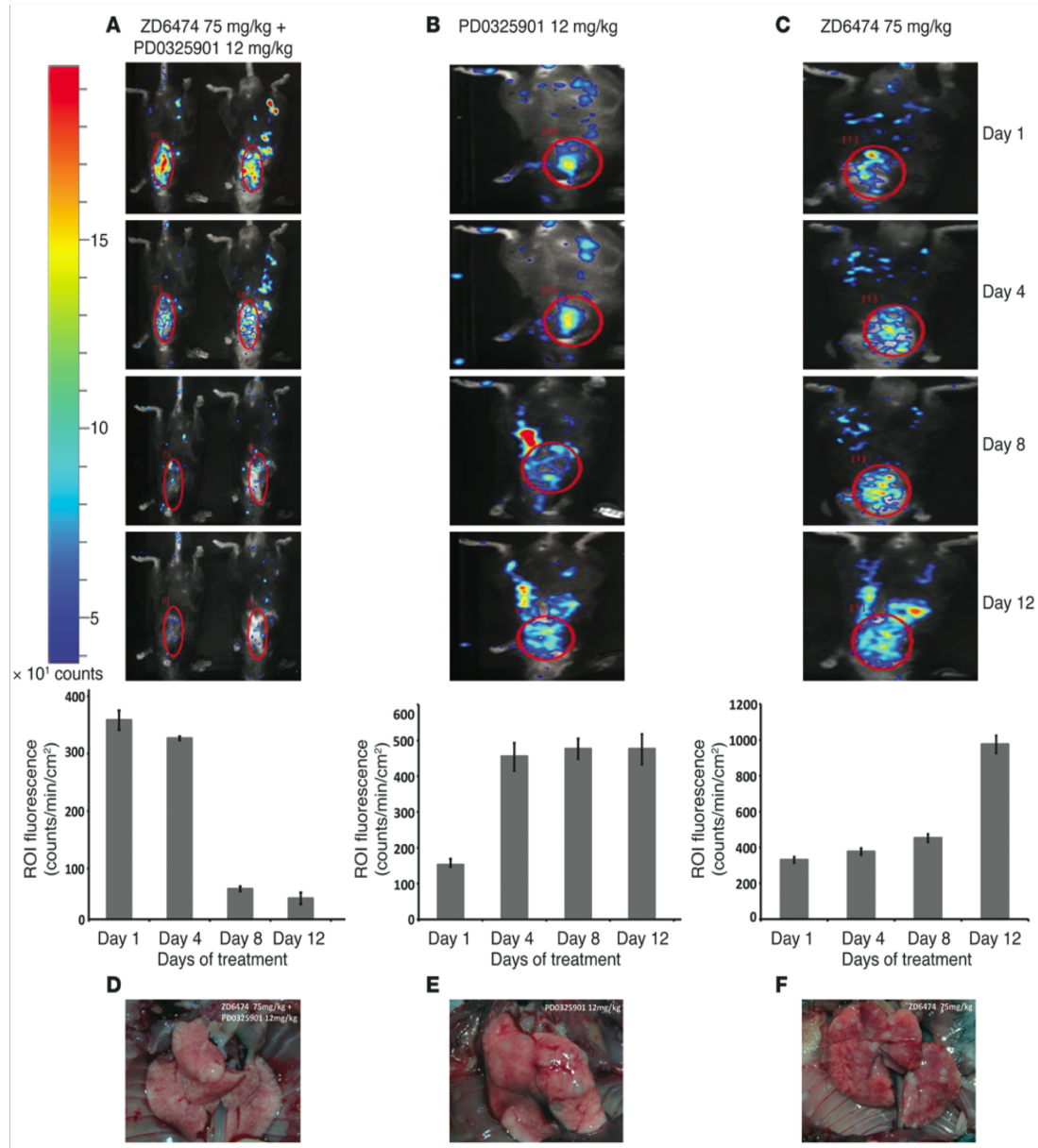
Figure 5
Combined inhibition of VEGFR2 and ERK signaling induces tumor shrinkage in an orthotopic Kras^{Val12}-driven murine lung lung cancer model (RasLo). (**A–C**) Kras^{Val12}-driven orthotopic murine lung tumors were induced; mice with Luc-positive tumors were treated, and BL imaging was performed on day 0 (before treatment) and at the indicated time points after treatment. Mice were treated with vehicle, ZD6474 alone, PD0325901 (12 mg/kg) alone, or a combination of PD0325901 plus ZD6474. The scale bar represents the luciferase activity in detected counts (photons/s/cm2/steradian × 10; red, high; blue, low). Graphs show quantification of change in BLI based on ROI analysis. (**D–F**) Images show representative lungs ex vivo, with macroscopic lung tumors in mice treated with (**E**) PD0325901 or (**F**) ZD6474 only.

Lentiviral RNAi, retroviral expression, and stable transduction. The VEGFR2 V916M mutation was introduced into H1975 cells using a pBABE vector by site-directed mutagenesis. Replication-incompetent retroviruses were produced by cotransfection with the pCL ampho plasmid in HEK 293T cells (Orbigen) using TRANS-IT (Mirus). Hairpins targeting the different genes were ordered from Sigma-Aldrich. Replication-incompetent lentiviruses were produced from *pLKO.1* vector (www.broad.mit.edu/genome_bio/trc/) by cotransfection with *Δ8.9* and *pMGD2* in HEK 293T cells (www.broadinstitute.org/rnai/trc/lib) using TRANS-IT. Cells were transduced in the presence of polybrene. After transduction, cells were selected with puromycin.

Western blotting. Western blotting was performed using the following antibodies: β-actin (clone C4) (MPBiomedicals LLC); pAKT (S473), AKT, pS6K, S6K, IRS-1, pERK, ERK, pVEGFR2, VEGFR2, VEGFR1, and pFoxO3a (all from Cell Signaling Technology); and anti-rabbit-HRP and anti-mouse-HRP antibodies (all from Millipore).

Immunoprecipitation. Protein A/G PLUS-Agarose Beads (Santa Cruz Biotechnology Inc.) were washed twice in PBS and resuspended in 500 μl of lysis buffer. Anti-phosphotyrosine antibody (clone 4G10) (Millipore), diluted 1:50, was added and incubated overnight in a rotating chamber at 4°C. Tubes were centrifuged at 1,000 *g* for 1 minute and washed 3 times in ice-cold PBS. 500 μg of cell lysate was added, and the volume of the tube was filled up to 1 ml with lysis buffer. Tubes were incubated in a similar manner and were centrifuged and washed as described above. After removing the supernatant, beads were resuspended in ×4 NuPage LDS buffer (Invitrogen) and heated at 80°C for 10 minutes. Supernatant was carefully pipetted and loaded in a gel for Western blotting. pVEGFR2 was used as the primary antibody.

ELISA assay. Cells were plated in 6-well plates and incubated for 24 hours in starving media. Cells were then stimulated with 40 ng VEGF-A 165 either alone or after pretreatment with the VEGFR2 inhibitor ZD6474 (1 μM) or with rapamycin (100 nM) for 4 hours. Secretion of VEGF into cell culture supernatants was measured with the VEGF Human ELISA Kit from Tebu-Bio GmbH (catalog no. ELH-VEGF-001) according to the manufacturer's instructions.

Flow cytometry. Cells were plated in 6-well plates and incubated for 24 hours in starving media. Cells were then either treated with DMSO or stimulated with 40 ng VEGF-A 165 alone or after pretreatment with ZD6474 (0.5 and 1 μM) for 4 hours. The incorporated BrdU was stained with specific anti-BrdU fluorescent antibodies. All protocols were performed according to instructions for the BrdU Flow Kit from BD Pharmingen (catalog no. 559619). The levels of cell-associated BrdU were then measured on a Gallios Flow Cytometer from Beckman Coulter. Results were calculated using Gallios FACS software.

PET and BLI. Nude mice bearing macroscopic H1975[WT] tumors were treated daily with an oral gavage of 75 mg/kg ZD6474 and investigated using a FOCUS microPET Scanner (Concord Microsystems Inc.). [18F]FLT and [11C]MET were synthesized as described previously (22). No-carrier-added [18F]FLT and [11C]MET were administered i.v. (tail vein) into experimental animals with a dose of 200 μCi per mouse and 400 μCi per mouse, respectively. [18F]FLT PET and [11C]MET PET imaging were performed 60 minutes and 20 minutes after injection, respectively. Evaluation of data was based on a ROI analysis of the entire tumor using in-house software (VINCI). For data analysis, we used the maximal voxel radioactivity within the tumors. The mediastinum was chosen as a reference for determination of uptake ratio, since we observed constant uptake for [18F]FLT and [11C]MET in this region. The heart was used as a reference for calculation of the [15O]H$_2$O. All data were decay corrected.

Analysis of luciferase gene expression was performed using an optical imaging system (Biospace). For bioluminescence detection, mice were injected intraperitoneally with D-luciferin (4 mg per animal in 200 μl PBS), and images were acquired 10 minutes after luciferin injection. Evaluation of data was performed using ROI analysis of BLI images to determine maximum values in photons. Data were background subtracted.

Mouse models. All animal procedures were approved by the local animal protection committee and the local authorities. For each tumor xenograft, 5×10^6 cells from individual cell lines suspended in plain RPMI were injected subcutaneously into male nude mice. Mice (with established tumors [70 mm^3] or 1 day after tumor cell inoculation) were treated daily by oral gavage of ZD6474 (75 mg/kg, dissolved in sterile, deionized water with 1% Tween 80), PD0325901 (12 mg/kg, dissolved in propylene glycol/water [1:1]), the combination of ZD6474 (75 mg/kg) and PD0325901 (12 mg/kg), or vehicle

alone. Avastin treatment was given i.p. (twice a week, 5 mg/kg). Tumor size was monitored by measuring perpendicular diameters. Tumor volumes were calculated by determination of the largest diameter and its perpendicular according to the following equation: tumor volume = $a \times (b^2/2)$, where a represents the largest diameter and b represents the perpendicular diameter.

The *RasLO* construct is under the β-actin promoter followed by a STOP codon flanked by *LoxP* sites. Human mutated *Kras*[Val12] and a fusion molecule consisting of ovalbumin, S-tag, and luciferase are expressed after excision of the STOP codon by Cre-recombinase encoded in adenoVirus. Tumor formation was then noninvasively monitored by BLI (Biospace). In order to induce tumor growth specifically in the lung, 10^7 PFUs of adeno-Cre were applied intranasally in *RasLO* genotyped positive mice between 6 to 8 weeks old that had been previously anesthetized with ketamine.

Tumor samples and immunohistochemistry. All tumor samples were received from the CIO Biobank at the Institute of Pathology, University of Bonn, Bonn, Germany. All tumors were clinically and pathologically identified as being the primary and only neoplastic lesion and classified according to WHO guidelines. Briefly, 3-μm-thick sections of FFPE tumors were deparaffinized, and antigen retrieval was performed by boiling the section in citrate buffer at pH 6 or EDTA at pH 9 for 20 minuets. Primary antibodies used were as follows: VEGF (sc-152, 1:100, pH 6, Santa Cruz Biotechnology Inc.), VEGF (bevacizumab, 1:100, pH 6, Roche; secondary anti-human IgG-FITC, Dako), CD31 (SZ31, 1:50, pH 6, Dianova), VEGFR2 (no. 2479, 1:200, pH 9, Cell Signaling Technology), Ki67 (mib-1, 1:100, pH 6, Thermo Scientific), pERK (no. 4376, 1:50, pH 6, Cell Signaling Technology), pMAPK (no. 4631, 1:50, pH 6, Cell Signaling Technology), IRS-1 (ab40777, 1:50, pH 6, Abcam), VEGF:VEGFR 2 (GV39M, 1:2, culture supernatant) (16), and HIF-1α (1:300, Cell Signaling Technology). Corresponding secondary antibody detection kits for reduced background on murine tissue were used (Histofine Simple Stain Mouse MAX PO, medac) and stained on an automated stainer (LabVision Autostainer 480S, Thermo Scientific). VEGF and VEGFR2 immunofluorescence was performed using the same primary antibodies and secondary antibodies. Staining intensities were individually evaluated by 3 independent observers, using a 4-tier scoring system. Statistical analysis was performed using a Fisher's exact test.

Statistics. Fisher's exact tests were performed using R version 2.7.1 (http://www.r-project.org/). A level of significance of $P < 0.05$ was chosen. Data are presented as mean ± SD in all figure panels in which error bars are shown.

Study approval. All animal procedures were in accordance with the German laws for animal protection and were approved by the local animal care committee and local governmental authorities (Recklinghausen, Germany).

Address correspondence to: Roland Ullrich, Max Planck Institute for Neurological Research, with Klaus-Joachim-Zülch Laboratories

of the Max Planck Society and the Medical Faculty of the University of Cologne, Gleueler Strasse 50, 50931 Cologne, Germany. Phone: 49.221.47262.306; Fax: 49.221.4726.298; E-mail: ullrich@nf.mpg.de.

Roman K. Thomas, Martin Peifer, and Mirjam Koker's present address is: Department of Translational Genomics, University of Cologne, Cologne, Germany.

1. Baeriswyl V, Christofori G. The angiogenic switch in carcinogenesis. *Semin Cancer Biol*. 2009; 19(5):329–337.
2. Carmeliet P. Mechanisms of angiogenesis and arteriogenesis. *Nat Med*. 2000;6(4):389–395.
3. Lee TH, et al. Vascular endothelial growth factor mediates intracrine survival in human breast carcinoma cells through internally expressed VEGFR1/ FLT1. *PLoS Med*. 2007;4(6):e186.
4. Chung GG, et al. Vascular endothelial growth factor, FLT-1, and FLK-1 analysis in a pancreatic cancer tissue microarray. *Cancer*. 2006; 106(8):1677–1684.
5. Silva SR, et al. VEGFR-2 expression in carcinoid cancer cells and its role in tumor growth and metastasis. *Int J Cancer*. 2011;128(5):1045–1056.
6. Lichtenberger BM, Tan PK, Niederleithner H, Ferrara N, Petzelbauer P, Sibilia M. Autocrine VEGF signaling synergizes with EGFR in tumor cells to promote epithelial cancer development. *Cell*. 2010; 140(2):268–279.
7. Yang F, et al. Increased VEGFR-2 gene copy is associated with chemoresistance and shorter survival in patients with non-small-cell lung carcinoma who receive adjuvant chemotherapy. *Cancer Res*. 2011; 71(16):5512–5521.
8. Wedge SR, et al. ZD6474 inhibits vascular endothelial growth factor signaling, angiogenesis, and tumor growth following oral administration. *Cancer Res*. 2002;62(16):4645–4655.
9. Pao W, et al. Acquired resistance of lung adenocarcinomas to gefitinib or erlotinib is associated with a second mutation in the EGFR kinase domain. *PLoS Med*. 2005;2(3):e73.
10. Shields AF, et al. Imaging proliferation in vivo with [F-18]FLT and positron emission tomography. *Nat Med*. 1998;4(11):1334–1336.
11. Blencke S, et al. Characterization of a conserved structural determinant controlling protein kinase sensitivity to selective inhibitors. *Chem Biol*. 2004; 11(5):691–701.
12. Fuchs BC, Bode BP. Amino acid transporters ASCT2 and LAT1 in cancer: partners in crime? *Semin Cancer Biol*. 2005;15(4):254–266.
13. Brugarolas JB, Vazquez F, Reddy A, Sellers WR, Kaelin WG. TSC2 regulates VEGF through mTOR-dependent and -independent pathways. *Cancer Cell*. 2003;4(2):147–158.
14. Kanai Y, Segawa H, Miyamoto K, Uchino H, Takeda E, Endou H. Expression cloning and characterization of a transporter for large neutral amino acids activated by the heavy chain of 4F2 antigen (CD98). *J Biol Chem*. 1998;273(37):23629–23632.
15. Vasudevan KM, et al. AKT-independent signaling downstream of oncogenic PIK3CA mutations in human cancer. *Cancer Cell*. 2009;16(1):21–32.
16. Brekken RA, Huang X, King SW, Thorpe PE. Vascular endothelial growth factor as a marker of tumor endothelium. *Cancer Res*. 1998;58(9):1952–1959.
17. Laking GR, Price PM. Positron emission tomographic imaging of angiogenesis and vascular function. *Br J Radiol*. 2003;1:S50–S59.
18. O'Reilly KE, et al. mTOR inhibition induces upstream receptor tyrosine kinase signaling and activates Akt. *Cancer Res*. 2006;66(3):1500–1508.
19. Takahashi O, et al. Combined MEK and VEGFR inhibition in orthotopic human lung cancer models results in enhanced inhibition of tumor angiogenesis, growth, and metastasis. *Clin Cancer Res*. 2012; 18(6):1641–1654.
20. Duvel K, et al. Activation of a metabolic gene regulatory network downstream of mTOR complex 1. *Mol Cell*. 2010;39(2):171–183.
21. Sos ML, et al. Predicting drug susceptibility of non-small cell lung cancers based on genetic lesions. *J Clin Invest*. 2009;119(6):1727–1740.
22. Ullrich R, et al. Glioma proliferation as assessed by 3'-fluoro-3'-deoxy-L-thymidine positron emission tomography in patients with newly diagnosed high-grade glioma. *Clin Cancer Res*. 2008; 14(7):2049–2055.

111

Transient Antiangiogenic Treatment Improves Delivery of Cytotoxic Compounds and Therapeutic Outcome in Lung Cancer

Sampurna Chatterjee[1,2,3], Caroline Wieczorek[1,2,3], Jakob Schöttle[1,2,3], Maike Siobal[1,2,3], Yvonne Hinze[4], Thomas Franz[4], Alexandra Florin[5], Joanna Adamczak[2], Lukas C. Heukamp[5], Bernd Neumaier[2], and Roland T. Ullrich[1,2,3]

Abstract

Extensive oncologic experience argues that the most efficacious applications of antiangiogenic agents rely upon a combination with cytotoxic drugs. Yet there remains a lack of clarity about how to optimize scheduling for such drug combinations. Prudent antiangiogenic therapy might transiently normalize blood vessels to improve tumor oxygenation and drug exposure. Using $[^{15}O]H_2O$ positron emission tomography imaging in a preclinical mouse model of non–small cell lung cancer, we observed that short-term treatment with the vascular endothelial growth factor receptor/platelet-derived growth factor receptor inhibitor PTK787 licensed a transient window of improved tumor blood flow. The improvement observed was associated with a reduced leakiness from tumor vessels, consistent with induction of a vascular normalization process. Initiation of a cytotoxic treatment in this window of tumor vessel normalization resulted in increased efficacy, as illustrated by improved outcomes of erlotinib administration after initial PTK787 treatment. Notably, intermittent PTK787 treatment also facilitated long-term tumor regression. In summary, our findings offer strong evidence that short-term antiangiogenic therapy can promote a transient vessel normalization process that improves the delivery and efficacy of a targeted cytotoxic drug. *Cancer Res; 74(10); 2816–24. ©2014 AACR.*

Introduction

Solid tumors cannot grow without access to and recruitment of blood vessels (1, 2). Tumor vessels are characterized by a leaky, disorganized, and abnormal phenotype (3). This leakiness leads to extravasation of plasma proteins, resulting in a high interstitial fluid pressure within tumors that interferes with the delivery of drugs (4). Moreover, this abnormal phenotype of tumor vasculature supports tumor progression and resistance to treatment. The goal of antiangiogenic treatment is to inhibit tumor vessel growth, thus abrogating the delivery of nutrients and oxygen to the tumor. Antiangiogenic compounds target either angiogenic growth factors such as bevacizumab (anti-VEGF) or receptor kinases that are known to regulate tumor angiogenesis such as vascular endothelial

growth factor receptor (VEGFR) and platelet-derived growth factor receptor (PDGFR). However, recent data indicate that a reduction in tumor vessels induced by antiangiogenic treatment using an antibody against VEGFR2 (DC101) results in an inhibition of tumor growth but on the other hand permits tumor invasiveness (5). This increase in invasiveness is most probably because of elevated hypoxia within the tumor during antiangiogenic therapy (6).

Nevertheless there is strong evidence that transient application of antiangiogenic agents can "normalize" the abnormal tumor microvessels (7, 8). This prudent application of antiangiogenic therapy might result in effective uptake of drugs and oxygen in the tumor-enhancing cytotoxic therapeutic outcome in cancer therapy (4, 9). Moreover, structurally and functionally abnormal blood vessels impair blood flow into the tumor contributing to an aggressive hypoxic microenvironment rendering the tumor unresponsive to traditional cytotoxic treatment regimes (10).

Using MRI we could recently demonstrate that short-term antiangiogenic treatment with a small molecule protein kinase inhibitor Vatalanib (PTK787) results in a reduction of vessel leakiness (11). Based on these findings we speculate that antiangiogenic treatment induced normalization of tumor vessels might increase tumor blood flow and reduce interstitial fluid pressure (IFP). This reduction of the IFP and increase of tumor blood flow during antiangiogenic treatment might improve anticancer drug delivery and, thus, treatment efficacy (12).

Authors' Affiliations: [1]Clinic I of Internal Medicine and Center for Integrated Oncology, University Hospital Cologne; [2]Max Planck Institute for Neurological Research; [3]Center for Molecular Medicine; [4]Max Planck Institute for Biology of Aging; and [5]Institute of Pathology, University Hospital Medical School, Cologne, Germany

Corresponding Author: Roland T. Ullrich, Max Planck Institute for Neurological Research with Klaus-Joachim-Zülch Laboratories of the Max-Planck-Society and the Medical Faculty of the University of Cologne, 50931 Cologne, Germany. Phone: 49-221-4726-306; Fax: 49-221-4726-298; E-mail: ullrich@nf.mpg.de

American Association for Cancer Research

113

PTK787 (ZK 222584) and ZD6474 are potent inhibitors of VEGFR tyrosine kinases, PDGFRβ tyrosine kinase and c-Kit whereas ZD6474 in addition targets the EGF receptor (EGFR) and RET (13, 14). We here sought to apply a multimodal imaging approach to monitor tumor blood flow *in vivo* to assess the normalization window during prudent antiangiogenic treatment using the tyrosine kinase inhibitors PTK787 and ZD6474. Imaging tumor vessel normalization induced by prudent antiangiogenic treatment was used to improve drug delivery of targeted compounds such as erlotinib and GDC0941.

Materials and Methods

Cell lines and reagents

Non–small cell lung cancer (NSCLC) cell line H1975 was purchased from the American Type Culture Collection. PC9 was purchased from European Collection of Cell Cultures. Both cell lines were maintained in RPMI-1640 medium enriched with 10% FCS and 1% penicillin + streptomycin. ZD6474, PTK787, and erlotinib were purchased from LC labs and GDC0941 from Axon Medchem. Compound stocks were stored at $-20°C$ and dissolved in dimethyl sulfoxide *in vitro*. For *in vivo* studies, erlotinib was dissolved in 6% Captisol (CyDex Inc.) at a concentration of 9 mg/mL. GDC0941 was dissolved in MCT (0.5% methylcellulose with 0.2% Tween-80 in distilled water) at concentrations of 22.5 mg/mL (monotherapy) and 15 mg/mL (in combination with antiangiogenic therapy). ZD6474 and PTK787 were dissolved in sterilized, deionized water with 1% Tween 80 at a concentration of 10 mg/mL. All solutions were stored on a rotating device at 4°C for animal therapy.

Western blotting

Western blotting was performed as described previously (15). For Western blotting, the following antibodies were used: β-actin (clone C4; MPBiomedicals LLC), pEGFR, pAKT (S473), pERK (Cell Signaling Technology), anti-rabbit-horseradish peroxidase (HRP) antibody, and anti-mouse-HRP antibody (Millipore).

Immunofluorescence

Vascular leakage was assessed by intravenous injection of 0.1 mL 10 mg/mL FITC-dextran (200,000 kDa) from Sigma. After 30 minutes, mice were anesthetized followed by perfusion with 4% paraformaldehyde injected into the aorta via an incision in the left ventricle and washed one time with PBS. Blood and fixative passaged out via the right atrium. Tumor sections were collected and immersed in 30% sucrose solution until samples dropped to the bottom of the vials. A cold bath was prepared with dry ice and methanol. Tissue Tek wells were labeled and filled up with Jung tissue freezing medium (Leica Biosystems). Excess sucrose was removed from tissues and placed in the center of wells and frozen by floating them on the methanol bath. Blocks were stored at $-20°C$ and sliced at 10 to 20 μm on cryostat. Slides were dried at room temperature for at least 2 hours and stained with anti-mouse CD31 (1:25; BD Pharmingen), anti-pVEGFR-2 (1:300; Cell Signaling Technology), fixed and processed for analysis in a Biorevo (Keyence) BZ-9000 microscope.

Tumor samples and immunohistochemistry

All tumors were collected after perfusion, stored in 4% paraformaldehyde overnight, and transferred to PBS. Tissues were embedded in paraffin following standard protocol and stained with primary antibodies as follows: mouse CD31 (1:25; BD Pharmingen), cleaved caspase-3 (1:750; Cell Signaling), pAKT (1:25; Cell Signaling), and α-smooth muscle actin α-SMA (1:50; Abcam) for marking pericytes. Corresponding secondary antibody detection kits for reduced background on murine tissue were used (Histofine Simple Stain Mouse MAX PO; medac) and stained on an automated stainer (LabVision Autostainer 480 S; Thermo Scientific).

Xenograft experiments

All animal procedures were approved by the local animal protection committee and the local authorities (Bezirksregierung Köln). Eight weeks old healthy *nu/nu* athymic male mice weighing 30 g in an average were purchased from Janvier. Tumors were generated by subcutaneous injection of PC9 and H1975 tumor cells (5×10^5 cells/tumor). Tumor-bearing mice were treated by oral gavage with the following set-ups: PTK787 ($n = 8$ mice with 3 tumors/mouse) or ZD6474 ($n = 8$ mice with 3 tumors/mouse) 75 mg/kg daily as monotherapy, erlotinib 30 mg/kg daily as monotherapy ($n = 8$ mice with 3 tumors/mouse), GDC0941 75 mg/kg daily as monotherapy ($n = 8$ mice with 3 tumors/mouse), vehicle ($n = 5$ mice with 3 tumors/mouse), erlotinib 30 mg/kg ($n = 14$ mice with 3 tumors/mouse), or GDC0941 50 mg/kg ($n = 8$ mice with 3 tumors/mouse) pretreated with PTK787 and continued as monotherapy during indicated timespan. The size of tumors ranged between 70 and 125 mm^3. Monotherapy and vehicle of each drug was used as control. Tumor volume was recorded accordingly.

[^{15}O]H$_2$O/[^{18}F]FLT positron emission tomography imaging

Animals bearing macroscopic tumors were investigated on day 0 followed by start of treatment with PTK787 75 mg/kg or ZD6474 75 mg/kg daily, day 4, day 8, and day 18 using a FOCUS microPET scanner (Siemens Microsystems, Inc; max. transaxial resolution 1.3 mm). In total, 25 animals underwent [^{15}O]H$_2$O and [^{18}F]FLT imaging, each animal carried 3 tumors. The PTK787-treated group contained 15 animals, the vehicle-treated group 10 mice. All animals underwent positron emission tomography (PET) imaging at 4 different time points. Initially 32 animals were included in the study, 7 of 32 mice died during PET imaging. We calculated percentage changes in tracer uptake with day 0 as baseline for each time point and tumor. [^{15}O]H$_2$O PET imaging was performed before [^{18}F]FLT PET. [^{18}F]FLT PET was measured 1 hour after [^{15}O]H$_2$O PET. [^{15}O]H$_2$O was injected dynamically via tail vein and PET images were acquired for 2 minutes after injection of 400 μCi/mouse. [^{18}F]FLT was administered intravenously (200 μCi/mouse). PET imaging was performed 60 minutes after injection (16). Data evaluation was performed using in-house VINCI software. Data evaluation was based on a region of interest (ROI) analysis. For data analysis we used the maximal and the mean voxel radioactivity of the defined ROI within the tumors. The

size of tumors ranged between 70 and 125 mm^3. The mediastinum was chosen as a reference for determination of uptake ratio, because we observed constant uptake for [^{18}F]FLT in this region. The heart was used as reference for calculation of the [^{15}O]H$_2$O. All data were decay corrected.

Mass spectrometry

For absolute quantification of erlotinib and OSI-420 in positive ESI MRM (multi reaction monitoring) mode, a Acquitiy UPLC/Xevo TQ (Waters) with MassLynx and absolute quantification TargetLynx (Waters) were used. An Acquity UPLC BEH C18 1.7 μm, 2.1 × 50 mm column was used at 25°C. Solvent A was 0.1% formic acid (Biosolve) and B acetonitrile (Biosolve). A linear gradient from 95% A to 5% in 4.10 min at a flow rate of 0.4 mL/min was used. The following MRM transitions were used for erlotinib m/z 394.03 (M+H$^+$)$^+$ to 277.95 (quantifier), m/z 394.03 to 303.95 (qualifier), m/z 394.03 to 335.94 (qualifier), for OSI-420 m/z 380.03 to 277.85 (quantifier), m/z 380.03 to 249.89 (qualifier), m/z 380.03 to 321.93 (qualifier). All compounds were fresh prepared during 2 months and dissolved in 0.1% formic acid (Biosolve) prepared with 0.22 μm MilliQ-Water. With erlotinib eluting at 2.94 minutes a standard calibration curve was calculated using following concentrations: 0.2, 0.5, 1, 5, 20, 50, 150, 300, 500, and 750 ng/mL (prepared individually from stock solutions 100 μg/mL). With OSI-420 eluting at 2.51 minutes a standard calibration curve was calculated using following concentrations: 0.1, 0.5, 1, 2, 4, 6, 8, and 10 ng/mL (prepared individually from stock solutions 100 μg/mL). Correlation coefficient: $r < 0.990$; response type: external standard, area; curve type linear; weighting 1/×. The peak integrations were corrected manually, if necessary. Quality control standards of each standard were used during sample analysis and showed between 0.5% and 40% deviation respectively. Blanks after the standards, quality control and sample batch proved to be sufficient. No carry over was detected.

Statistics

Fisher exact tests were performed using R version 2.7.1 (http://www.r-project.org). Data are presented as mean ± SD in all figures where error bars are shown. A level of significance of $P < 0.05$ was chosen (where mentioned).

Results

Short-term anti-VEGFR/PDGFR treatment induces a time window of improved blood flow into the tumor

We used the human lung cancer cell line PC9. PTK787 treatment improved tumor blood flow after 4 days of treatment by 12% (day 0: SD = 7.47, range = 22.42%; day 4: SD = 9.15, range = 35.04%), as determined by changes of maximal voxel activity in [^{15}O]H$_2$O PET ([^{15}O]H$_2$O; Fig. 1A, right and B). We could measure a steady and significant increase in tumor blood flow by 33.58% (day 8: SD = 5.52, range = 34.57%) until day 8 of treatment with PTK787 (P-value < 0.001) probably mediated by a transient normalization of vessels followed by a sharp decrease of 17.23% (day 18: SD = 12.63, range = 48.66%) till day 18. In contrast, blood flow decreased consistently from day 4 to day 8 by 20.42% (day 0: SD = 4.52, range = 9.39%; day 4: SD

= 4.67, range = 8.60%; day 8: SD = 5.58, range = 12.89%), and by 30.75% until day 18 (day 18: SD = 0.63, range = 10.53%) in the vehicle-treated tumors (Fig. 1A, left and B). Simultaneously, uptake of 3′-deoxy-3′-[^{18}F]-fluoro-L-thymidine, [^{18}F]FLT), a marker of proliferation (17), was increased by 51.08% from day 0 to day 4 (day 4: SD = 26.81, range = 527.31%) and by 76% form day 0 to day 8 (day 8: SD = 44.99, range = 532.67%; Supplementary Fig. S1A–S1C), suggesting that the cells continued to progress through the cell cycle. In concordance with the [^{18}F]FLT PET data, treatment of H1975 and PC9 cells with 10 or 20 μmol/L PTK787 did not reduce tumor cell proliferation *in vitro* (Supplementary Fig. S1D and S1E).

To investigate if improvement in blood flow can be also achieved by using other antiangiogenic agents, we used ZD6474, a tyrosine kinase inhibitor, that targets VEGFR2 and EGFR with additional activity against VEGFR3, VEGFR1, PDGFRβ, and the RET tyrosine kinase. We treated H1975 xenografts with ZD6474, which are resistant to EGFR inhibition because of the presence of T790M gatekeeper mutation of EGFR (15). There was an increase in blood flow by 21.39% (day 0: SD = 0.91, range = 10.12%; day 4: SD = 9.23, range = 38.58%, day 8: SD = 5.82, range = 30.15%) from day 0 to day 8 of ZD6474 treatment followed by a drop of 20.95% from day 0 to day 18. Vehicle-treated tumors displayed a stable decrease in blood flow by 8.95% from day 0 to day 8 and by 14.78% on day 18 (SD = 4.32, range = 12.11%; Supplementary Fig. S2A and S2B). Proliferation remained unaffected as measured by an increase in [^{18}F]FLT uptake by 67.1% from day 0 to day 4 (day 4: SD = 3.17, range = 193.5%) and by 78.02% form day 0 to day 8 (day 8: SD = 20.49, range = 675.8%; Supplementary Fig. S3A and S3B).

These data indicate that prudent anti-VEGFR/PDGFR treatment produces a short-lived time window of about 7 days when tumor vessels are transiently normalized, which can be monitored by an increase in blood flow by up to 50% into the tumor.

Short-time antiangiogenic treatment reduces leakiness and improves pericyte coverage in tumor blood vessels in xenografts

To elucidate if the improved blood flow into the tumors was indeed because of vessel normalization, permeability of the blood vessels were examined by fluorescence microscopy after tumor-bearing animals were perfused with FITC-dextran. Blood vessels of vehicle-treated tumors were dilated with aberrant morphologic pattern and displayed extensive leakiness associated with massive extravasation of FITC-dextran (Fig. 2A, left and Supplementary Fig. S3C) and correlated with high expression of CD31 and p-VEGFR2 (Fig. 2A, left). However, in tumors that were treated with PTK787 for 4 days, blood vessels showed strikingly reduced leakiness with almost no extravasation of FITC-dextran (Fig. 2A, right and Supplementary Fig. S3C) supported by 8-fold reduction in signal intensity (Fig. 2B) accompanied by diminished CD31 and p-VEGFR2 expression. (Fig. 2A, right). Tumor vasculature was characterized by abnormal and discontinuous pericyte lining of vessels as indicated by arrows on day 0 (Fig. 2C). Antiangiogenic treatment for 4 days transiently improved pericyte coverage in contrast to vehicle-treated tumors, which still exhibited incoherent pericyte coverage (Fig. 2C and Supplementary Fig.

Figure 1. Multimodal imaging of tumor blood flow using $[^{15}O]H_2O$ PET in xenografts (PC9). A, PET imaging was performed on nude mice with macroscopic subcutaneous tumors on day 0 (before start of therapy) and at the indicated time points after treatment with vehicle (left) and PTK787 (right). B, quantitative analysis of tumor blood perfusion before (day 0) and after 4, 8, and 18 days of PTK787 treatment (blue line) compared with vehicle sets (red line).
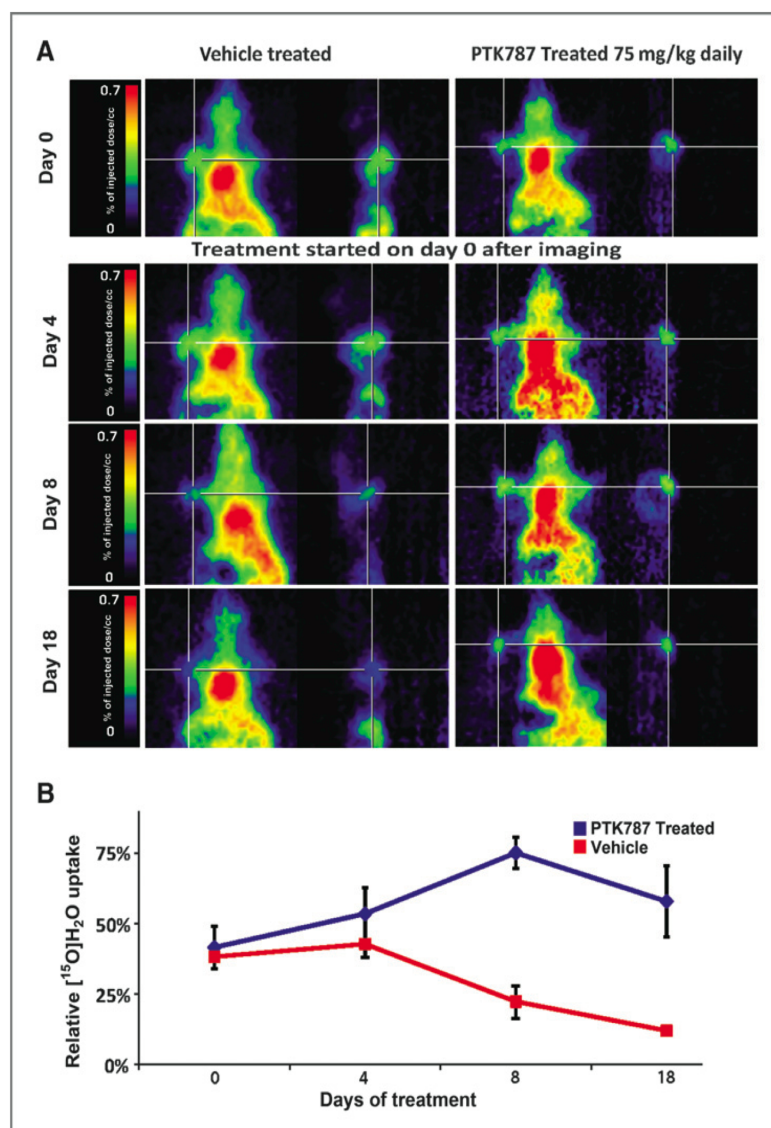
4A). PTK787 treatment also corrected the morphologic aberrations of the vessels with reduced tortuosity and improved maturity (Fig. 2C).

Pretreatment with antiangiogenic agents improves cytotoxic therapeutic outcome in NSCLC with enhanced delivery of erlotinib into the tumor

In the next step, we investigated if augmented blood flow induced by short-term antiangiogenic treatment had any improved therapeutic efficacy in NSCLC. Mice bearing macroscopic PC9 tumors were treated by an oral gavage of PTK787 (75 mg/kg daily) for 1 week. Because $[^{15}O]H_2O$ PET data indicated that tumor blood flow improves within a time window of 7 days of antiangiogenic therapy, erlotinib treatment was started within this "normalization window" from day 4 onward and continued as monotherapy for 13 days. Mice receiving erlotinib therapy pretreated with PTK787 had a sharp initial increase in tumor volume from 100% on day 1 to 221.28% (SD = 27.09, range = 162%) on day 4 followed by a massive reduction to 45.63% (SD = 7.11, range = 6.9%) on day 7, and finally almost complete shrinkage of tumor after 16 days of treatment (9.14% (SD = 3.2, range = 7.2%) of original mass left; Fig. 3A). Erlotinib as monotherapy restricted tumor proliferation, resulting in a slow reduction (up to 50% of tumor mass), but not as strong as with intermittent PTK787 treatment (P-value <
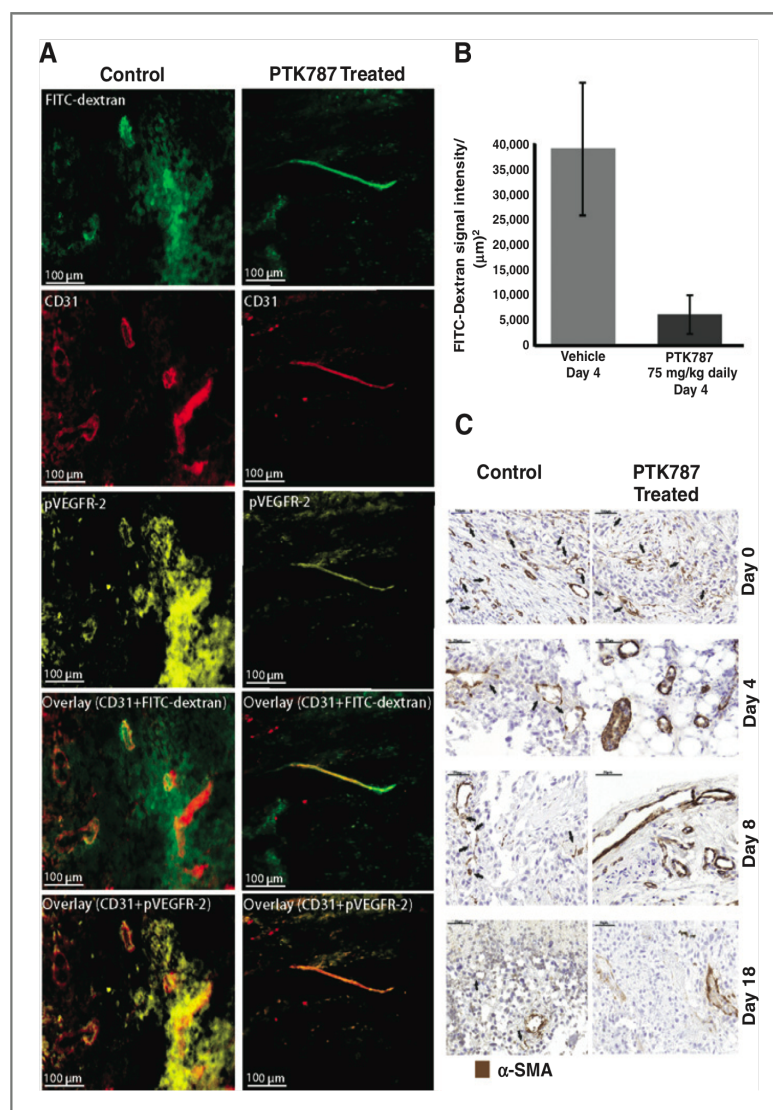
116

Figure 2. Blood vessel morphology and permeability. A, vascular leakage was assessed by intravenous injection of 0.1 mL 10 mg/mL FITC-dextran (200,000 kDa). Perfused tumors were collected and 10- to 20-μm-thick slices were stained with anti-mouseCD31 and anti-pVEGFR2 antibody, fixed and processed for microscopy control set (left) and PTK787-treated tumors (right). B, signal intensity of the total area of green staining (FITC-dextran) was quantified (4 fields per tumor in both control- and PTK787-treated groups). C, histology of tumors stained for α-SMA (brown, pericytes) comparing untreated vasculature (left) with PTK787 sets (right).

0.001; Fig. 3A). PTK787 monotherapy had similar effects like vehicle treatment (with an increase from 100% on day 1 to 245% and 220% (SD = 17.9, range = 38.8%) respectively on day 4; Fig. 3A).

To check if the normalized blood vessels were effectively delivering drugs into the tumors, we measured erlotinib concentration within the tumor via mass-spectrometric analysis. Under monotherapy with erlotinib, there was a slight improvement of the drug uptake into the tumor from day 1 (start of treatment) to day 4 by 20% (SD = 5.2, range = 34.16%; Fig. 3B). In contrast, tumors pretreated with PTK787 for 4 days displayed an increased erlotinib uptake by 140% (SD = 10.56, range = 35.64%) on the first day of erlotinib treatment (day 4), which improved up to 160% (SD = 11.04, range = 25.64%) on

day 8 (Fig. 3B). Monotherapy sets showed no further improvement in drug uptake, which was reduced by 42% (SD = 4.32, range = 23.72) on day 8 (Fig. 3B).

Western blot analysis of lysates from tumors treated with PTK787 and erlotinib showed an overtime decrease in pEGFR signal from day 1 to day 4 of treatment corresponding to pAKT and pERK levels (Fig. 3C). There was no change in signal intensity of pEGFR, pAKT, or pERK in the vehicle or monotherapy sets (PTK787 alone or erlotinib alone; Fig. 3C). Western blot analysis results correlated with histology where Ki67-positive cells were dramatically reduced in PTK787 pretreated tumors receiving erlotinib on day 1 compared with tumors receiving erlotinib as monotherapy on day 1 (Supplementary Fig. S4B). Ki67-positive cells were reduced further in number

Figure 3. Prudent antiangiogenic treatment improves delivery of erlotinib into the tumor and promotes therapeutic outcome. A, tumor volumes in nude mice were recorded over time under treatment with PTK787 (75 mg/kg), erlotinib (30 mg/kg), and PTK787 (75 mg/kg) + erlotinib (30 mg/kg) and vehicle control at indicated days. B, quantification of erlotinib uptake as measured by mass spectrometry in PTK787 pretreated tumors (blue column) between day 4 and 8 compared with uptake in the tumors receiving erlotinib just as monotherapy (four independent tumors from different mice per set-up). C, tumor lysates were prepared from different therapy modules (as indicated) and immunoblotted with phospho-specific antibodies. Representative Western blots are shown. D, histology of tumor samples from C comparing pAKT expression between erlotinib monotherapy and erlotinib pretreated with PTK787 tumors on day 0 (before start of treatment) and on indicated days after therapy. E, induction of apoptosis (cleaved caspase-3) in erlotinib monotherapy and erlotinib pretreated with PTK787 tumors on day 0 (before start of treatment) and on indicated days after therapy.
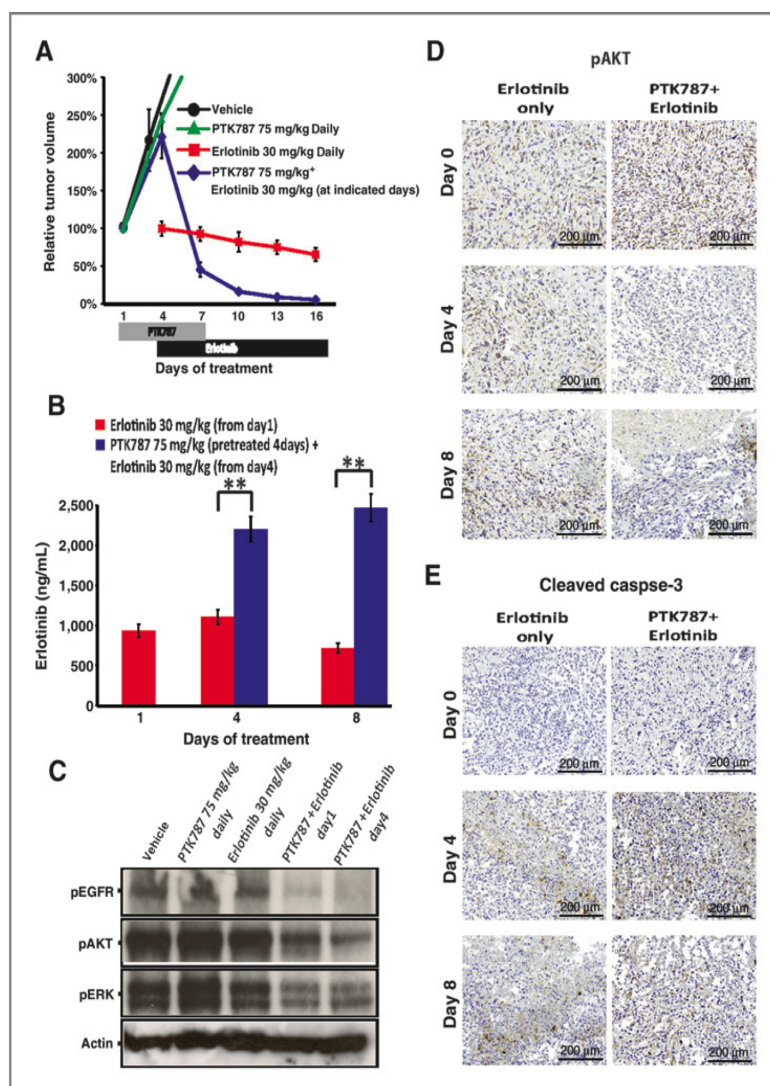
from day 0 to day 4 until only a few Ki67-positive cells were left on day 8 in the tumors receiving erlotinib pretreated with PTK787 (Supplementary Fig. S4B). Histology results also showed complete inhibition of pAKT from day 0 to day 4 in PTK787 pretreated tumors receiving erlotinib (Fig. 3D). pAKT levels remain inhibited on day 8 with induction of necrosis (Fig. 3D). Even though tumor cells were healthy in both sets on day 0 (Fig. 3E), heavy induction of apoptosis (cleaved caspase-3) was detected in tumors receiving erlotinib pretreated with PTK787 on day 4 (Fig. 3E, right), which remained consistent on day 8 (Fig. 3E, right). However, in erlotinib monotherapy sets, there was only moderate induction of apoptosis overtime (Fig. 3E, left).

To confirm that this effect of tumor shrinkage was only because of better drug delivery facilitated by prudent anti-

angiogenic treatment, macroscopic H1975 tumor bearing mice pretreated with PTK787 were treated with phosphoinositide 3-kinase inhibitor GDC0941. Tumors receiving GDC0941 therapy pretreated with PTK787 receded by 50% (SD = 4.7, range = 10.07) more than 28 days compared with just a mild growth inhibition observed in GDC0941 monotherapy sets, which tumor volumes surpassed by 250% (SD = 10.41, range = 22,10) on day 22 (Fig. 4A).

Intermittent antiangiogenic treatment facilitates long-term tumor regression

A long-term xenograft study with subcutaneous PC9 tumors was performed where mice were treated with a continuous dose of erlotinib combined with a short PTK787 treatment every 10 days. Tumors remained regressed in this combination
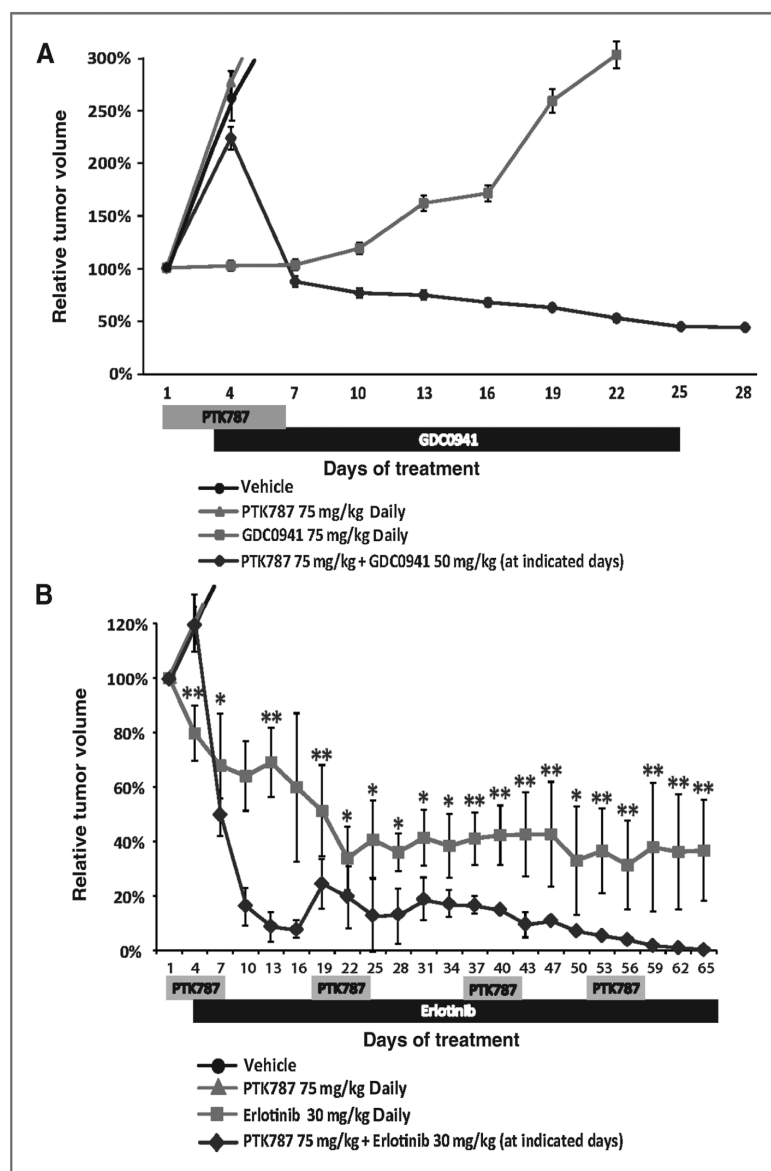

Figure 4. Short antiangiogenic treatment improves therapeutic outcome of GDC0941; long-term tumor regression with intermittent antiangiogenic therapy. PC9 cells were engrafted subcutaneously in nude mice and tumor volumes were recorded over time for either 28 days under treatment with PTK787 (75 mg/kg), GDC0941 (75 mg/kg) and PTK787 (75 mg/kg) + GDC0941 (50 mg/kg) at indicated days ($n = 6$ mice with 3 tumors/mouse for each set-up; A) or for 65 days under treatment with PTK787 (75 mg/kg), erlotinib (30 mg/kg), and erlotinib (30 mg/kg) with intermittent PTK787 treatment from day 1 to day 7, day 17 to day 25, day 35 to day 43 and day 51 to day 58 ($n = 6$ mice with 3 tumors/mouse for each set-up; B).

model over the entire time span of 65 days (Fig. 4B). However, in mice treated with erlotinib only, there was an initial tumor regression up to 40% of original tumor volume until day 22 followed by a stable disease (Fig. 4B).

Discussion

Using *in vivo* PET imaging we demonstrate that transient antiangiogenic treatment using PTK787 improves tumor blood flow *in vivo*. This transient tumor vessel normalization results in an improved delivery of targeted compounds such as erlotinib into the tumor. Most strikingly, enhanced availability and distribution of erlotinib within the tumor induced by transient PTK787 treatment was followed by a significant increase in tumor shrinkage. This improvement in tumor response is consistent with recent findings demonstrating that high-dose EGFR-targeted drug exposure results in more efficient target inhibition (18).

Several mechanisms have been described as potential targets to improve the function of tumor vessels. Recently, Chakroborty and colleagues described Dopamine as a potential drug to improve the function of tumor vessels. The

normalization effect was mainly mediated by an upregulation of angiopoetin-1 and the Krüppel-like factor 2 (19). Similarly, treatment with the Cox-2 inhibitor apricoxib increased the maturity of tumor vessel *in vivo* (20). In line with our findings this vascular normalization effect was associated with a significantly enhanced efficacy of gemcitabine plus erlotinib (21). Tumor vessel normalization upon apricoxib treatment was primarily induced by a transient reduction in VEGF secretion within the tumor *in vivo*. Of note, the tumor vessel normalization effect was time and dose dependent (20). Rakesh Jain recently reported that the tumor vessel normalization effect induced by inhibition of the VEGF-VEGFR2 axis is time and dose dependent (22, 23). We applied $[^{15}O]H_2O$ PET imaging to decipher this time-dependent tumor vessel normalization effect. In line with the tumor vessel normalization hypothesis, tumor blood flow increased within the first 8 days of PTK787 treatment but again declined till day 18 of treatment accompanied by a decrease in pericyte coverage (19, 24). Thus, our data strongly indicate that tumor vessel normalization induced by PTK787 is time dependent. We found similar results with ZD6474, a tyrosine kinase inhibitor that primarily targets EGFR and VEGFR2 (13). As we applied H1975 xenografts that are resistant to EGFR treatment, the ZD6474 induced effect on the tumor vasculature seems to be mainly driven by inhibition of VEGFR2. Similarly, Huang and colleagues found that low-dose treatment with an anti-VEGFR2-antibody (DC101) results in an increase in pericyte coverage in a breast cancer *in vivo* model (25). These and our data indicate that the primary target to induce tumor vessel normalization is most probably VEGFR2. However, further investigations are required to decipher in detail the responsible tyrosine kinases that drive tumor vessel normalization.

In our study the implication of $[^{15}O]H_2O$-PET–guided use of PTK787 and ZD6474 treatment significantly improved the delivery of the cytotoxic compounds erlotinib and GDC0941. $[^{15}O]H_2O$ PET has been already successfully applied in patients with human lung cancer (26). Thus, $[^{15}O]H_2O$ PET reflects a highly accurate method that can easily be translated into clinical application. The implementation of $[^{15}O]H_2O$ PET enables to establish combined antiangiogenic and cytotoxic PET-guided treatment protocols in individual patients to improve the delivery of cytotoxic compounds.

Cytotoxic agents combined with antiangiogenic therapy has shown only little efficacy in patients with advanced stage NSCLC. In a recent phase III trial, the addition of bevacizumab to chemotherapy for newly diagnosed glioblastoma did not improve overall survival (27). In a recent human study, docetaxel uptake was reduced in NSCLC after patients were administered with bevacizumab (28). These data indicate that inhibition of VEGF potentially bears an antivascular than tumor vessel normalization effect supporting the notion that scheduling and dosing of the antiangiogenic treatment is essential to induce and maintain tumor vessel normalization. This is also confirmed by our PET data as the vascular normalization effect seems to be transient as continuous treatment with PTK787 or ZD6474 result in a reduction in tumor flow after more than 8 days of treatment. Our data strengthen the use of $[^{15}O]H_2O$ PET in clinical studies to define the optimal dose and schedule of antiangiogenic drugs such as bevacizumab and PTK787 to improve the delivery of cytotoxic drugs in to the tumor.

In summary, our findings are consistent with the vascular normalization hypothesis and are indicative of the fact that prudent antiangiogenic therapy leads to evanescent vessel normalization, resulting in better cytotoxic therapeutic outcome. However, optimal designs of drug scheduling and efficient imaging techniques are absolutely indispensable to achieve maximal clinical outcome.

Disclosure of Potential Conflicts of Interest

No potential conflicts of interest were disclosed.

Authors' Contributions

Conception and design: S. Chatterjee, B. Neumaier, R.T. Ullrich
Development of methodology: S. Chatterjee, B. Neumaier, R.T. Ullrich
Acquisition of data (provided animals, acquired and managed patients, provided facilities, etc.): S. Chatterjee, C. Wieczorek, J. Schöttle, M. Siobal, Y. Hinze, T. Franz, A. Florin, L.C. Heukamp, R.T. Ullrich
Analysis and interpretation of data (e.g., statistical analysis, biostatistics, computational analysis): S. Chatterjee, J. Schöttle, L.C. Heukamp, R.T. Ullrich
Writing, review, and or revision of the manuscript: S. Chatterjee, T. Franz, B. Neumaier, R.T. Ullrich
Administrative, technical, or material support (i.e., reporting or organizing data, constructing databases): S. Chatterjee, M. Siobal, A. Florin, J. Adamczak, L.C. Heukamp, B. Neumaier, R.T. Ullrich
Study supervision: R.T. Ullrich

References

1. Folkman J. Tumor angiogenesis: therapeutic implications. N Engl J Med 1971;285:1182–6.
2. Rak J, Yu JL, Kerbel RS, Coomber BL. What do oncogenic mutations have to do with angiogenesis/vascular dependence of tumors? Cancer Res 2002;62:1931–4.
3. Mazzone M, Dettori D, Leite de Oliveira R, Loges S, Schmidt T, Jonckx B, et al. Heterozygous deficiency of PHD2 restores tumor oxygenation and inhibits metastasis via endothelial normalization. Cell 2009;136: 839–51.
4. Jain RK. Normalization of tumor vasculature: an emerging concept in antiangiogenic therapy. Science (New York, NY). 2005;307:58–62.
5. Paez-Ribes M, Allen E, Hudock J, Takeda T, Okuyama H, Vinals F, et al. Antiangiogenic therapy elicits malignant progression of tumors to increased local invasion and distant metastasis. Cancer Cell 2009; 15:220–31.
6. Rapisarda A, Melillo G. Role of the hypoxic tumor microenvironment in the resistance to anti-angiogenic therapies. Drug Resist Updat 2009; 12:74–80.

120

7. Jain RK. Normalizing tumor vasculature with anti-angiogenic therapy: a new paradigm for combination therapy. Nat Med 2001;7:987–9.

8. Zhang Q, Bindokas V, Shen J, Fan H, Hoffman RM, Xing HR. Time-course imaging of therapeutic functional tumor vascular normalization by antiangiogenic agents. Mol Cancer Ther 2011;10:1173–84.

9. Winkler F, Kozin SV, Tong RT, Chae SS, Booth MF, Garkavtsev I, et al. Kinetics of vascular normalization by VEGFR2 blockade governs brain tumor response to radiation: role of oxygenation, angiopoietin-1, and matrix metalloproteinases. Cancer Cell 2004;6:553–63.

10. Fukumura D, Duda DG, Munn LL, Jain RK. Tumor microvasculature and microenvironment: novel insights through intravital imaging in pre-clinical models. Microcirculation 2010;17:206–25.

11. Ullrich RT, Jikeli JF, Diedenhofen M, Bohm-Sturm P, Unruh M, Vollmar S, et al. In vivo visualization of tumor microvessel density and response to anti-angiogenic treatment by high resolution MRI in mice. PLoS ONE 2011;6:e19592.

12. Kerbel RS. Antiangiogenic therapy: a universal chemosensitization strategy for cancer? Science (New York, NY) 2006;312:1171–5.

13. Wedge SR, Ogilvie DJ, Dukes M, Kendrew J, Chester R, Jackson JA, et al. ZD6474 inhibits vascular endothelial growth factor signaling, angiogenesis, and tumor growth following oral administration. Cancer Res 2002;62:4645–55.

14. Wood JM, Bold G, Buchdunger E, Cozens R, Ferrari S, Frei J, et al. PTK787/ZK 222584, a novel and potent inhibitor of vascular endothe-lial growth factor receptor tyrosine kinases, impairs vascular endothe-lial growth factor-induced responses and tumor growth after oral administration. Cancer Res 2000;60:2178–89.

15. Chatterjee S, Heukamp LC, Siobal M, Schottle J, Wieczorek C, Peifer M, et al. Tumor VEGF:VEGFR2 autocrine feed-forward loop triggers angiogenesis in lung cancer. J Clin Invest 2013;123:3183.

16. Ullrich RT, Zander T, Neumaier B, Koker M, Shimamura T, Waerzeg-gers Y, et al. Early detection of erlotinib treatment response in NSCLC by 3′-deoxy-3′-[F]-fluoro-L-thymidine ([F]FLT) positron emission tomography (PET). PLoS ONE 2008;3:e3908.

17. Shields AF, Grierson JR, Dohmen BM, Machulla HJ, Stayanoff JC, Lawhorn-Crews JM, et al. Imaging proliferation in vivo with [F-18]FLT and positron emission tomography. Nat Med 1998;4:1334–6.

18. Shah NP, Kasap C, Weier C, Balbas M, Nicoll JM, Bleickardt E, et al. Transient potent BCR-ABL inhibition is sufficient to commit chronic myeloid leukemia cells irreversibly to apoptosis. Cancer Cell 2008; 14:485–93.

19. Chakroborty D, Sarkar C, Yu H, Wang J, Liu Z, Dasgupta PS, et al. Dopamine stabilizes tumor blood vessels by up-regulating angiopoie-tin 1 expression in pericytes and Kruppel-like factor-2 expression in tumor endothelial cells. Proc Natl Acad Sci U S A 2011;108:20730–5.

20. Kirane A, Toombs JE, Larsen JE, Ostapoff KT, Meshaw KR, Zaknoen S, et al. Epithelial-mesenchymal transition increases tumor sensitivity to COX-2 inhibition by apricoxib. Carcinogenesis 2012; 33:1639–46.

21. Kirane A, Toombs JE, Ostapoff K, Carbon JG, Zaknoen S, Braunfeld J, et al. Apricoxib, a novel inhibitor of COX-2, markedly improves stan-dard therapy response in molecularly defined models of pancreatic cancer. Clin Cancer Res 2012;18:5031–42.

22. Jain RK. Normalizing tumor microenvironment to treat cancer: bench to bedside to biomarkers. J Clin Oncol 2013;31:2205–18.

23. Huang Y, Stylianopoulos T, Duda DG, Fukumura D, Jain RK. Benefits of vascular normalization are dose and time dependent–letter. Cancer Res 2013;73:7144–6.

24. Jain RK, Booth MF. What brings pericytes to tumor vessels? J Clin Invest 2003;112:1134–6.

25. Huang Y, Yuan J, Righi E, Kamoun WS, Ancukiewicz M, Nezivar J, et al. Vascular normalizing doses of antiangiogenic treatment reprogram the immunosuppressive tumor microenvironment and enhance immuno-therapy. Proc Natl Acad Sci U S A 2012;109:17561–6.

26. de Langen AJ, van den Boogaart V, Lubberink M, Backes WH, Marcus JT, van Tinteren H, et al. Monitoring response to antiangiogenic therapy in non-small cell lung cancer using imaging markers derived from PET and dynamic contrast-enhanced MRI. J Nucl Med 2011; 52:48–55.

27. Gilbert MR, Dignam J, Won M, Blumenthal DT, Vogelbaum MA, Aldape KD, et al. Phase III double-blind placebo-controlled trial evaluating bevacizumab (Bev) in patients (Pts) with newly diagnosed glioblastoma (GBM). J Clin Oncol 31, 2013 (suppl; abstr 1). 2013;2013 ASCO Annual Meeting.

28. Van der Veldt AA, Lubberink M, Bahce I, Walraven M, de Boer MP, Greuter HN, et al. Rapid decrease in delivery of chemotherapy to tumors after anti-VEGF therapy: implications for scheduling of anti-angiogenic drugs. Cancer Cell 2012;21:82–91.

121

8.3. Additional publications

1. **Intermittent high-dose treatment with erlotinib enhances therapeutic efficacy in EGFR-mutant lung cancer**

   Jakob Schöttle, **Sampurna Chatterjee**, Caroline Volz, Maike Siobal, Alexandra Florin, Dennis Rokitta, Yvonne Hinze, Felix Dietlein, Dennis Plenker, Katharina König, Kerstin Albus, Johannes Heuckmann, Daniel Rauh, Thomas Franz, Bernd Neumaier, Uwe Fuhr, Lukas C. Heukamp, Roland T. Ullrich, Roman K. Thomas.
   Clinical Cancer Research, August 2014 (under review).

2. **Prediction of therapy response to irreversible EGFR tyrosine kinase inhibitors in NSCLC using a novel 18F-labelled anilinoquinazoline derivative by PET**

   Jakob Schöttle*, **Sampurna Chatterjee***, René Kandler, Diana Kobus, Maike Siobal, Roland T. Ullrich, Bernd Neumaier (*co first authors)
   Journal of Nuclear Medicine, August 2014 (under review).

3. **The bispecific immunoligand ULBP2-aCEA re-directs natural killer cells to tumor cells and reveals potent antitumor activity against colon carcinoma.**

   Achim Rothe, Ron D Jachimowicz, Sven Borchmann, Marie Madlener, Jörg Keßler, Katrin S Reiners, Maike Sauer, Hinrich P Hansen, Roland T. Ullrich, **Sampurna Chatterjee**, Peter Borchmann, Paul Yazaki, Thomas C Koslowsky, Andreas Engert, Lukas C. Heukamp, Micheal Hallek, Elke Pogge von Strandmann.
   International Journal of Cancer, 2013.

4. **Targeted expression of mutated ALK induces neuroblastoma in transgenic mice.**

Lukas C. Heukamp, Theresa Thor, Alexander Schramm, Katleen De Preter, Candy Kumps, Bram De Wilde, Andrea Odersky, Martin Peifer, Sven Lindner, Annika Spruessel, Filip Pattyn, Pieter Mestdagh, Björn Menten, Steffi Kuhfittig-Kulle, Annette Künkele, Katharina König, Lydia Meder, **Sampurna Chatterjee**, Roland T. Ullrich, Stefanie Schulte, Jo Vandesompele, Frank Speleman, Reinhard Büttner, Angelika Eggert, Johannes H. Schulte (July 2012).
Science Translational Medicine, 2012.

5. **Cytohesins are cytoplasmic ErbB Receptor Activators.**

Anke Bill, Anton Schmitz, Barbara Albertoni, Jin-Na Song, Lukas C. Heukamp, David Walrafen, Franziska Thorwirth, Peter J. Verveer, Sebastian Zimmer, Lisa Meffert, Arne Schreiber, **Sampurna Chatterjee**, Roman K. Thomas, Roland T. Ullrich, Thorsten Lang, Michael Famulok.
Cell, 2010.

8.4. Erklärung / Declaration

Ich versichere, dass ich die von mir vorgelegte Dissertation selbständig angefertigt, die benutzten Quellen und Hilfsmittel vollständig angegeben und die Stellen der Arbeit – einschließlich Tabellen, Karten und Abbildungen -, die anderen Werken im Wortlaut oder dem Sinn nach entnommen sind, in jedem Einzelfall als Entlehnung kenntlich gemacht habe; dass diese Dissertation noch keiner anderen Fakultät oder Universität zur Prüfung vorgelegen hat; dass sie – abgesehen von unten angegebenen Teilpublikationen – noch nicht veröffentlicht worden ist sowie, dass ich eine solche Veröffentlichung vor Abschluss des Promotionsverfahrens nicht vornehmen werde. Die Bestimmungen dieser Promotionsordnung sind mir bekannt. Die von mir vorgelegte Dissertation ist von PD. Dr. med. Dr. nat. med. Roland Ullrich betreut worden.

I confirm that the submitted dissertation is my own work and has not been written for me, in whole or in part, by any other person. I undertake that all the materials that have been presented in this thesis including tables and figures are my own work and have not been submitted elsewhere for examination. Any source of information (quotation, paraphrase, figure, table etc) has been duly acknowledged. I have read and understood the regulations concerning plagiarism for writing a doctoral thesis. This dissertation submitted by me has been supervised by PD. Dr. med. Dr. nat. med. Roland Ullrich.

……………………………………………..

Cologne, 26.08.2014.

8.5. Affiliations and Funding

8.6. Acknowledgement

(Head, Institute for Biochemistry II and Chair of the IPMM-PhD-Examination Board) have been very gracious and generous with their time and evaluation of my thesis. I owe a lot to Dr. **Debora Grosskoph-Kroiher** (Managing Director, IPMM) who devoted a lot of energy and time to ensure that my graduation procedure runs smoothly from beginning to the end.

I am immensely grateful to Prof. Dr. **Bernd Neumaier**, Dr. **Rainer Wagner** and Dr. **Bernd Bauer** from the department of Radiochemistry at the MPI for Metabolism Research, Cologne for pushing my projects by consistently synthesizing radiotracers according to my convenience.

I thank all my co-authors for contributing into my projects resulting in fruitful collaborations and publications. I acknowledge **Alexandra Florin** from department of Pathology, University Hospital Cologne and **Melanie Nelles** from NMR group, MPI for their continuous inputs in my research and endless patience. Alex supported me unconditionally by performing countless number of histologies of tumor samples while Melanie taught me immunofluorescence for my second project.

A good support system is essential to survive and stay sane during the PhD time and my working group has served that purpose perfectly. **Maike Siobal** (technical assistant) assisted me extensively in successfully carrying out my projects. **Caroline Volz** (fellow PhD student turned into a great friend) and me not only shared the same lab but also our fears, worries and major set backs. She along with Dr. **Jakob Schöttle** (medical PhD student) provided me ample enthusiasm and optimism to sustain the last four years. I will definitely miss those days at and outside work when we spent hours talking gibberish and participating in silly discussions. **Kristina Golfmann** and **Alina Zaplatina**, the juniors, have been like a fresh breeze in the group cheering me up with many lively conversations and after-work outings.

My future work group from Harvard Medical School, Boston, deserves an exclusive mention here. I praise the enormous backing and perseverance from Prof. Dr. **Rakesh Jain** (Director, Edwin L. Steele lab), Dr. **Timothy Padera** and Dr. **Jonas Kloepper**. Their keenness in having me in their group and constant cooperation catalysed my finishing phase here in Cologne.

Living and studying in a foreign country can be exciting because evey now and then you get to confront with unexpected challanges. Dozens of people have helped me out in overcoming many unforeseen hurdles during my almost five-year-long stay in Germany. I could always go to **Caroline**, **Jakob**, Dr. **Joanna Adamczak** and **René Kandler** who readily translated the official documents (in German) to English. **Caroline** and **René** frequently accompanied me to the City Council of Foreign Affairs to ensure that the bureaucratic affairs run smoothly saving me a lot of trouble. Prof. Dr. **Helmut Lamm** whom I met by coincidence has a been a friend , phillosopher and guide throughout the last four years. With his calm and reserved personality, he was a great source of strength and advice whenever I needed. Pursuing my PhD in Germany has been one of the best decisions I have taken in my life. I arrived here as an amateur and this country shaped my mind and anchored my identity. I learnt from the Germans that working hard and honestly, being humble, behaving politely and helping people out define the identity of a person.

Prof. **David. I. Stott**, my former supervisor (University of Glasgow) has been the invisible man behind my success all the time since the beginning of my scientific career. His undeterred encouragement kept me moving forward no matter what and his recommendation letters earned me every single position I applied for in every country until now.

I am heavily indebted to **Avina Dey**, **Eric Dietrich** and **Florian Wodlei**. These terrific trio redefined the meaning of friendship by pulling me up when I stumbled in my otherwise smooth journey of pursuing a PhD. Their indomitable inspiration and rock-solid trust in my capabilities motivated me to pace up again and complete my thesis in just one month. It was always a pleasure to babble nonstop in our mother tongue Bengali with **Avina**, solve riddles with **Eric** and engage in scientific discussions with **Florian**. **Joanna**, **Somayyeh Hamzei Taj**, Dr. **Jochen Michely** and **Petra Weiß** from the MPI provided me constant enthusiam in accomplishing my target. **Eleni Kalisperati,** the sweet girl from Greece have been a great friend and support since the time I got to know her from our German lessons.

Words will fall short when I talk about the contributions of my family and friends nine thousand kilometres away. I have the typical stereotypical family however standing out to be unique and amazing in many ways. My **parents** and **grandparents**, **Saikat**, **Dola**, **Tumpa** and **Ayesha** have been like a powerhouse of positive energy, unconditional love and steadfast backing during all those years. I salute their unlimited patience and faith in me. My maternal grandmother with her tender heart, my maternal grandfather with the most detached outlook towards mundane things, my paternal grandfather (who taught me English) with his intense desire to know and understand everything this world contains and my paternal grandmother (beloved Nani whom we lost this year in January) with her cheerful temparament and vibrant smile have defined many traits of my personality and made me who I am today. My deeply emotional **father** have shown me that it is ok to fall or loose once in a while in the race of life as long as I manage to get up and move on. Finally it is the moment that I mention this very special lady, whose intrepid struggle with life, unflinching dedication towards me and unapprehensive ways of strengthening my personality by exposing the harsh reality of the world to me have made me fearless and undaunted in approaching life and dealing with any obstacle coming in my way; my **mother**, the most amazing woman in my life, I would not have made it up till here without you.

I would specially like to acknowledge my **father's colleagues** whose appreciation for every little step that I put forward made me feel special and powerful since I was a child.

Last but not the least, I owe my success and achievements to that one person who never doubted my potential. Dr. **Roland Ullrich**, my supervisor and phillosopher has curved out the whole trajectory for me ensuring that my PhD time in his lab becomes interesting and rewarding laying the path for future advances in my scientific career.

8.7. Curriculum Vitae

Sampurna Chatterjee

City of Birth   Kolkata / Calcutta / KalKutta

Nationality   Indian

Address: Centre for Molecular Medicine Cologne

                                 Group: Cancer Therapy and Molecular Imaging

                                 Robert Koch straße 21,

                                 50931 Cologne.

                                 Germany.

Scientific Career

Till 07.2014   Doctoral study at the Max Planck Institute for Metabolic Research, Department I of Internal Medicine with Centre for Integrated oncology, University Hospital of Cologne and Centre for Molecular Medicine of University of Cologne in the group of Cancer Therapy and Molecular Imaging headed by PD. Dr. Dr. Roland Ullrich.

09.2007 – 12.2008   Master of Research (M.Res) study in Biomedical and Life Sciences at University of Glasgow, Scotland, UK.

08.2004 – 07.2007   Bachelor of Science (B.Sc) study in Microbiology from University of Calcutta, India.

06.2002 – 04.2004   Higher Secondary Study, Patha Bhavan School, Calcutta.

12.1990 – 03.2002   Secondary Study, Nava Nalanda School, Calcutta.